FIRE RESISTANCE ASSESSMENT OF PARTIALLY PROTECTED COMPOSITE FLOORS (FRACOF): ENGINEERING BACKGROUND

Contents

SUMMARY

Large-scale fire tests conducted in a number of countries and observations of actual building fires have shown that the fire performance of composite steel framed buildings is much better than is indicated by fire resistance tests on isolated elements. It is clear that there are large reserves of fire resistance in modern steel-framed buildings and that standard fire resistance tests on single unrestrained members do not provide a satisfactory indicator of the performance of such structures.

As a result of observation and analysis of the BRE Cardington large-scale building fire test programme carried out during 1995 and 1996, a simple design model on the basis of membrane action of steel and concrete composite floor has been developed which allows designers to take advantage of the inherent fire resistance of a composite floor plate without the need to resort to complex finite element analysis of whole building behaviour.. However, because of its specific feature, this innovative design concept remains still unfamiliar to most of engineers and authorities. In consequence, this technical document is established to provide all necessary background information in order to assist the reader to understand easily the basis of the design recommendations of above simple design model.

In this technical document, the theoretical basis of the simple design method and its development for application to fire engineering is described. An important review of existing relevant fire tests carried out in full scale buildings around the world is described and the corresponding test data are summarized as well in this document. Information is also included on observations of the behaviour of multi-storey buildings in accidental fires. On the other hand, the document gives detailed explanation of the new large-scale fire tests of composite floor systems conducted under long duration ISO fire which provides more evidences about the validity of the simple design model. The conservativeness of the simple design model is also clearly illustrated through the comparison with the parametric numerical study conducted with help of advanced calculation models.

1 INTRODUCTION

Large-scale fire tests conducted in a number of countries and observations of actual building fires have shown that the fire performance of composite steel framed buildings with composite floors (concrete slabs connected to steel beams by means of headed studs) is much better than indicated by standard fire resistance tests on composite slabs or composite beams as isolated structural elements. It is clear that there are large reserves of fire resistance in modern steel-framed buildings and that standard fire resistance tests on single unrestrained members do not provide a satisfactory indicator of the real performance of such structures.

Analysis reveals that this excellent fire performance is due to the development of tensile membrane action in the reinforced concrete slab and the catenary action of steel beams.

As a result of the above observation and analysis, a new fire design concept for modern multi-storey steel-framed buildings was developed in the UK. Design guidance and software design tools for composite floor plates based on this method were first published in 2000. Many buildings in the UK have since benefited from the application of the simple design method, resulting in reduced fire protection costs[1].

The design concept allows designers to take advantage of whole building behaviour, allowing some members to remain unprotected while maintaining the safety levels expected from fully fire-protected structures. The design method allows the fire resistance of partially protected composite floors to be assessed for natural fire or standard fire exposure. The latter is of particular interest because it means that the design concept may be applied by design engineers without the need for specialist fire engineering knowledge.

Although widely used in the UK, the enhancement of fire resistance provided by membrane and catenary actions is still a very new concept for the majority of engineers and regulatory authorities within Europe. To inform these potential user groups, this document aims to provide a solid technical support package for this design concept, comprising:

- a review of the evidence available about the performance of composite structures in large-scale fire tests and accidental building fires;
- a detailed explanation of the theoretical basis of the simple design model for composite floor systems;
- a description of the fundamental assumptions adopted in the simple design model for fire resistance assessment of steel and concrete composite floor systems;
- details of a demonstration fire test on a full scale steel and concrete composite floor system using the standard time-temperature curve in accordance with EN 1365-2, for a duration of more than 120 minutes
- a detailed numerical parametric investigation to verify the output from the simple design model.

2 CARDINGTON FIRE TEST PROGRAM

2.1 Research programme

In September 1996, a programme of fire tests was completed in the UK at the Building Research Establishment's Cardington Laboratory. The tests were carried out on an eight-storey composite steel-framed building that had been designed and constructed as a typical multi-storey office building. The purpose of the tests was to investigate the behaviour of a real structure under real fire conditions and to collect data that would allow computer programs for the analysis of structures in fire to be verified.

Figure 2.1 *Cardington test building prior to concreting of the floors*

The test building (see Figure 2.1.) was designed to be a typical example of both the type of braced structure and the load levels that are commonly found in the UK. In plan, the building covered an area of 21 m × 45 m and had an overall height of 33 m. The beams were designed as simply supported, acting compositely with a 130 mm floor slab. Normally, a building of this type would be required to have 90 minutes fire resistance. Fin-plates were used for the beam-to-beam connections and flexible end plates for the beam-to-column connections. The structure was loaded using sandbags distributed over each floor to simulate typical office loading.

There were two projects in the research programme. One project was funded by Corus (formerly British Steel) and the European Coal and Steel Community (ECSC); the other was funded by the UK Government via the Building Research Establishment (BRE). Other organisations involved in the research programme included Sheffield University, TNO (The Netherlands), CTICM (France) and The Steel Construction Institute. Fire tests took place between January 1995 and July

1996. The tests were carried out on various floors; the location of each test is shown on the floor plan in Figure 2.2.

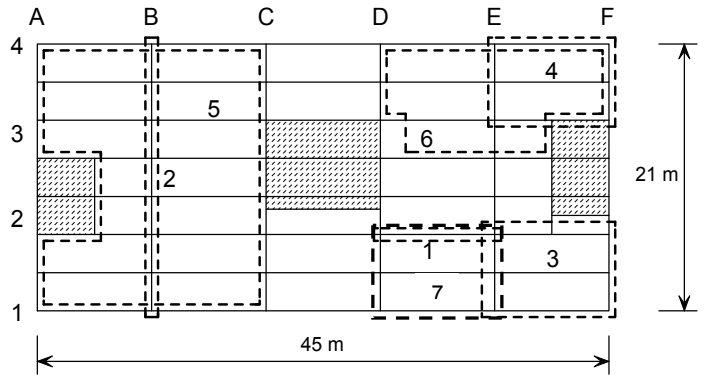

1. Restrained beam (ECSC)
2. Plane frame (ECSC)
3. Corner (ECSC)
4. Corner (BRE)
5. Large compartment (BRE)
6. Office demonstration (ECSC)
7. Central compartment (CTU)

Figure 2.2 *Test Locations*

Test 1 involved a single secondary beam and the surrounding floor slab, which was heated by a purpose-built gas-fired furnace. Test 2 was also heated using gas, and was conducted on a plane frame spanning across the building on one floor; the test included primary beams and associated columns. Tests 3, 4 and 5 involved compartments of various sizes subjected, in each case, to a natural fire fuelled by timber cribs. The columns in these tests were protected up to the underside of the floor slab and the beams and floor slab were left unprotected. Test 6 was a demonstration, which used furniture and contents typically found in modern offices as the fire load, leading to the most severe fire.

A detailed description of the tests has been published[1]. The complete test data, in electronic form with accompanying instrument location maps, is available for Tests 1, 2, 3 and 6 from Corus RD&T (Swinden Technology Centre) and for Tests 4 and 5 from BRE[3,4].

2.2 Test 1: Restrained beam

The test was carried out on the seventh floor of the building. A purpose-built gas fired furnace, 8.0 m long and 3.0 m wide, was designed and constructed to heat a secondary beam (D2/E2) spanning between two columns and part of the surrounding structure. The beam was heated over the middle 8.0 m of its 9.0 m length, thus keeping the connections relatively cool. The purpose of the test was to investigate the behaviour of a heated beam surrounded by an unheated floor slab and study the restraining effect of the unheated parts of the structure.

The beam was heated at between 3 and 10°C per minute until temperatures approaching 900°C were recorded. At the peak temperature, 875ºC in the lower flange, the mid span deflection was 232 mm (span/39) (see Figure 2.3). On cooling, the mid-span deflection recovered to 113 mm.

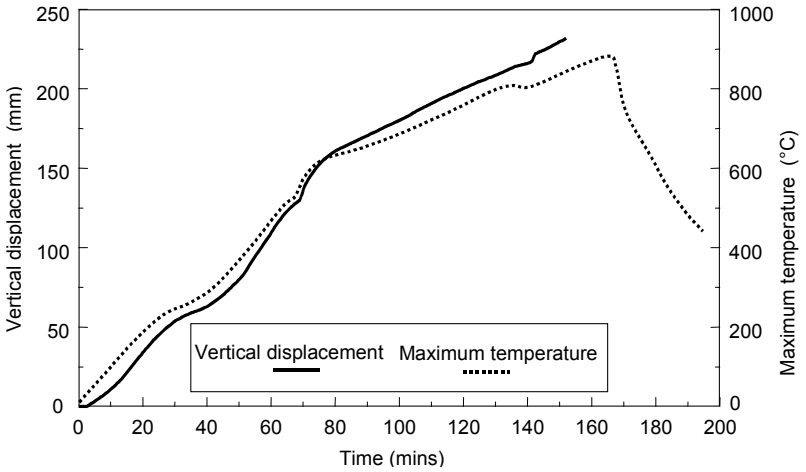

Figure 2.3 *Central displacement and maximum temperature in restrained beam test*

The contrast between the behaviour of this beam and a similar unprotected beam tested in a standard fire test under a similar load[5] is shown in Figure 2.4. The 'runaway' displacement typical of simply supported beams in the standard test did not occur to the beam in the building frame even though, at a temperature of about 900ºC, structural steel retains only about 6% of its yield strength at ambient temperature.

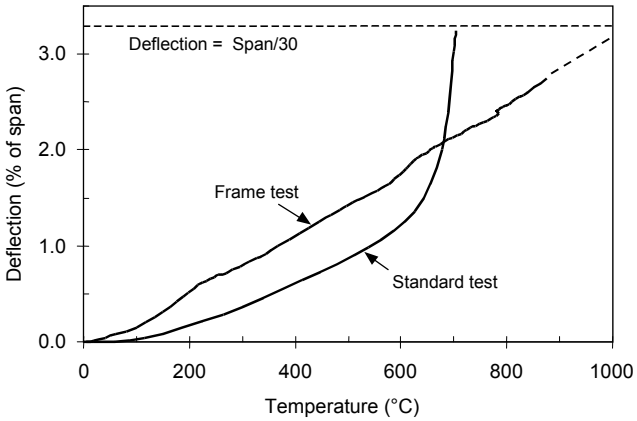

Figure 2.4 *Central displacement and maximum temperature in standard fire test and restrained beam test*

During the test, local buckling occurred at both ends of the test beam, just inside the furnace wall (see Figure 2.5).

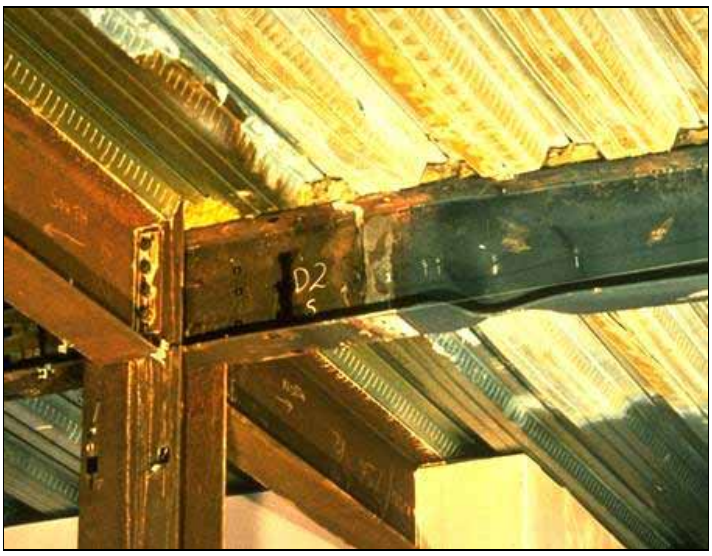

Figure 2.5 *Flange buckling in restrained beam*

Visual inspection of the beam after the test showed that the end-plate connection at both ends of the beam had fractured near, but outside, the heat-affected zone of the weld on one side of the beam. This was caused by thermal contraction of the beam during cooling, which generated very high tensile forces. Although the plate sheared down one side, this mechanism relieved the induced tensile strains, with the plate on the other side of the beam retaining its integrity and thus providing shear capacity to the beam. The fracture of the plate can be identified from the strain gauge readings, which indicate that, during cooling, the crack progressed over a period of time rather than by a sudden fracture.

2.3 Test 2: Plane frame

This test was carried out on a plane frame consisting of four columns and three primary beams spanning across the width of the building on gridline B, as shown in Figure 2.2.

A gas-fired furnace 21 m long × 2.5 m wide × 4.0 m high was constructed using blockwork across the full width of the building.

The primary and secondary beams, together with the underside of the composite floor, were left unprotected. The columns were fire protected to a height at which a suspended ceiling might be installed (although no such ceiling was present). This resulted in the top 800 mm of the columns, which incorporated the connections, being unprotected.

The rate of vertical displacement at midspan of the 9 m span steel beam increased rapidly between approximately 110 and 125 minutes (see Figure 2.6). This was caused by vertical displacements of its supporting columns. The exposed areas of the internal columns squashed by approximately 180 mm (see Figure 2.7). The temperature of the exposed part of the column was approximately 670°C when local buckling occurred.

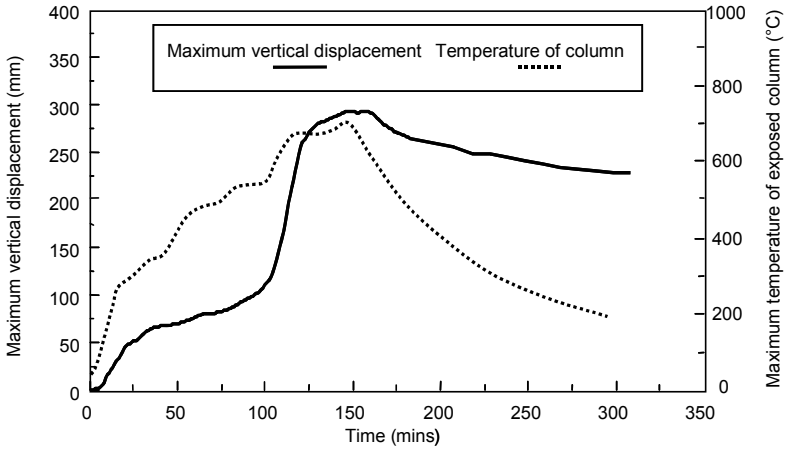

Figure 2.6 *Maximum vertical displacement of central 9 m beam and temperature of exposed top section of internal column*

The reduction in column height which resulted from this local buckling caused a permanent deformation of approximately 180 mm in all the floors above the fire compartment. To avoid this behaviour, columns in later tests were protected over their full height.

Figure 2.7 *Squashed column head following the test*

On both sides of the primary beams, the secondary beams were each heated over a length of approximately 1.0 m. After the test, investigation showed that many of the bolts in the fin-plate connections had sheared (see Figure 2.8). The bolts had only sheared on one side of the primary beam. In a similar manner to the fracturing of the plate in Test 1, the bolts sheared due to thermal contraction of the beam during cooling. The thermal contraction generated very high tensile forces, which were relieved once the bolts sheared in the fin-plate on one side of the primary beam.

Figure 2.8 *Fin-plate connection following test*

2.4 Test 3: Corner

The objective of this test was to investigate the behaviour of a complete floor system and, in particular, the role of 'bridging' or membrane action of the floor in providing alternative load paths as the supporting beams lose strength. Using concrete blockwork, a compartment 10 m wide × 7.6 m deep was constructed in one corner of the first floor of the building (E2/F1).

To ensure that the compartment walls did not contribute to supporting the applied loads, all the restraints and ties in the gable wall and the top layer of blockwork were removed. The mineral fibre board in the expansion joints was replaced with a ceramic blanket.

Similarly, the wind posts on the external wall were detached from the edge beam above the compartment opening, to ensure that this edge beam did not have additional support.

All columns, beam-to-column connections and edge beams were fire protected.

The fire load was 45 kg/m^2, in the form of timber cribs. This fire load is quite high and is equivalent to the 95% fractile loading for office buildings. Fire safety engineering calculations are normally based on the 80% fractile loading. Ventilation was provided by a single 6.6 m wide × 1.8 m high opening. The peak atmospheric temperature recorded in the compartment was 1071ºC.

The maximum steel temperature was 1014ºC, recorded on the inner beam on gridline 2 (E2/F2). The maximum vertical displacement of 428 mm (just less than span/20) occurred at the centre of the secondary beam, which had a peak temperature of 954ºC. On cooling, this beam recovered to a permanent displacement of 296 mm. The variations of deflection and temperature with time are shown in Figure 2.9.

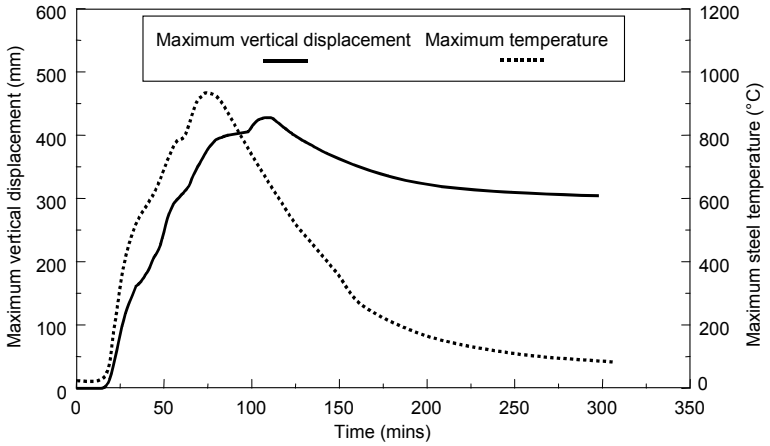

Figure 2.9 *Maximum vertical displacement and temperature of secondary beam*

All the combustible material within the compartment was consumed by the fire. The structure behaved extremely well, with no signs of collapse (see Figure 2.10).

Buckling occurred in the proximity of some of the beam-to-column connections but, unlike Test 2, bolts in the connections did not suffer shear failure. This might indicate either that the high tensile forces did not develop or that the connection had adequate ductility to cope with the tensile displacements.

Figure 2.10 *View of structure following test*

2.5 Test 4: Corner

This test was carried out on the second floor, in a corner bay (E4/F3) with an area of 54 m^2. The internal boundaries of the compartment on gridlines E and 3 were constructed using steel stud partitions with fire resistant board. The stud partition was specified to have 120 minutes fire resistance, with a deflection head of 15 mm. An existing full-height blockwork wall formed the boundary on the gable wall on gridline F; the outer wall, gridline 4, was glazed above 1 metre of blockwork. The compartment was totally enclosed, with all windows and doors closed. The columns were fire protected up to the underside of the floor slab, including the connections but, unlike Test 3, the lintel beam (E4/F4) was unprotected and the wind posts above it remained connected. Twelve timber cribs were used to give a fire load of 40 kg/m^2.

The development of the fire was largely influenced by the lack of oxygen within the compartment. After an initial rise in temperature, the fire died down and continued to smoulder until, after 55 minutes, the fire brigade intervened to vent the compartment by removal of a single pane of glazing. This resulted in a small increase in temperature followed by a decrease. A second pane, immediately above the first, was broken at 64 minutes and temperatures began to rise steadily; between 94 and 100 minutes the remaining panes shattered. This initiated a sharp increase in temperature that continued as the fire developed. The maximum recorded atmospheric temperature in the centre of the compartment was 1051°C after 102 minutes (see Figure 2.11). The maximum steel temperature of 903°C was recorded after 114 minutes in the bottom flange of the central secondary beam.

The maximum slab displacement was 269 mm and occurred in the centre of the compartment after 130 minutes. This recovered to 160 mm after the fire.

The unprotected edge beam on gridline 4 was observed during the test to be completely engulfed in fire. However, the maximum temperature of this beam was 680°C, which is relatively low compared to that of the internal beams, as shown by Figure 2.12. The corresponding maximum displacement of the edge beam was 52 mm, recorded after 114 minutes. This small displacement was attributed to the additional support provided by wind posts above the compartment, which acted in tension during the test.

The internal compartment walls were constructed directly under unprotected beams and performed well. Their integrity was maintained for the duration of the test. On removal of the wall, it could be seen that one of the beams had distortionally buckled over most of its length. This was caused by the high thermal gradient through the cross section of the beam (caused by the positioning of the compartment wall), together with high restraint to thermal expansion.

No local buckling occurred in any of the beams, and the connections showed none of the characteristic signs of high tensile forces that were seen on cooling in the other tests.

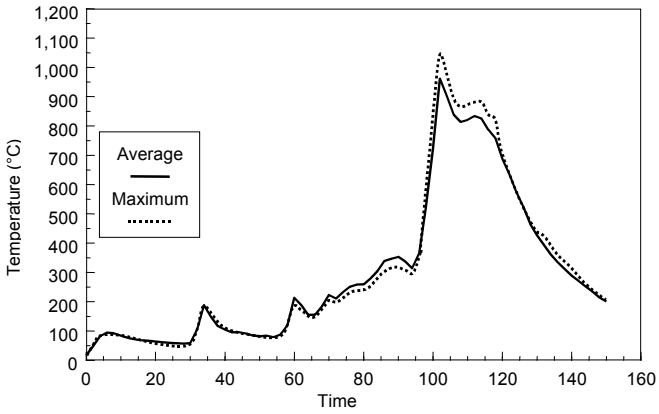

Figure 2.11 *Furnace gas temperatures recorded in Test 4*

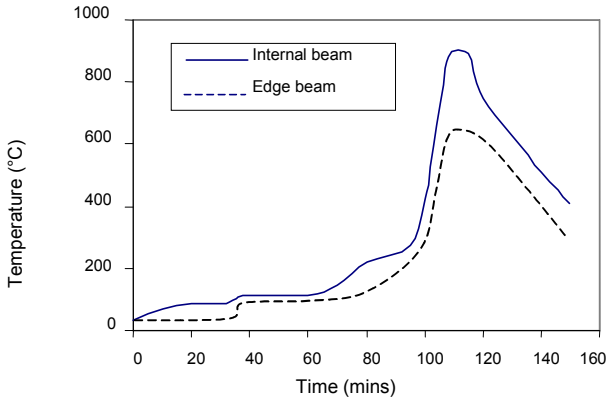

Figure 2.12 *Maximum flange temperature of internal beam and edge beam*

2.6 Test 5: Large compartment

This test was carried out between the second and third floor, with the fire compartment extending over the full width of the building, covering an area of 340 m^2.

The fire load of 40 kg/m^2 was provided by timber cribs arranged uniformly over the floor area. The compartment was constructed by erecting a fire resistant stud and plasterboard wall across the full width of the building and by constructing additional protection to the lift shaft. Double glazing was installed on two sides of the building, but the middle third of the glazing on both sides of the building was left open. All the steel beams, including the edge beams, were left unprotected. The internal and external columns were protected up to and including the connections.

The ventilation condition governed the severity of the fire. There was an initial rapid rise in temperature as the glazing was destroyed, creating large openings on both sides of the building. The large ventilation area in two opposite sides of the compartment gave rise to a fire of long duration but lower than expected temperatures. The maximum recorded atmosphere temperature was 746°C, with a

maximum steel temperature of 691°C, recorded at the centre of the compartment. The recorded atmospheric temperatures in the compartment are shown by Figure 2.13. The structure towards the end of the fire is shown in Figure 2.14.

The maximum slab displacement reached a value of 557 mm. This recovered to 481 mm when the structure cooled.

Extensive local buckling occurred in the proximity of the beam-to-beam connections. On cooling, a number of the end-plate connections fractured down one side. In one instance the web detached itself from the end-plate such that the steel-to-steel connection had no shear capacity. This caused large cracks within the composite floor above this connection, but no collapse occurred, with the beam shear being carried by the composite floor slab.

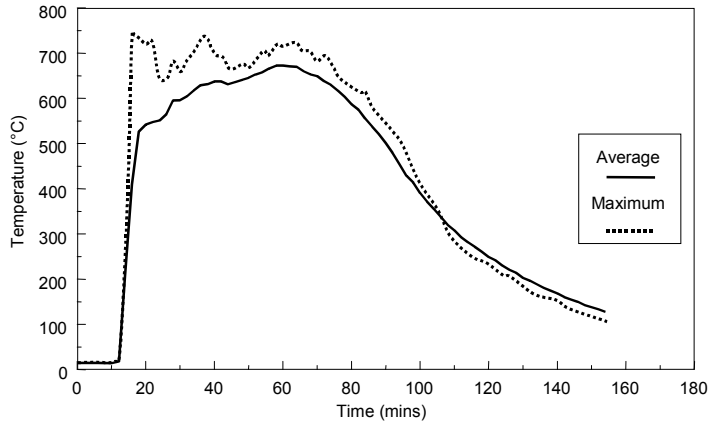

Figure 2.13 *Maximum and average recorded atmosphere temperature*

Figure 2.14 *Deformed structure during fire*

2.7 Test 6: The office demonstration test

The aim of this test was to demonstrate structural behaviour in a realistic fire scenario.

A compartment 18 m wide and up to 10 m deep with a floor area of 135 m^2, was constructed using concrete blockwork. The compartment represented an open plan office and contained a series of work-stations consisting of modern day furnishings, computers and filing systems (see Figure 2.15). The test conditions were set to create a very severe fire by incorporating additional wood/plastic cribs to create a total fire load of 46 kg/m^2 (less than 5% of offices would exceed this level) and by restricting the window area to the minimum allowed by regulations for office buildings. The fire load was made up of 69% wood, 20% plastic and 11% paper. The total area of windows was 25.6 m^2 (19% of the floor area) and the centre portion of each window, totalling 11.3 m^2, was left unglazed to create the most pessimistic ventilation conditions at the start of the test.

Figure 2.15 *Office before test*

Within the compartment, the columns and the beam-to-column connections were fire protected. Both the primary and secondary beams, including all the beam-to-beam connections, remained totally exposed.

The wind posts were left connected to the edge beams, and thus gave some support during the fire.

The maximum atmospheric temperature was 1213°C and the maximum average temperature was approximately 900°C, as shown by Figure 2.16. The maximum temperature of the unprotected steel was 1150°C. The maximum vertical displacement was 640 mm, which recovered to a permanent deformation of 540 mm on cooling (see Figure 2.17). The peak temperature of the lintel beams, above the windows, was 813ºC. All the combustible material in the compartment was completely burnt, including the contents of the filing cabinets. Towards the back of the compartment, the floor slab deflected and rested on the blockwork wall. The structure showed no signs of failure.

An external view of the fire near its peak is shown in Figure 2.18. The structure following the fire is shown in Figure 2.19 and Figure 2.20. Figure 2.19 shows a general view of the burned out compartment and Figure 2.20 shows the head of one of the columns. During the test, the floor slab cracked around one of the column heads, as shown in Figure 2.21. These cracks occurred during the cooling phase, possibly due to a partial failure of the steel beam to column connection in this location. Investigation of the slab after the test showed that the reinforcement had not been lapped correctly and that, in this area, adjacent sheets of mesh were simply butted together. This illustrates the importance of using full tension laps between adjacent sheets of mesh reinforcement.

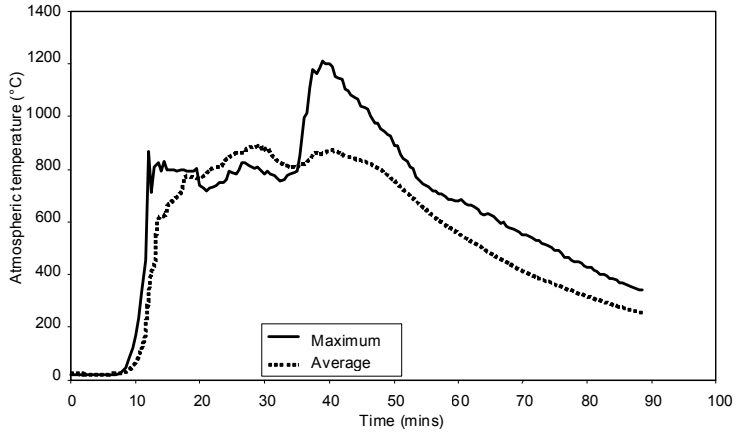

Figure 2.16 *Measured atmosphere temperature*

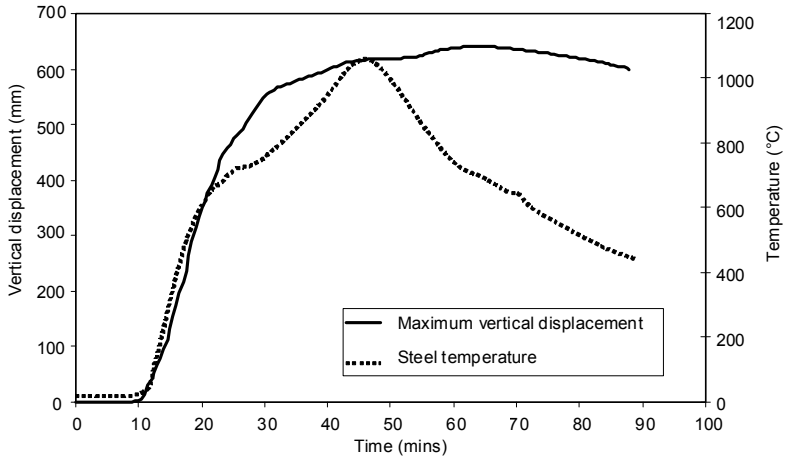

Figure 2.17 *Maximum steel temperature and vertical displacement*

Figure 2.18 *External view of fire*

Figure 2.19 *Measured atmosphere temperature in the compartment*

Figure 2.20 *Column head showing buckled beams*

Figure 2.21 *Cracked floor slab in region of non-overlapped mesh*

2.8 Test 7: Central compartment

The test was carried out in a centrally located compartment on the fourth floor of the building, which is 11 m wide and 7 m deep. The steel structure exposed to fire consists of two primary beams in 356x171x51 UB, two columns in 305x305x198 UC and 305x305x137 UC, and three secondary beams in 305x165x40 UB, respectively.

The fire load was provided by wood cribs of 40 kg/m^2 covering whole compartment floor area. The ventilation was provided by a 1.27m high and 9m long opening on the façade.

About 130 thermocouples were disposed in the compartment and at various locations along the beams in both the steel profile and the composite slabs, as well as in the steel connections (fin plate and end plate). An additional 14 thermocouples were also disposed in the protected columns. In order to measure the distribution of internal forces, 2 different types of strain gauges were used: high

temperature ones in the connection and ambient temperature ones in the protected column and un-exposed elements. As for the instrumentation of the deflected shape of the floor and of the main structural members, a total of 37 displacement transducers were used to measure the deformation of the concrete slab and the horizontal movement of the columns. In addition, 10 video cameras and two thermo imaging cameras recorded the fire and smoke development, the structural deformations and the temperature distribution with time.

Komentář [MR1]: Bin, tu peux voir si c'est nécessaire de citer les descriptifs du banc d'essai

The recorded temperatures in different places of the compartment are compared with the parametric curve presented in prEN 1991-2, Annex B [37] (see figure 2.22). The maximum recorded compartment temperature was 1107.8 °C after 54 minutes of fire.

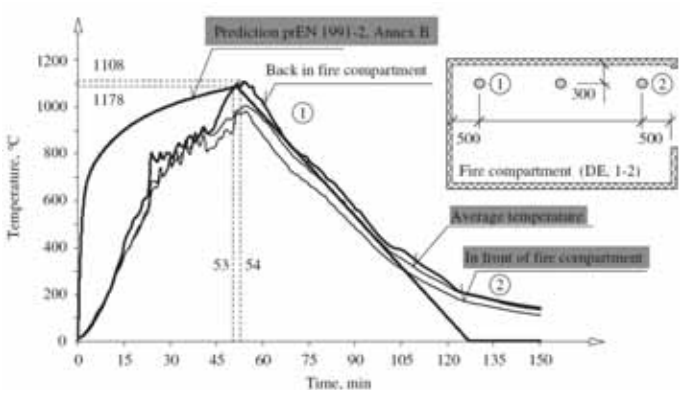

Figure 2.22 *Compartment following fire*

As far as the heating of steel beams is concerned, the unprotected steel beams were heated up to around 1087.5 °C which occurred after 57 min of fire on the bottom flange of the steel beam D2-E2 in the middle of the section (see figure 2.23). The maximum temperature recorded at the joints was around 200 °C.

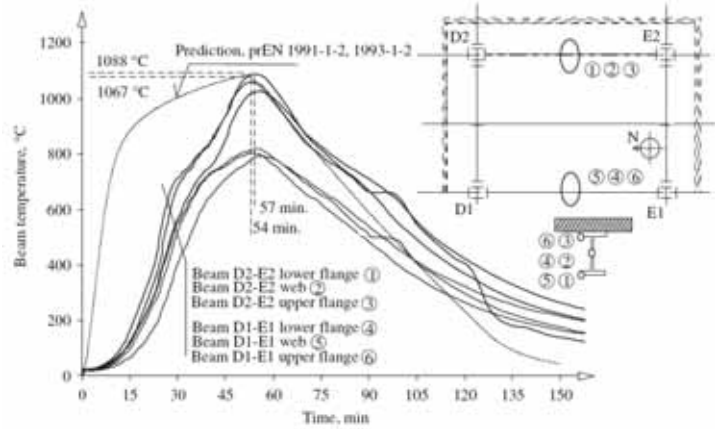

Figure 2.23 *Temperatures variations in steel beams*

A summary of the temperatures recorded in the composite slab is shown in 2.24 for temperatures in the reinforcement over the rib. It can be found that the maximum

heating measured at the unexposed side of the composite slab was less than 100 °C which was in accordance with the insulation criteria.

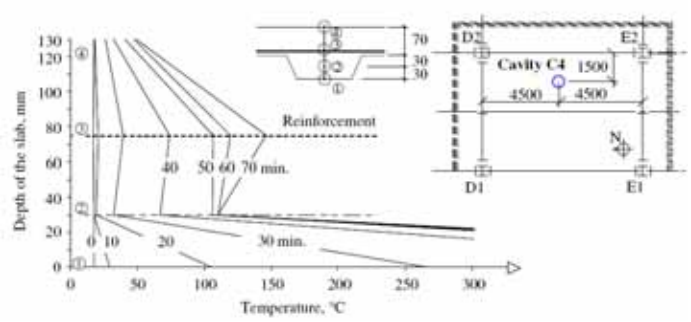

Figure 2.24 *Composite floor temperature variation*

As far as the global deflection of the floor is concerned, the maximum deflections were about 1200 mm. Despite the occurrence of such an important deflection, the predicted collapse of the floor was not reached, as shown in Figure 2.25. During cooling phase, the deflection recovery of the floor was about 925 mm.

Figure 2.25 *View of the floor after the test*

Buckling occurred in the lower beam flange and web adjacent to the joints during the heating phase after about 23 min of fire (see figure 2.26). This local buckling is caused by restraint to thermal expansion provided by the surrounding structure. In addition, the formation of a flexural plastic hinge was occurred in the beam's cross section adjacent to the protected zone due to the restraint to thermal elongation provided by the adjacent protected section.

Figure 2.26 *Various deformed steel beams*

Figure 2.27 shows the open cracks in the concrete slab around one of the column heads. This crack developed along a line of mesh reinforcement overlap without adequate attachment.

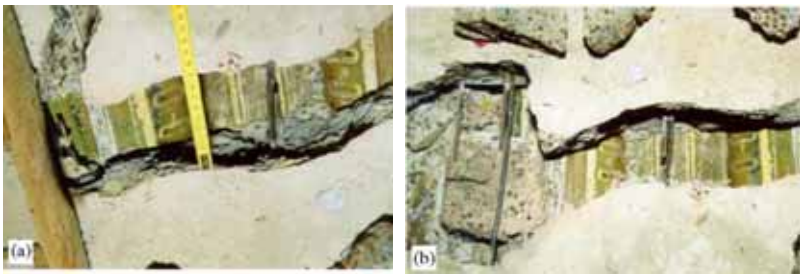

Figure 2.27 *Cracked floor slab around one of the column heads*

2.9 General comments on observed behaviour

In all tests, the structure performed very well and overall structural stability was maintained.

The performance of the whole building in fire is manifestly very different from the behaviour of single unrestrained members in the standard fire test. It is clear that there are interactions and changes in load-carrying mechanisms in real structures that dominate the way they behave; it is entirely beyond the scope of the simple standard fire test to reproduce or assess such effects.

The Cardington tests demonstrated that modern steel frames acting compositely with steel deck floor slabs have a coherence that provides a resistance to fire far greater than that normally assumed. This confirms evidence from other sources.

3 CAR PARK FIRE TESTS, FRANCE

Between 1998 and 2001, as part of an ECSC funded project, fire tests were performed on an open car park with a composite steel and concrete structure.

A single storey composite steel-framed open car park was constructed specifically for full scale fire tests. The floor of the car park occupied an area of 32 × 16 m², which is equivalent to a 48 space car park and the storey height was 3 m (see Figure 3.1).

The structure was composed of:

- unprotected steel columns: HEA180 (edge columns) and HEB200 (central columns),
- composite beams: unprotected steel beams (IPE 550, IPE 400 and IPE 500) connected to the composite slab,
- composite slab with a total thickness of 120 mm (steel deck: COFRASTRA40).

The structural design of the open car park was based on a fire safety engineering method developed specifically for open car parks during an earlier European research project. For this method, a fire scenario was defined based on statistics of real car park fires. The structural resistance of the open car park was checked with an advanced model using 2D frame analysis that neglected the influence of membrane effects in the composite slab (see Figure 3.2).

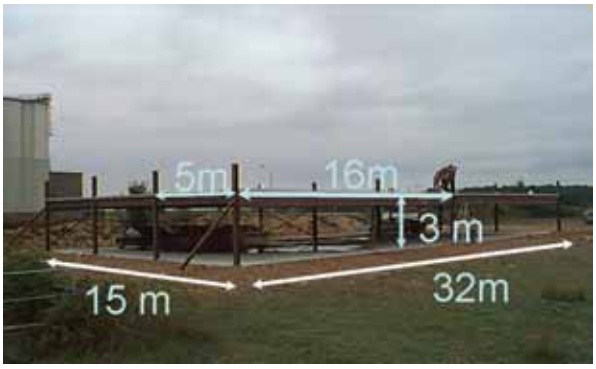

Figure 3.1 *Open car parks prior to fire tests*

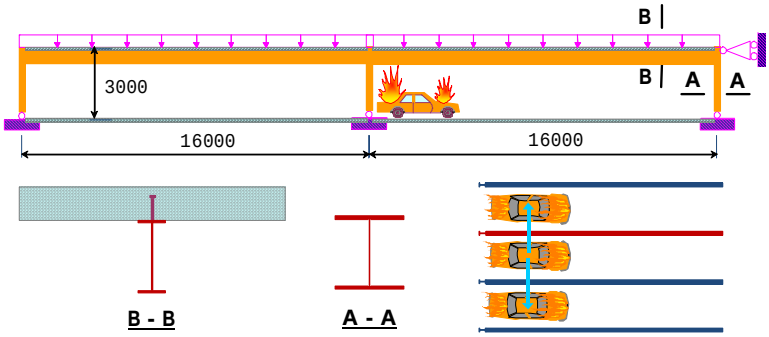

Figure 3.2 *2D modelling of tested open car park with planar composite frame*

Three tests were performed on the open car park. The first two tests involved three cars; the third test was performed to assess the spread of fire between two cars placed facing each other. During each test the cars were allowed to burn themselves out.

The most severe fire was obtained in the second test, during which, under the affect of a strong wind, three cars burned together 10 minutes after the ignition of the first car (see Figure 3.3), which led to an significant area of the floor being exposed to the flames which reached a temperature of more than 800 °C (see Figure 3.4). The steel beams above the burned cars were heated up to at least 700 °C (see Figure 3.5).

Figure 3.3 *Full fire development during one fire test*

Although the heating of steel beams would result in a significant reduction of steel strength, no collapse of the unprotected steel structure occurred during these fire tests. Moreover, with respect to the structural behaviour, the measured maximum deflection of the composite floor was relatively low and did not exceed 150 mm.

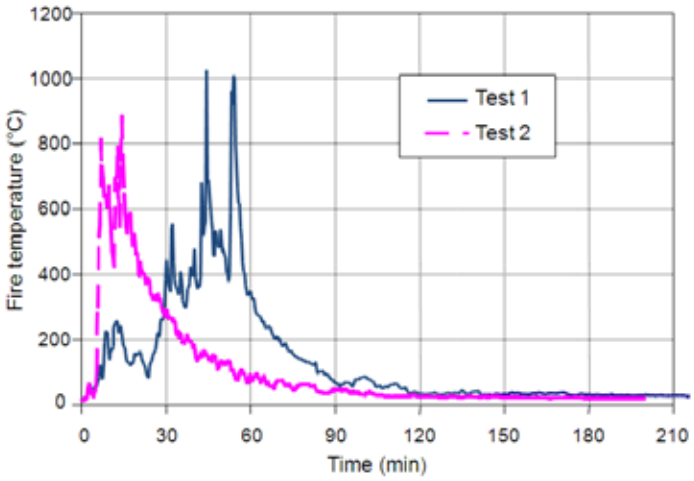

Figure 3.4 *Measured temperature of hot gases (fire) above burned cars*

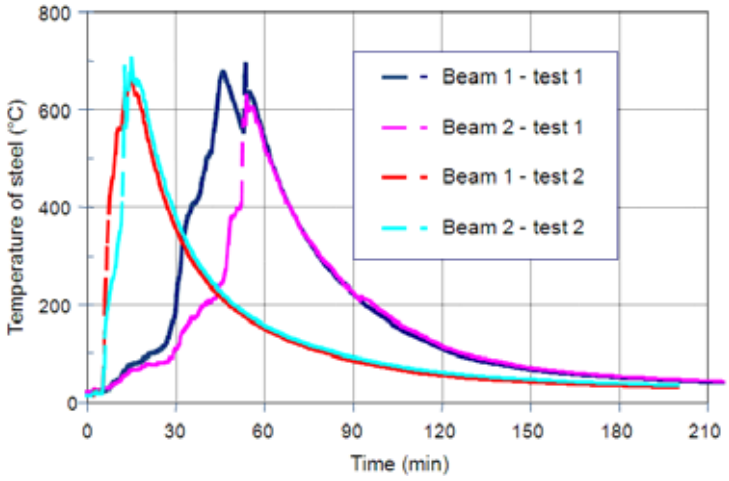

Figure 3.5 *Measured temperature of steel beams above burned cars*

It was observed that the deflections predicted by a two-dimensional simulation were higher than the measured deflections recorded during the test. Therefore, a three-dimensional model was created to predict the structural behaviour of the car park (see Figure 3.6), using the modelling techniques that had been developed during the second phase of Cardington research project.

Figure 3.7 shows a comparison between measured deflections recorded in the test and those predicted by the two and three dimensional models, from which it can be seen that the predictions of the 3D modelling results in a closer correlation with the test results. It is clear that the membrane effect of the composite slab has already started to play a positive role even under relatively low deflection.

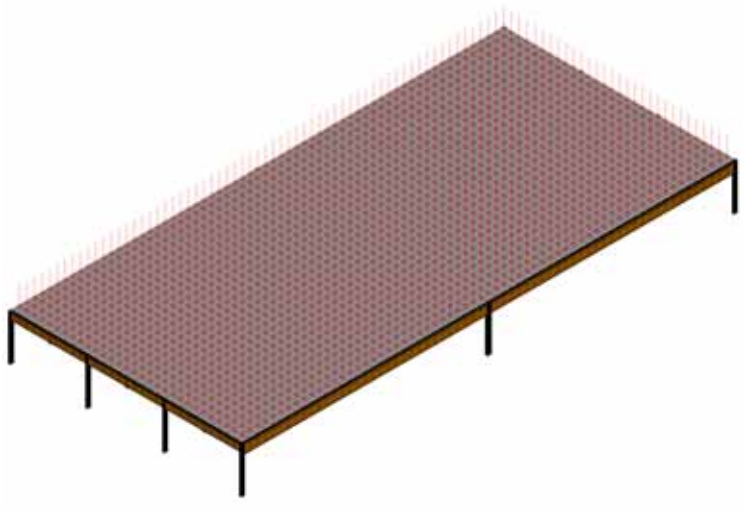

Figure 3.6 *3D modelling of an open car park*

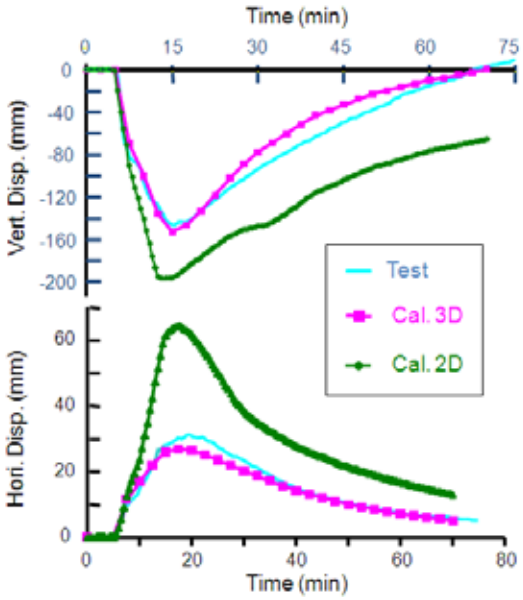

Figure 3.7 *Comparison of vertical displacement between calculation and test*

Nevertheless, according to the fire scenario adopted in fire safety engineering, the steel members of an open car park could be heated up to around 950°C. It is evident that under such heating, the deflection of the floor will be amplified and its structural resistance will rely strongly on the membrane effect (see Figure 3.8).

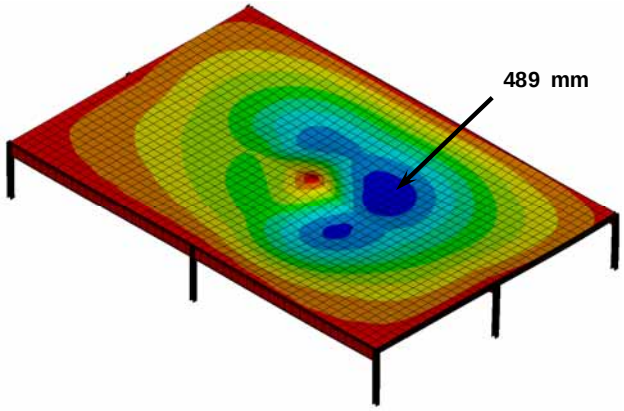

Figure 3.8 *Example of the deflection of an open car park under fire scenario according to French regulation*

In consequence, the methodology based on 3D modelling of the composite floor of open car parks developed during this project was then used in various fire safety engineering projects in France to check the stability of unprotected composite steel-framed open car parks. It can be easily understood that the basis of this methodology is of course the membrane effect of the composite steel and concrete floor. In addition, in order to facilitate the application of this methodology, several design tables[38] were provided in which the standard sizes of steel members, the concrete slab as well as the necessary reinforcing steel mesh are recommended according to both applied load and structural frame system. One example of these design tables is given in Table 3.1.

~~Table 3.2~~Table 3.1 *Design table of open car parks related to fire resistance*

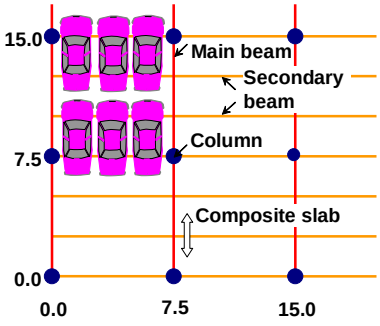

Slab span: 2.5 m
Secondary beam span: 7.5 m
Main beam span: 7.5 m
Spacing of columns: 7.5 m

Applied load (except selfweight) :
- Standard level:
  - deal load : 0.20 kN/m²
  - imposed load : 2.50 kN/m²
- Last level:
  - dead load : 1.45 kN/m²
  - imposed load: 2.50 kN/m²
- Selfweight of facade: 7.5 kN/m

Orientation of parking place:
- Perpendicular to secondary beam

Net height beneath steel beam: 2.1 m		
Minimum size of secondary beam cross section	Standard level	IPE240
	Last level	IPE270
Minimum size of main beam cross section	Standard level	IPE400
	Last level	IPE450
Design of column cross section	Available of section type	HEA, HEB et HEM
	Maximum load level (**)	0.35
Requirement to be applied to concrete slab	Total depth of slab	≥ 120 mm &≤ 140 mm
	Maximum height of steel deck	62 mm
	Minimum compactness of rib of steel deck (*)	0.393
	Minimum thickness of steel sheet	0.75 mm
	Minimum mesh of reinforcing steel	ϕ7 150 mmx150 mm
	location of reinforcing steel mesh	30 mm from top of slab

(*) compactness of rib of steel deck

$$\frac{(\ell_1 + \ell_2)}{2(\ell_1 + \ell_3)}$$

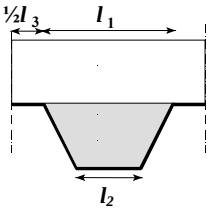

(**) Load level: ratio of applied load under fire situation over ultimate load at room temperature design

4 EVIDENCE FROM ACCIDENTAL FIRES AND OTHER COUNTRIES

Two building fires in England during the early 1990's (Broadgate and Churchill Plaza) provided the opportunity to observe how modern steel-framed buildings performed in fire. The experience from these fires was influential in stimulating thought about how buildings might be designed to resist fire and in bringing about the Cardington experiments.

Evidence of building behaviour is also available from large-scale fire tests in Australia and Germany. In both Australia and New Zealand, design approaches that allow the use of unprotected steel in multi-storey, steel-framed buildings have been developed.

4.1 Broadgate

In 1990, a fire occurred in a partly completed 14-storey office block on the Broadgate development in London[6]. The fire began inside a large site hut on the first level of the building. Fire temperatures were estimated to have reached over 1000°C.

The floor was constructed using composite long-span lattice trusses and composite beams supporting a composite floor slab. The floor slab was designed to have 90 minutes fire resistance. At the time of the fire, the building was under construction and the passive fire protection to the steelwork was incomplete. The sprinkler system and other active measures were not yet operational.

After the fire, a metallurgical investigation concluded that the temperature of the unprotected steelwork was unlikely to have exceeded 600°C. A similar investigation on the bolts used in the steel-to-steel connections concluded that the maximum temperature reached in the bolts, either during manufacture or as a consequence of the fire, was 540°C.

The distorted steel beams had permanent deflections of between 270 mm and 82 mm. Beams with permanent displacements at the higher end of that range showed evidence of local buckling of the bottom flange and web near their supports. From this evidence, it was concluded that the behaviour of the beams was influenced strongly by restraint to thermal expansion. This restraint was provided by the surrounding structure, which was at a substantially lower temperature than the fire-affected steel. Axial forces were induced into the heated beams resulting in an increase in vertical displacement due to the *P-delta* effect. The buckling of the lower flange and web of the beam near its supports was due to a combination of the induced axial force and the negative moment caused by the fixity of the connection.

Although the investigation showed the visually unfavourable effects of restraint on steel beams, the possible beneficial effects were not evident because only relatively low steel temperatures were reached during the fire. The beneficial effects that could have developed were catenary action of the beams and bridging or membrane action of the composite slab.

The fabricated steel trusses spanned 13.5 m and had a maximum permanent vertical displacement of 552 mm; some truss elements showed signs of buckling. It

was concluded that the restraint to thermal expansion provided by other elements of the truss, combined with non-uniform heating, caused additional compressive axial forces, which resulted in buckling.

At the time of the fire, not all the steel columns were fire protected. In cases where they were unprotected, the column had deformed and shortened by approximately 100 mm (see Figure 4.1). These columns were adjacent to much heavier columns that showed no signs of permanent deformation. It was thought that this shortening was a result of restrained thermal expansion. The restraint to thermal expansion was provided by a rigid transfer beam at an upper level of the building, together with the columns outside the fire affected area.

Figure 4.1 *Buckled column and deformed beams at Broadgate*

Although some of the columns deformed, the structure showed no signs of collapse. It was thought that the less-affected parts of the structure were able to carry the additional loads that were redistributed away from the weakened areas.

Following the fire, the composite floor suffered gross deformations with a maximum permanent vertical displacement of 600 mm (see Figure 4.2). Some failure of the reinforcement was observed. In some areas, the steel profiled decking had debonded from the concrete. This was considered to be caused mainly by steam release from the concrete, together with the effects of thermal restraint and differential expansion.

A mixture of cleat and end-plate connections was used. Following the fire, none of the connections was observed to have failed, although deformation was evident. In cleated connections, there was some deformation of bolt holes. In one end-plate connection, two of the bolts had fractured; in another, the plate had fractured down one side of the beam but the connection was still able to transfer shear. The main cause of deformation was thought to be due to the tensile forces induced during cooling.

Following the fire, structural elements covering an area of approximately 40 m x 20 m were replaced, but it is important to note that no structural failure had occurred and the integrity of the floor slab was maintained during the fire. The direct fire loss was in excess of £25M, of which less than £2M was attributed to the repair of the structural frame and floor damage; the other costs resulted from smoke damage. Structural repairs were completed in 30 days.

Figure 4.2 *View of deformed floor above the fire (the maximum deflection was about 600 mm)*

4.2 Churchill Plaza building, Basingstoke

In 1991, a fire took place in the Mercantile Credit Insurance Building, Churchill Plaza, Basingstoke. The 12-storey building was constructed in 1988. The columns had board fire protection and the composite floor beams had spray-applied protection. The underside of the composite floor was not fire protected. The structure was designed to have 90 minutes fire resistance.

The fire started on the eighth floor and spread rapidly to the ninth and then the tenth floor as the glazing failed. During the fire, the fire protection performed well and there was no permanent deformation of the steel frame. The fire was believed to be comparatively 'cool' because the failed glazing allowed a cross wind to increase the ventilation. The protected connections showed no deformation.

In places, the dovetail steel decking showed some signs of debonding from the concrete floor slab. (as had also been observed in the Broadgate fire). A load test was conducted on the most badly affected area, with a load of 1.5 times the total design load being applied. The test showed that the slab had adequate load-carrying capacity and could be reused without repair.

The protected steelwork suffered no damage. The total cost of repair was in excess of £15M, most of which was due to smoke contamination, as in the Broadgate fire. Sprinklers were installed in the refurbished building.

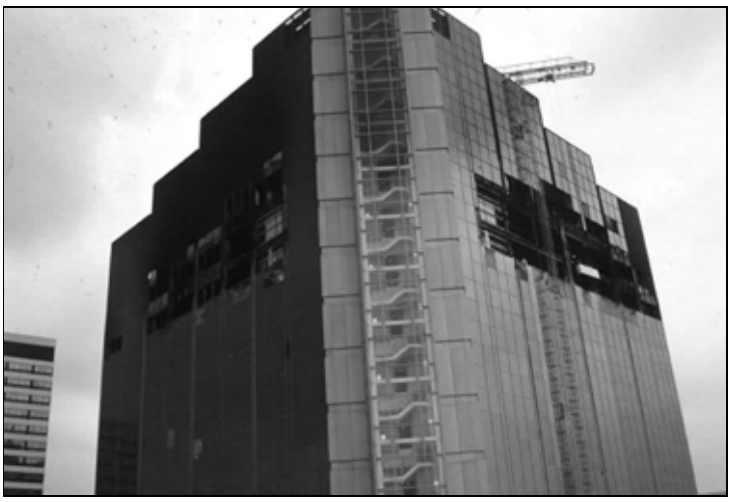

Figure 4.3 *Churchill Plaza, Basingstoke following the fire*

4.3 Australian fire tests

BHP, Australia's biggest steel maker, has been researching and reporting[7,8] fire-engineered solutions for steel-framed buildings for many years. A number of large-scale natural fire tests have been carried out in specially constructed facilities at Melbourne Laboratory, representing sports stadia, car parks and offices. The office test programme focussed on refurbishment projects that were to be carried out on major buildings in the commercial centre of Melbourne.

William Street fire tests and design approach

A 41-storey building in William Street in the centre of Melbourne was the tallest building in Australia when it was built in 1971. The building was square on plan, with a central square inner core. A light hazard sprinkler system was provided. The steelwork around the inner core and the perimeter steel columns were protected by concrete encasement. The beams and the soffit of the composite steel deck floors were protected with asbestos-based material. During a refurbishment programme in 1990, a decision was made to remove the hazardous asbestos.

The floor structure was designed to serviceability rather than strength requirements. This meant that there was a reserve of strength that would be very beneficial to the survival of the frame in fire, as higher temperatures could be sustained before the frame reached its limiting condition.

At the time of the refurbishment, the required fire resistance was 120 minutes. Normally this would have entailed the application of fire protection to the steel beams and to the soffit of the very lightly reinforced slab (Australian regulations have been revised and now allow the soffit of the slab to be left unprotected for 120 minutes fire resistance). In addition, the existing light hazard sprinkler system required upgrading to meet the prevailing regulations.

During 1990, the fire resistance of buildings was subject to national debate; the opportunity was therefore taken to conduct a risk assessment to assess whether fire protecting the steelwork and upgrading the sprinkler system was necessary for this building. Two assessments were made. The first was made on the basis that the building conformed to current regulations with no additional safety measures; the

second was made assuming no protection to the beams and soffit of the slab, together with the retention of the existing sprinkler system. The effect of detection systems and building management systems were also included in the second assessment. The authorities agreed that if the results from the second risk assessment were at least as favourable as those from the first assessment, the use of the existing sprinkler system and unprotected steel beams and composite slabs would be considered acceptable.

A series of four fire tests was carried out to obtain data for the second risk assessment. The tests were to study matters such as the probable nature of the fire, the performance of the existing sprinkler system, the behaviour of the unprotected composite slab and castellated beams subjected to real fires, and the probable generation of smoke and toxic products.

The tests were conducted on a purpose-built test building at the Melbourne Laboratories of BHP Research (see Figure 4.4). This simulated a typical storey height 12 m × 12 m corner bay of the building. The test building was furnished to resemble an office environment with a small, 4 m × 4 m, office constructed adjacent to the perimeter of the building. This office was enclosed by plasterboard, windows, a door, and the facade of the test building. Imposed loading was applied by water tanks.

Figure 4.4 *BHP test building and fire test*

Four fire tests were conducted. The first two were concerned with testing the performance of the light hazard sprinkler system. In Test 1, a fire was started in the small office and the sprinklers were activated automatically. This office had a fire load of 52 kg/m^2. The atmosphere temperatures reached 60°C before the sprinklers

controlled and extinguished the fire. In Test 2, a fire was started in the open-plan area midway between four sprinklers. This area had a fire load of 53.5 kg/m^2. The atmosphere temperature reached 118°C before the sprinklers controlled and extinguished the fire. These two tests showed that the existing light hazard sprinkler system was adequate.

The structural and thermal performance of the composite slab was assessed in Test 3. The supporting beams were partially protected. The fire was started in the open plan area and allowed to develop with the sprinklers switched off. The maximum atmosphere temperature reached 1254°C. The fire was extinguished once it was considered that the atmosphere temperatures had peaked. The slab supported the imposed load. The maximum temperature recorded on the top surface of the floor slab was 72°C. The underside of the slab had been partially protected by the ceiling system, which remained substantially in place during the fire.

In Test 4, the steel beams were left unprotected and the fire was started in the small office. The fire did not spread to the open-plan area despite manual breaking of windows to increase the ventilation. Therefore fires were ignited from an external source in the open-plan area. The maximum recorded atmosphere temperature was 1228°C, with a maximum steel beam temperature of 632°C above the suspended ceiling. The fire was extinguished when it was considered that the atmosphere temperatures had peaked. Again, the steel beams and floor were partially shielded by the ceiling. The central displacement of the castellated beam was 120 mm and most of this deflection was recovered when the structure cooled to ambient temperature.

Three unloaded columns were placed in the fire compartment to test the effect of simple radiation shields. One column was shielded with galvanized steel sheet, one with aluminised steel sheet and one was an unprotected reference column. The maximum recorded column temperatures were 580ºC, 427ºC and 1064ºC respectively, suggesting that simple radiation shields might provide sufficient protection to steel members in low fire load conditions.

It was concluded from the four fire tests that the existing light hazard sprinkler system was adequate and that no fire protection was required to the steel beams or soffit of the composite slab. Any fire in the William Street building should not deform the slab or steel beams excessively, provided that the steel temperatures do not exceed those recorded in the tests.

The temperature rise in the steel beams was affected by the suspended ceiling system, which remained largely intact during the tests.

The major city centre office building that was the subject of the technical investigation was owned by Australia's largest insurance company, which had initiated and funded the test programme. It was approved by the local authority without passive fire protection to the beams but with a light hazard sprinkler system of improved reliability and the suspended ceiling system that had proved to be successful during the test programme.

4.3.2 Collins Street fire tests

This test rig was constructed to simulate a section of a proposed steel-framed multi-storey building in Collins Street, Melbourne. The purpose of the test was to record temperature data in fire resulting from combustion of furniture in a typical office compartment.

The compartment was 8.4 m × 3.6 m and filled with typical office furniture, which gave a fire load between 44 and 49 kg/m^2. A non-fire-rated suspended ceiling system was installed, with tiles consisting of plaster with a fibreglass backing blanket. An unloaded concrete slab formed the top of the compartment. During the test, temperatures were recorded in the steel beams between the concrete slab and the suspended ceiling. The temperatures of three internal free-standing columns were also recorded. Two of these columns were protected with aluminium foil and steel sheeting, acting simply as a radiation shield; the third remained unprotected. Three unloaded external columns were also constructed and placed 300 mm from the windows around the perimeter of the compartment.

The non-fire-rated ceiling system provided an effective fire barrier, causing the temperature of the steel beams to remain low. During the test the majority of the suspended ceiling remained in place. Atmosphere temperatures below the ceiling ranged from 831°C to 1163°C, with the lower value occurring near the broken windows. Above the ceiling, the air temperatures ranged from 344°C to 724°C, with higher temperatures occurring where the ceiling was breached. The maximum steel beam temperature was 470°C.

The unloaded indicative internal columns reached a peak temperature of 740°C for the unprotected case and below 403°C for the shielded cases. The bare external columns recorded a peak temperature of 490°C.

This fire test showed that the temperatures of the beams and external columns were sufficiently low to justify the use of unprotected steel and, as in the William Street tests, the protection afforded by a non-fire-rated suspended ceiling was beneficial.

Conclusions from Australian research

The Australian tests and associated risk assessments concluded that, provided that high-rise office buildings incorporate a sprinkler system with a sufficient level of reliability, the use of unprotected beams would offer a higher level of life safety than similar buildings that satisfied the requirements of the Building Code of Australia by passive protection. Up to the beginning of 1999, six such buildings between 12 and 41 storeys were approved in Australia.

4.4 German fire test

In 1985, a fire test was conducted on a four storey steel-framed demonstration building constructed at the Stuttgart-Vaihingen University in Germany[9]. Following the fire test, the building was used as an office and laboratory.

The building was constructed using many different forms of steel and concrete composite elements. These included water filled columns, partially encased columns, concrete filled columns, composite beams and various types of composite floor.

The main fire test was conducted on the third floor, in a compartment covering approximately one-third of the building. Wooden cribs provided the fire load and oil drums filled with water provided the gravity load. During the test, the atmosphere temperature exceeded 1000°C, with the floor beams reaching temperatures up to 650°C. Following the test, investigation of the beams showed that the concrete in-filled webs had spalled in some areas exposing the reinforcement. However, the beams behaved extremely well during the test with no significant permanent deformations following the fire. The external columns and those around the central core showed no signs of permanent deformation. The

composite floor reached a maximum displacement of 60 mm during the fire and retained its overall integrity.

Following the fire, the building was refurbished. The refurbishment work involved the complete replacement of the fire damaged external wall panels, the damaged portions of steel decking to the concrete floor slab, and the concrete infill to the beams. Overall, it was shown that refurbishment to the structure was economically possible.

4.5 Experimental work at room temperature

The simple design method presented in Section 5 has been based on theoretical models developed for room temperature design and verified with experimental investigations. Since 1961, a number of such experimental investigations have been conducted to investigate membrane action in concrete slabs (15,18,22,23,24) with no in-plane horizontal restraint. In all the tests, the specimen failed due to large cracks through the full depth of the slab across the shorter span and membrane action was clearly observed, as shown by Table 4.1

Table 4.1 *Comparison between the simple design method and previous room temperature tests*[26]

Reference	Test No.	Slab Size (m)	Yield-line load (kN/m^2)	Test load (kN/m^2)	Enhancement observed from test	Calculated enhancement
Hayes & Taylor[22]	R11	0.914x0.914	15.43	31.97*	2.07	2.07
	R12	0.914x0.914	55.64	89.0*	1.60	2.11
	R13	0.914x0.914	29.05	60.8*	2.09	2.09
	R21	1.372x0.914	20.24	36.48*	1.80	1.80
	R31	1.828x0.914	16.37	25.08*	1.53	1.49
Taylor, Maher & Hayes [23]	S1	1.829x1.829	23.83	42.90*	1.80	1.48
	S7	1.829x1.829	23.83	39.03*	1.64	1.68
	S9	1.829x1.829	23.83	38.13*	1.60	1.31
Sawczuk & Winnicki [18]	Type 1 (α = 2.0)	2.0x1.0	20.6	38.26*	1.86	1.71
	Type 2 (α = 2.0)	2.0x1.0	10.99	17.18*	1.56	1.46
	Type 1 (α = 1.45)	1.6x1.1	21.04	45.13*	2.14	2.15
Wood[15]		0.610 x0.610	10.45 (kN)	17.14* (kN)	1.64	1.36
BRE[20]		9.5 x 6.46	2.58	4.81	1.86	1.68

* denotes that slab failure did not occur.

A series of 22 tests were recently conducted on horizontally unrestrained small-scale concrete slabs, with an aspect ratio of 1.0 or 1.55, by Bailey and Toh[27]. Two different modes of failure were generally witnessed in these ambient tests dependent to the reinforcement ratio, aspect ratio and the reinforcement ductility. Fracture of the reinforcement across the shorter span (Figure 4.5(a)) was the dominant failure mode in most of the lightly reinforced slabs whilst the heavily reinforced slabs and the ones with highly ductile reinforcement mostly failed due to the compressive failure at the corners of the slab (Figure 4.5(b)). These experimental data provided the necessary information to extend the method to orthotropic reinforcement and to include compressive failure in the concrete as an additional failure mode to be considered.

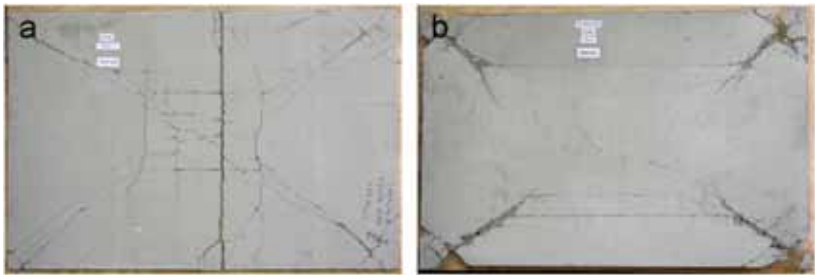

Figure 4.5 *Two typical modes of failure for test slabs at ambient temperature*

4.6 Experimental work at elevated temperature

In addition to the seven full-scale tests carried out on the full scale eight-storey steel framed building with composite floors at Cardington in 1996 and 2003[28,29] further small scale tests have also been conducted at elevated temperature by Bailey and Toh[27] in order to further investigate tensile membrane action in composite slabs. As a result of these tests the design method originally developed by Bailey and Moore has been modified, resulting in the formulation presented in Section 5.

Bailey and Toh[27] carried out a series of 15 small scale tests on horizontally unrestrained concrete slabs, with aspect ratios of 1.0 or 1.55. They concluded that unlike the slabs tested in ambient conditions, where the failure mode was influenced by compressive failure of the concrete, in all 15 slabs tested in fire conditions, the fracture of the reinforcement across the shorter span governed the failure, as shown in Figure 4.6.

Figure 4.6 *Mode of failure for test slabs at elevated temperatures*

5 SIMPLE DESIGN METHOD

Since Johansen's pioneering work on yield line analysis[10] researchers have observed the beneficial effects of membrane forces in improving the load bearing capacity of concrete slabs, compared to estimates of capacity based only on flexural behaviour[11].

A number of experimental and theoretical investigations have been carried out to investigate the beneficial effects of in-plane forces at room temperature, leading to a good theoretical understanding of the behaviour. Following the experimental work carried out at Cardington, this theory has been extended to fire design scenarios, as discussed below.

The experimental work at Cardington and evidence from other real fires in building structures had served to illustrate that there are significant reserves of strength in composite steel concrete buildings, which means that the performance of the structure in fire exceeds the expectations created by standard fire tests on individual structural elements. Cardington demonstrated that it was possible to leave the composite steel beams that supported the concrete floor slab unprotected; work commenced to investigate suitable design models to allow structural engineers to justify the fire design of a floor slab supported by unprotected steel beams.

Researchers at the Building Research Establishment (BRE), with funding from the Steel Construction Institute, developed a simple design method for composite steel concrete floor slabs following the experimental work at Cardington[12,13]. The BRE model has been validated against the Cardington large scale fire test results and previous experimental work conducted at room temperature. This method is presented and discussed in detail in Section 5.2.

The simple design method differs from the simple design procedures provided in design codes[32,33], as it considers the behaviour of an assembly of structural members acting together, rather than individual elements. While it would also be technically possible to use non-linear finite elements to determine the load bearing capacity in fire, that is a more expensive solution requiring a significant amount of expertise and prior knowledge. The method presented in this document is more accessible to structural engineers with only a basic appreciation of fire engineering.

5.1 Introduction to yield line theory and membrane action

The yield line theory pioneered by Johansson is an ultimate load theory based on assumed collapse mechanisms and plastic properties of under-reinforced concrete slabs. The collapse mechanism is defined by a pattern of yield lines along which the reinforcement yields and the slab undergoes plastic deformations. The areas bounded by the yield lines are assumed to remain rigid with all rotation taking place at the yield line.

For yield line theory to be valid, shear failures, bond failures and compression failures must be prevented. The moment-curvature response of the slab must be sufficiently ductile to allow a mechanism to form; in practice this is not a problem as slabs are always under-reinforced, leading to ductile yielding of the

reinforcement before more brittle modes of failure such as compressive failure in the concrete.

For square and rectangular slabs that are simply supported along their free edges, the patterns of yield lines shown in Figure 5.1 are expected to occur. These are the yield line patterns which are assumed in the following theoretical development. In reality, for a steel framed building, the slab is supported on steel beams which will have a finite stiffness between column positions. This will be discussed in Section 6.

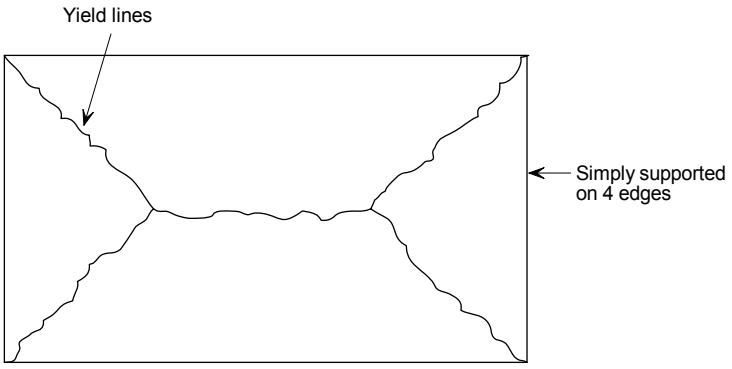

Figure 5.1 *A typical yield line pattern for a rectangular slab simply supported on four sides*

An upper bound solution may be obtained for an assumed yield line pattern. The solution is based on energy theory, with the external work done by the applied load due to a unit displacement of the rigid regions being equated to the internal work done by the rotation of the yield lines. The load which corresponds to any assumed failure mechanism will be greater than or equal to the true collapse load of the structure, thus giving an upper bound solution.

However, due to membrane action in the slab and strain hardening of the reinforcement after yielding, this theoretical upper bound solution from the yield line analysis tends to be significantly lower than the actual failure load of the slab observed during experiments.

Membrane action in slabs creates in-plane forces that are governed by the in-plane boundary conditions of the slab. Two extreme cases, of full restraint and no restraint, are considered below.

Slab with full in-plane restraint

With full in-plane restraint to the slab boundaries, the initial small bending deflections of a slab result in compressive membrane action[14,15]. This mechanism is illustrated in Figure 5.2, for a one way spanning element. A compressive action along a path from the bottom surface at the boundary to the top surface at mid-span develops, inducing a compressive arching action in the slab, which results in an enhanced resistance as shown in Figure 5.3. However, this arching action becomes unstable once the magnitude of the vertical deflection exceeds a value equal to approximately half the slab thickness, resulting in the rapid decrease of resistance. The slab can then go on to develop tensile membrane action at larger displacements.

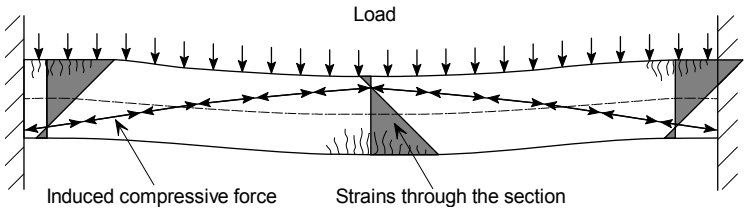

Figure 5.2 *Compressive membrane action in a restrained slab*

Park[14] illustrated the effect of compressive membrane action on a restrained slab using a figure similar to Figure 5.3. The initial peak load shown in this figure at displacements less than the slab thickness is due to compressive membrane action. When compression failure occurs in the concrete a sudden drop in capacity is observed, accompanied by an increase in displacement. The load capacity then increases with increasing deflection until fracture of the reinforcement occurs.

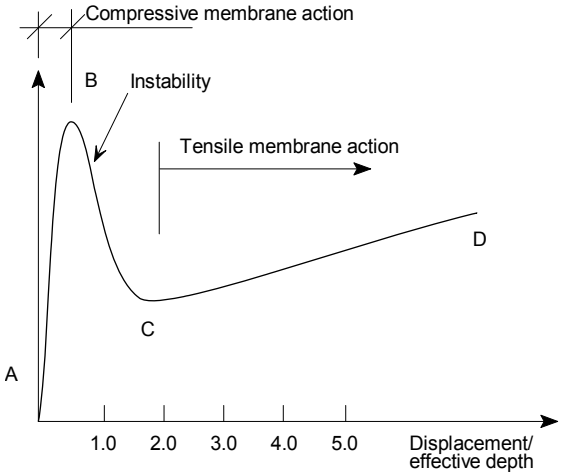

Figure 5.3 *Membrane action in a slab with restrained in-plane boundaries[15]*

Slab with no in-plane restraint

Where the boundary of the slab is unrestrained, the slab behaviour is different. Compressive membrane action cannot occur and the post-yielding behaviour is characterised by tensile membrane action. For a one-way spanning element, large vertical displacements will cause end shortening of the member. If this end shortening is prevented then tensile forces will develop. For a one-way spanning member, these restraint forces would have to be developed externally at the supports. However, for a two way spanning slab, i.e. a slab with simple supports on four edges, external horizontal restraints are not required as the slab can develop an internal system of in-plane forces which has the same effect.

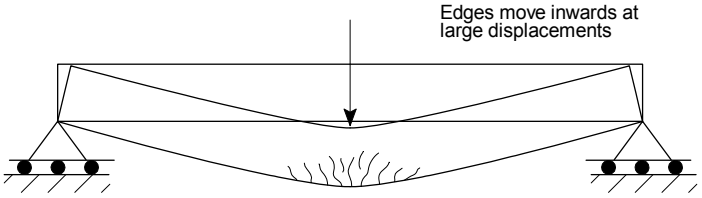

Figure 5.4 *One way spanning structural members*

Considering the case of a two-way spanning slab, as shown in Figure 5.5. This slab has vertical supports around its perimeter but no in-plane horizontal restraints. The strip at the centre of the slab denoted X-X will tend to have end shortening behaviour similar to the one-way spanning element shown in Figure 5.4. However, the strips denoted Y-Y on a supported edge do not have the same vertical displacement and will therefore not have significant end shortening. In-plane forces will therefore occur at the interface of these strips of slab in order to maintain equilibrium, thus inducing tensile stresses in strips such as X-X and compressive stresses in strips such as Y-Y. As this behaviour occurs in two directions the result is an area of tensile stress in the centre of the slab denoted by the shaded area in Figure 5.5 and a compressive ring around the perimeter.

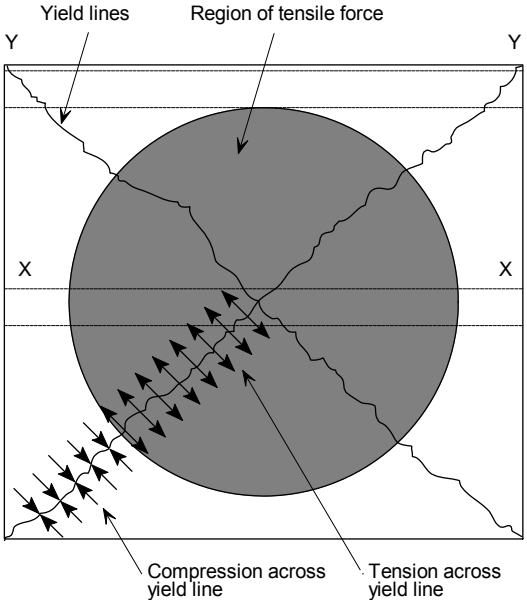

Figure 5.5 *Development of in-plane membrane forces*

Effect of membrane stresses on yield lines

The development of tensile and compressive in-plane forces will influence the yield line moments developed in the slab, with reductions in bending resistance occurring in the tensile zone and enhancement of the bending resistance of the yield lines in the compression zone. In addition to this influence on bending resistance, there is also the additional load bearing capacity due to tensile membrane action.

Following the work of Johansson on yield line analysis, tests to destruction of a complete building were reported by Ockleston[11]. These test revealed that the loads that could be sustained by the floor slabs were considerably greater than those

predicted by yield line theory. This generated considerable interest in research into membrane effects and a number of researchers investigated these effects both experimentally and analytically in subsequent years.

Observations from tests on unrestrained slabs show that the pattern of yield lines is unchanged at large displacements. The ultimate mode of failure has also been shown to be the development of large cracks across the shorter span of the slab and fracture of the reinforcement, as reported by Wood[15]

Methods of analysis taking account of membrane action have been developed for unrestrained slabs by Wood[15], Kemp[17], Taylor[16], Sawczuk[18], Hayes[19] and Bailey and Moore[12,13]

Wood developed a solution for a circular slab with simply supported boundaries subject to distributed loading. A similar solution was developed for square slabs by Kemp. Kemp's method involved a rigorous rigid-plastic solution, in which the load bearing capacity is determined from consideration of the equilibrium of the rigid regions of the slab. This enables the magnitude of the membrane forces and yield line moments to be determined as a function of the slab deflection. Kemp's theory demonstrates that the capacity of the slab is a function of the slab deflection. He notes that in practice a collapse load would be reached when fracture of the reinforcement occurs or when the concrete in the outer region crushes, although his model does not attempt to define this end point on the load deflection response.

In the approach used by Sawczuk, the formation of the crack across the short span was included. Sawczuk identified that the rigid triangular elements of the slab are subject to in-plane moments due to the variation of membrane forces along the yield lines. By estimating the bending resistance of the rigid regions, Sawczuk predicted the development of bending hinges along the centre line of the slab and cracking across the short span. This cracking is not allowed for by the methods developed by Taylor and Kemp. Sawczuk's energy based method, considered two possible crack formations, as shown in Figure 5.6. The conclusion was that the critical mode of failure was caused by cracks forming across the shorter span, at the intersection of the yield lines, as shown in Figure 5.6(a).

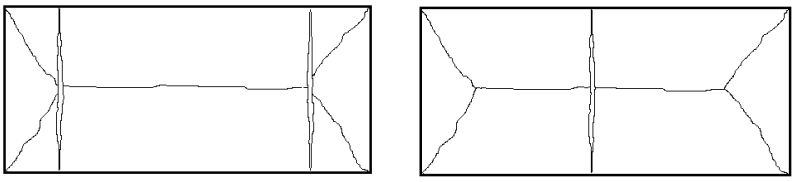

(a) Crack forming at the intersection of the yield lines

(b) Crack forming at the centre of the slab

Figure 5.6 *Failure modes identified by Sawczuk*

Hayes noted that the Sawczuk's analysis implied that boundary forces were present, when in reality these forces could not exist at an unrestrained simply supported edge. Hayes also observed that no increase in the load bearing capacity was apparent when moment equilibrium of the rigid regions was considered. Hayes went on to develop a solution for orthotropically reinforced rectangular slabs which addressed his criticisms of Sawczuk method and which was in good agreement with Kemp's solution for square slabs. In his method, Hayes also assumed that the cracks across the short span occur at the intersection of the yield lines. Comparing his method with Sawczuk's, Hayes concluded that the differences were not

significant. Importantly, Hayes also noted that the enhancement due to membrane effects decreases with increase in the aspect ratio of the slab or the orthotropy of the reinforcement.

Sawczuk's assumption, which was also adopted by Hayes, that the failure mode includes two cracks across the short span of the slab at the intersection of the yield lines contradicts a large portion of the test results, including a test conducted by Building Research Establishment in 2000[20]. Therefore, Bailey and Moore[12,13] modified the method developed by Hayes's approach and based their equilibrium method on the formation of a single crack in the centre of the slab, the mode of failure commonly observed in the tests conducted at ambient and elevated temperatures, Figure 5.7(b). The derivation used by Bailey and Moore is described in Section 5.2. Initially this was developed for isotropic reinforcement, but has been updated to include the effects of the orthotropic reinforcement and the catenary action of the steel beams[21].

5.2 Calculation of resistance of composite floors in accordance with the simple design method

This Section describes the development of a simple design method that can be used to calculate the resistance of rectangular composite floor plates. The method has developed over a number of years. The initial development [12,13] of the method for use with isotropic reinforcement only considered one failure mode, due to fracture of the mesh across the short span, as shown by Figure 5.7(a). Later developments[21,25] included a more general derivation allowing the use of orthotropic reinforcement, and also the inclusion of compression failure of the concrete at the slab corners (see Figure 5.7(b)).

5.2.1 Calculation of resistance

The load bearing capacity of a two-way spanning simply supported slab, with no in-plane horizontal restraint at its edges, is greater than that calculated using the normal yield line theory. The enhancement of the resistance is as a result of tensile membrane action developing in the slab at large displacement and also due to the increase of the yield moment in the outer regions of the slab, where compressive stresses occur across the yield lines (see Figure 5.8).

The enhancement of the resistance determined as a lower bound solution for yield line failure is based on the assumption that at ultimate conditions the yield line pattern will be as shown in Figure 5.7(a) and that failure will occur due to fracture of the mesh across the short span at the centre of the slab. A second mode of failure might, in some cases, occur due to crushing of the concrete in the corners of the slab where high compressive in-plane forces occur as shown by Figure 5.7(b). This mode of failure is discussed in Section 5.3.

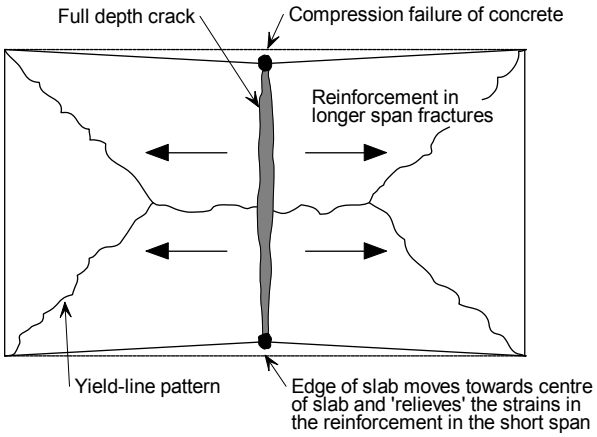

(a) Tensile failure of mesh reinforcement

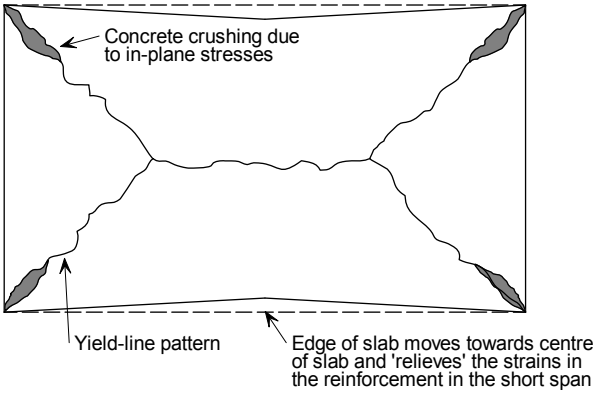

(b) compressive failure of concrete

Figure 5.7 *Assumed failure mode for composite floor*

The first failure mode will occur when the compressive strength of the concrete exceeds the ultimate strength of the mesh in tension, leading to fracture of the mesh. The second failure mode will occur in cases were the ultimate strength of the mesh exceeds the compressive strength of the concrete, resulting in compression failure of the concrete at the corners of the slab.

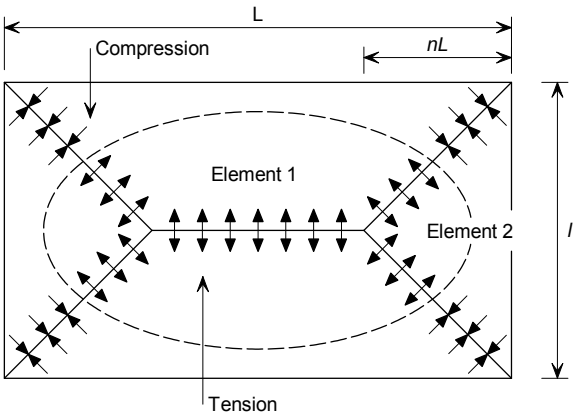

Figure 5.8 *Rectangular slab simply supported on four edges showing in-plane forces across the yield lines due to tensile membrane action.*

Figure 5.8 shows a rectangular slab simply supported on its perimeter and the expected lower bound yield line pattern that would develop due to uniformly distributed loading. The intersection of the yield lines is defined by the parameter n calculated using the general yield line theory and given by:

$$n = \frac{1}{2\sqrt{\mu a^2}}\left(\sqrt{3\mu a^2 + 1} - 1\right), \qquad (11)$$

where

a is the aspect ratio of the slab (L/l)

μ is the ratio of the yield moment capacity of the slab in orthogonal directions (should always be less than or equal to 1.0)

The shorter span should be defined by the span with the lower moment capacity resulting in coefficient of orthography (μ) being always less than, or equal to one. Therefore n would be limited to maximum of 0.5 resulting in a valid yield line pattern.

The resistance of the mechanism which occurs due to the formation of these yield lines is given by the following equation:

$$\mathrm{P} = \frac{24\mu M}{l^2}\left[\sqrt{3 + \frac{1}{(a')^2}} - \frac{1}{a'}\right]^{-2}$$

where

a' $= \sqrt{\mu a}$

Hayes[19] noted that assuming rigid-plastic behaviour, only rigid body translations and rotations are allowed. Further assumptions that the neutral axes along the yield lines are straight lines and that the concrete stress-block is rectangular, means that the variations in membrane forces along the yield lines become linear, as shown in Figure 5.9. These assumptions and the resulting distribution of membrane forces were also adopted by Bailey[12,26].

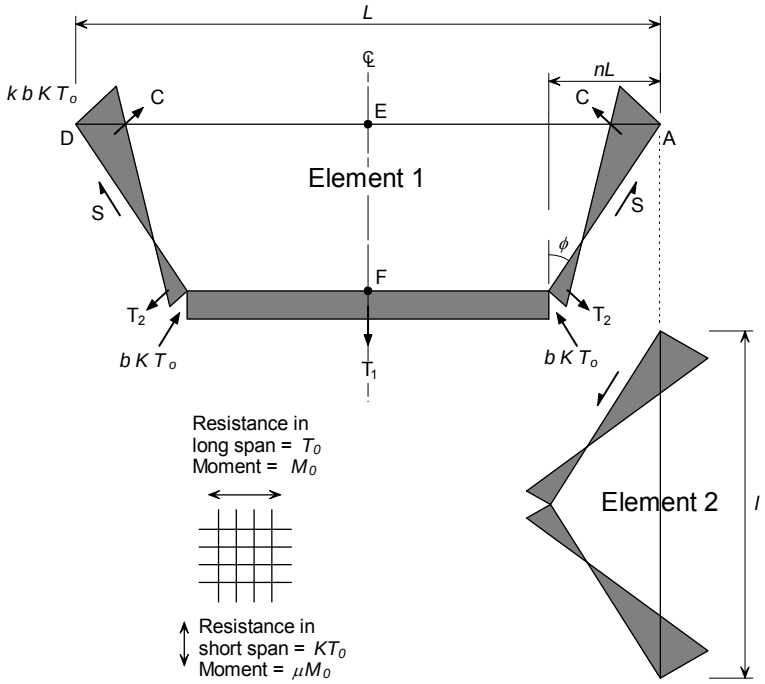

Figure 5.9 *In-plane stress distribution for the elements 1 and 2*

Derivation of an expression for parameter k

Considering the equilibrium of the in-plane forces T_1, T_2 and C acting on Element 1 allows the following relationships to be derived:

$$S\sin\phi = (C - T_2)\cos\phi$$

and

$$-S\cos\phi = (C - T_2)\sin\phi - \frac{T_1}{2}$$

Therefore,

$$\frac{T_1}{2}\sin\phi = (C - T_2) \qquad (1)$$

where

ϕ is the angle defining the yield line pattern.

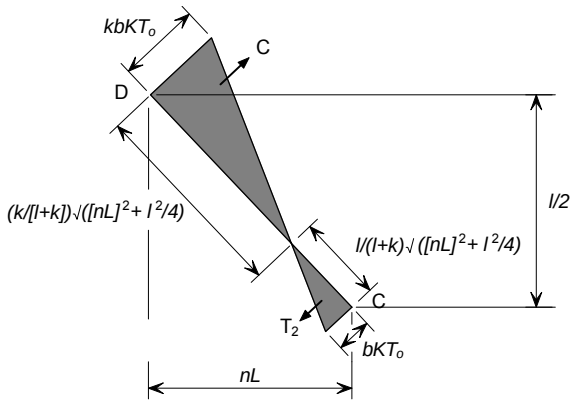

Figure 5.10 *In-plane stress distribution along yield line CD*

Figure 5.10 shows the geometry of the stress distribution along yield line CD. Considering Figure 5.9 and Figure 5.10,

$$T_1 = bKT_0\,(L - 2nL)$$

$$T_2 = \frac{bKT_0}{2}\left(\frac{1}{1+k}\right)\sqrt{(nL)^2 + \frac{l^2}{4}}$$

$$C = \frac{kbKT_0}{2}\left(\frac{k}{1+k}\right)\sqrt{(nL)^2 + \frac{l^2}{4}}$$

$$\sin\phi = \frac{nL}{\sqrt{(nL)^2 + \frac{l^2}{4}}}$$

where

b, k	are parameters defining the magnitude of the membrane force,
KT_0	is the resistance of the steel reinforcing mesh per unit width,
n	is a parameter defining the yield line pattern

Substituting the above values into Equation (1) gives,

$$\frac{bKT_0(L-2nL)}{2}\,\frac{nL}{\sqrt{(nL)^2 + \frac{l^2}{4}}} = \frac{kbKT_0}{2}\left(\frac{k}{1+k}\right)\sqrt{(nL)^2 + \frac{l^2}{4}} - \frac{bKT_0}{2}\left(\frac{1}{1+k}\right)\sqrt{(nL)^2 + \frac{l^2}{4}}$$

This expression can then be rearranged to give an expression for parameter k.

$$k = \frac{4na^2(1-2n)}{4n^2a^2 + 1} + 1 \qquad (2)$$

Derivation of an expression for parameter b

Considering the fracture of the reinforcement across the short span of the slab, an expression for the parameter b can be developed. The line EF shown in Figure 5.11 represents the location of the mesh fracture, which will result in a full depth crack across the slab. An upper bound solution for the in-plane moment of resistance along the line EF can be obtained by assuming that all the reinforcement along the section is at ultimate stress (f_u) and the centroid of the compressive stress block is at location E in Figure 5.11.

It is assumed that,

$$f_u = 1.1 f_y$$

where

f_y is the yield stress.

Taking moment about E in Figure 5.11,

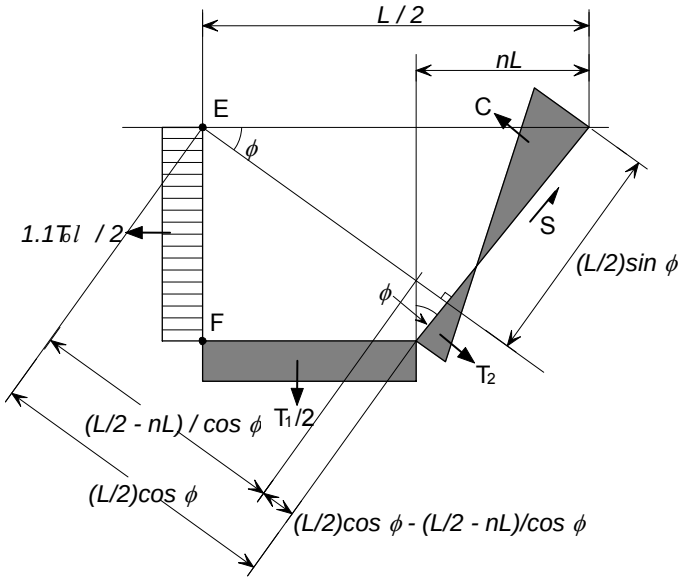

Figure 5.11 *In-plane stress distribution along fracture line EF*

$$T_2\left[\left(\frac{L}{2}\cos\phi - \frac{\left(\frac{L}{2}-nL\right)}{\cos\phi}\right)\frac{1}{\tan\phi} - \frac{1}{3}\left(\frac{1}{1+k}\right)\sqrt{(nL)^2+\frac{l^2}{4}}\right]$$
$$+C\left[\frac{L}{2}\sin\phi - \frac{l}{3}\left(\frac{k}{k+1}\right)\sqrt{(nL)^2+\frac{l^2}{4}}\right] \qquad (3)$$
$$+S\frac{L}{2}\cos\phi - \frac{T_1}{2}\left[\frac{1}{2}\left(\frac{L}{2}-nL\right)\right] = \frac{1.1T_o l^2}{8}$$

where

$$\frac{T_1}{2} = bKT_o\left(\frac{L}{2} - nL\right)$$

$$T_2 = \frac{bKT_o}{2}\left(\frac{1}{1+k}\right)\sqrt{(nL)^2 + \frac{l^2}{4}}$$

$$C = \frac{kbKT_o}{2}\left(\frac{k}{k+1}\right)\sqrt{(nL)^2 + \frac{l^2}{4}}$$

$$S = \frac{bKT_o l}{4nL}(k-1)\sqrt{(nL)^2 + \frac{l^2}{4}}$$

$$\cos\phi = \frac{(l/2)}{\sqrt{(nL)^2 + \frac{l^2}{4}}}$$

$$\sin\phi = \frac{nL}{\sqrt{(nL)^2 + \frac{l^2}{4}}}$$

$$\tan\phi = \frac{nL}{(l/2)}$$

Substituting these expressions into Equation (3) leads to,

$$\frac{bKT_o}{2}\left(\frac{1}{1+k}\right)\sqrt{(nL)^2 + \frac{l^2}{4}}\left[\left(\frac{\left(\frac{l}{2}\right)}{\sqrt{(nL)^2 + \frac{l^2}{4}}}\frac{L}{2} - \frac{\left(\frac{L}{2} - nL\right)}{\left(\frac{l}{2}\right)}\sqrt{(nL)^2 + \frac{l^2}{4}}\right)\frac{\left(\frac{l}{2}\right)}{nL} - \frac{1}{3}\left(\frac{1}{1+k}\right)\sqrt{(nL)^2 + \frac{l^2}{4}}\right]$$

$$+\frac{kbKT_o}{2}\left(\frac{k}{k+1}\right)\sqrt{(nL)^2 + \frac{l^2}{4}}\left[\frac{nL}{\sqrt{(nL)^2 + \frac{l^2}{4}}}\frac{L}{2} - \frac{1}{3}\left(\frac{k}{1+k}\right)\sqrt{(nL)^2 + \frac{l^2}{4}}\right]$$

$$+\frac{bKT_o l}{4nL}(k-1)\sqrt{(nL)^2 + \frac{l^2}{4}}\frac{\left(\frac{l}{2}\right)}{\sqrt{(nL)^2 + \frac{l^2}{4}}}\left(\frac{L}{2}\right) - bKT_o\left(\frac{L}{2} - nL\right)\left[\frac{l}{2}\left(\frac{L}{2} - nL\right)\right] = \frac{1.1T_o l^2}{8}$$

which can be rearranged to give,

$$\frac{b}{2}\left(\frac{1}{1+k}\right)\left[\left(\frac{l^2}{8n}-\frac{\left(\frac{L}{2}-nL\right)}{nL}\left((nL)^2+\frac{l^2}{4}\right)-\frac{1}{3}\left(\frac{1}{1+k}\right)\left((nL)^2+\frac{l^2}{4}\right)\right)\right]$$
$$+\frac{b}{2}\left(\frac{k^2}{1+k}\right)\left[\frac{nL^2}{2}-\frac{k}{3(1+k)}\left((nL)^2+\frac{l^2}{4}\right)\right] \qquad (4)$$
$$+\frac{bl^2}{16n}(k-1)-b\left(\frac{L}{2}-nL\right)\left(\frac{L}{4}-\frac{nL}{2}\right)=\frac{1.1l^2}{8K}$$

Equation (4) can be rewritten as,

$$Ab+Bb+Cb-Db=\frac{1.1l^2}{8K}$$

Whence:

$$b=\frac{1.1l^2}{8K(A+B+C-D)} \qquad (5)$$

where

$$A=\frac{1}{2}\left(\frac{1}{1+k}\right)\left[\frac{l^2}{8n}-\frac{\left(L/2-nL\right)}{nL}\left((nL)^2+\frac{l^2}{4}\right)-\frac{1}{3}\left(\frac{1}{1+k}\right)\left((nL)^2+\frac{l^2}{4}\right)\right],$$

$$B=\frac{1}{2}\left(\frac{k^2}{1+k}\right)\left[\frac{nL^2}{2}-\frac{k}{3(1+k)}\left((nL)^2+\frac{l^2}{4}\right)\right],$$

$$C=\frac{l^2}{16n}(k-1),$$

$$D=\left(\frac{L}{2}-nL\right)\left(\frac{L}{4}-\frac{nl}{2}\right).$$

The parameters *k* and *b,* which define the in-plane forces, can be calculated using equations (2) and (5) respectively.

Membrane forces

The load bearing capacity for Elements 1 and 2 of the slab can be determined by considering the contribution of the membrane forces to the resistance and the increase in bending resistance across the yield lines separately as shown below. These effects are expressed in terms of an enhancement factor, to be applied to the lower bound yield line resistance. Initially, the effects of the in-plane shear *S* (Figure 5.9) or any vertical shear on the yield line was ignored, resulting in two unequal loads being calculated for Elements 1 and 2 respectively. An averaged value was then calculated, considering contribution of the shear forces.

Contribution of membrane forces to load bearing capacity.

a) Element 1

According to Figure 5.12, the moment about the support due to membrane force is given by:

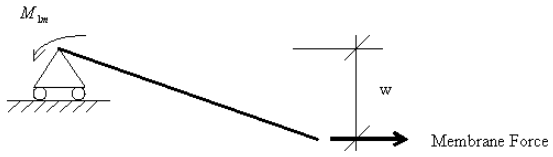

Figure 5.12 *Calculating the moment caused by the membrane force*

$$M_{1m} = bKT_0 (L - 2nL)w + bKT_0 nLw\left(\frac{3k+2}{3(1+k)^2}\right) - bKT_0 nLw\left(\frac{k^3}{3(1+k)^2}\right)$$

where

M_{1m} is the moment about the support due to membrane forces for element 1.

The expression reduces to:

$$M_{1m} = KT_0 Lbw\left((1-2n) + \frac{n(3k+2) - nk^3}{3(1+k)^2}\right).$$

The above formulation defines the contribution from the membrane forces to the load bearing capacity that needs to be added to the contribution due to the enhanced bending capacity in the areas where the slab is experiencing compression forces. For simplicity, the contribution from the membrane forces and enhanced bending action is related to the normal yield line load. This allows an enhancement factor to be calculated for both the membrane force and also the enhanced bending moments. These enhancement factors can finally be added to give the overall enhancement of the slab due to membrane action.

Dividing M_{1m} by $\mu M_o L$, the moment of resistance of the slab, when no axial force is present, allows the effect of tensile membrane action to be expressed as an enhancement of yield line resistance (Figure 5.13).

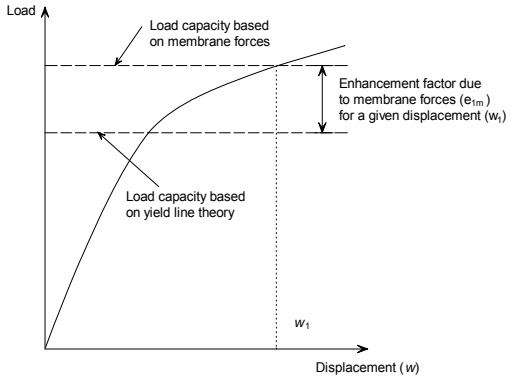

Figure 5.13 *Enhancement factor due to membrane force*

The value of μM_o is obtained by considering Figure 5.14.

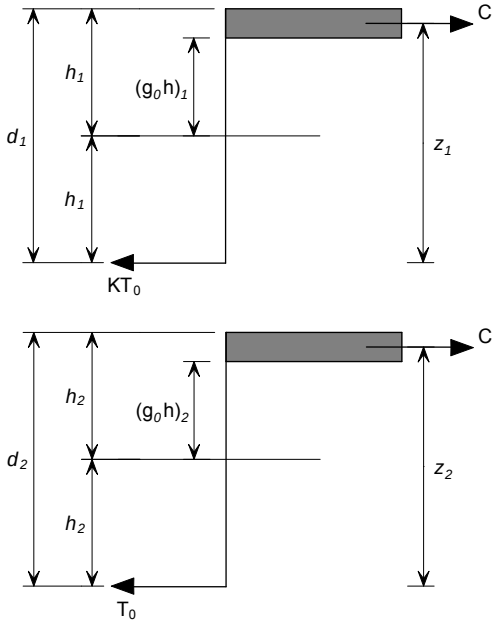

Figure 5.14 *Calculation of the moment resistance*

The bending moments μM_0 and M_o per unit width of slab in each orthogonal direction are given by:

$$\mu M_0 = KT_0 d_1 \left(\frac{3 + (g_0)_1}{4} \right)$$

$$M_0 = T_0 d_2 \left(\frac{3 + (g_0)_2}{4} \right)$$

where

$(g_0)_1$, $(g_0)_2$ are parameters which define the flexural stress block in the two orthogonal directions (see Figure 5.14)

d_1 , d_2 are the effective depths of the reinforcement in each direction.

The enhancement factor, e_{1m} , is given by:

$$e_{1m} = \frac{M_{1m}}{\mu M_0 L} = \frac{4b}{3+(g_0)_1}\left(\frac{w}{d_1}\right)\left((1-2n)+\frac{n(3k+2)-nk^3}{3(1+k)^2}\right) \quad (6)$$

b) Element 2

The moment about the support due to the membrane forces is given by:

$$M_{2m} = KT_0 lbw\left(\frac{2+3k-k^3}{6(1+k)^2}\right)$$

where

M_{2m} is the moment about support due to membrane force for element 2.

The effect of tensile membrane action can be expressed as an enhancement of yield line resistance by dividing the moment about the support due to membrane action, M_{2m} by the moment resistance in the longitudinal direction, when no axial force is present, $M_0 l$, which results in,

$$e_{2m} = \frac{M_{2m}}{M_0 l} = \frac{4bK}{3+(g_0)_2}\left(\frac{w}{d_2}\right)\left(\frac{2+3k-k^3}{6(1+k)^2}\right) \quad (7)$$

The effect of the membrane forces on the bending resistance along the yield lines is evaluated by considering the yield criterion when axial load is also present, as given by Wood [6]. In the case of the short span the bending moment in the presence of an axial force is given by

$$\frac{M_N}{\mu M_0} = 1+\alpha_1\left(\frac{N}{KT_0}\right)-\beta_1\left(\frac{N}{KT_0}\right)^2 \quad (8a)$$

where

$$\alpha_1 = \frac{2(g_0)_1}{3+(g_0)_1}$$

and

$$\beta_1 = \frac{1-(g_0)_1}{3+(g_0)_1}$$

Similarly for the long span,

$$\frac{M_N}{\mu M_0} = 1+\alpha_2\left(\frac{N}{T_0}\right)-\beta_2\left(\frac{N}{T_0}\right)^2 \quad (8b)$$

where

$$\alpha_2 = \frac{2(g_0)_2}{3+(g_0)_2}$$

and

$$\beta_2 = \frac{1-(g_0)_2}{3+(g_0)_2}$$

Effect of membrane forces on bending resistance

a) Element 1

The effect of the membrane forces on the bending resistance is considered separately for the each yield line,

For the yield line BC, the membrane force is constant and equals $-bKT_0$ and therefore:

$$\left(\frac{M_N}{M_0}\right)_{BC} = 1-\alpha_1 b-\beta_1 b^2$$

For the yield line AB (Figure 5.15),

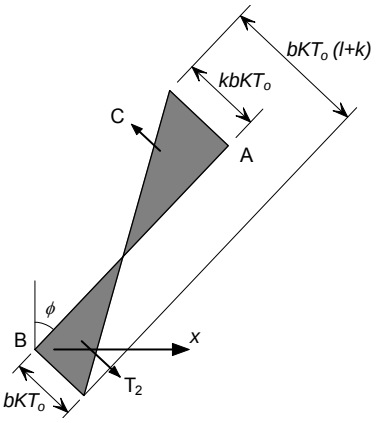

Figure 5.15 *Forces applied to element 1, yield line CD*

The membrane force across the yield line, at a distance of x from B is given by:

$$N_x = -bKT_0 + \frac{x}{nL}(K+1)bKT_0$$

$$N_x = bKT_0\left(\frac{x(k+1)}{nL}-1\right)$$

Substitution into Equation (8a) gives, for yield lines AB and CD:

$$2\int_0^{nL}\frac{M}{M_0}dx = 2\int_0^{nL}\left[1+\alpha_1 b\left(\frac{x(k+1)}{nL}-1\right)-\beta_1 b^2\left(\frac{x(k+1)}{nL}-1\right)^2\right]dx$$

This results in:

$$2\int_0^{nL}\frac{M}{M_0}dx = 2nL\left[1+\frac{\alpha_1 b}{2}(k-1)-\frac{\beta_1 b^2}{3}\left(k^2-k+1\right)\right]$$

The enhancement of bending resistance due to membrane forces on Element 1 is given by:

$$e_{1b} = \frac{M}{\mu M_0 L} = 2n\left[1+\frac{\alpha_1 b}{2}(k-1)-\frac{\beta_1 b^2}{3}\left(k^2-k+1\right)\right]+(1-2n)\left(1-\alpha_1 b-\beta_1 b^2\right) \quad (9)$$

b) Element 2

Referring to Figure 5.16 for element 2, the force at a distance y from B can be expressed as:

$$N_y = -bKT_0 + \frac{y}{l/2}(k+1)bKT_0$$

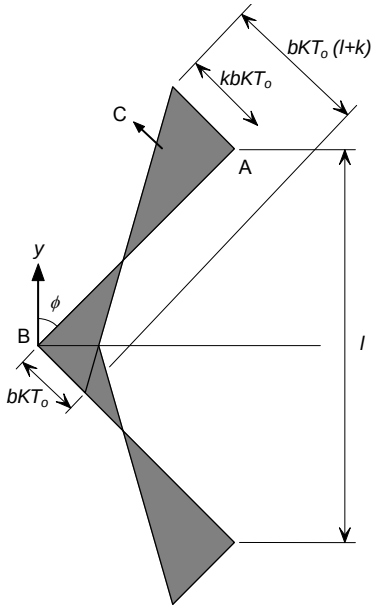

Figure 5.16 *Forces applied to element 2*

By rearranging

$$N_y = bKT_0\left(\frac{2y(k+1)}{l}-1\right)$$

Substitution into Equation (8b) gives:

$$\int_0^{1/2}\frac{M}{M_0}dy = 2\int_0^{1/2}\left[1+\alpha_2 bK\left(\frac{2y(k+1)}{l}-1\right)-\beta_2 b^2 K\left(\frac{2y(k+1)}{l}-1\right)^2\right]dy$$

Resulting in,

$$2\int_0^{1/2}\frac{M}{M_0}dx = l\left[1+\frac{\alpha_2 b}{2}(k-1)-\frac{\beta_2 b^2}{3}(k^2-k+1)\right]$$

Which gives the enhancement factor due to the effect of the membrane forces on the bending resistance according to the following formulation,

$$e_{2b}=\frac{M}{M_0 l}=1+\frac{a_2 bK}{2}(k-1)-\frac{\beta_2 b^2 K}{3}(k^2-k+1) \qquad (10)$$

Equations (6), (7), (9) and (10) provide the contribution to the load bearing capacity due to the membrane forces and the effect of the membrane forces on the bending resistance of the slab..

Consequently, the combined enhancement factor is obtained for each element as follows

$$e_1 = e_{1m} + e_{1b}$$

$$e_2 = e_{2m} + e_{2b}$$

As stated earlier, the values e_1 and e_2 calculated based on the equilibrium of elements 1 and 2 will not be the same and Hayes suggests that these differences can be explained by the effect of the vertical or in-plane shear and that the overall enhancement is given by.

$$e = e_1 - \frac{e_1 - e_2}{1+2\mu a^2}$$

5.3 Compressive failure of concrete

The enhancement factor in Section 5.2.1 was derived by considering tensile failure of the mesh reinforcement. However, compressive failure of the concrete in the proximity of the slab corners must also be considered as a possible mode of failure, which in some cases may precede mesh fracture. This was achieved by limiting the value of the parameter '*b*', which represents the magnitude of the in-plane stresses.

According to Figure 5.9, the maximum in-plane compressive force at the corners of the slab is given by $kbKT_0$. The compressive force due to the bending should also be considered. By assuming that the maximum stress-block depth is limited to 0.45d, and adopting an average effective depth to the reinforcement in both orthogonal directions results in:

$$kbKT_0 + \left(\frac{KT_0 + T_0}{2}\right) = 0.85 f_{ck} \times 0.45\left(\frac{d_1 + d_2}{2}\right)$$

Where, f_{ck} is the concrete cylinder strength.

Solving for the constant *b* gives:

$$b = \frac{1}{kKT_o}\left(0.85 f_{ck} \times 0.45\left(\frac{d_1 + d_2}{2}\right) - T_0\left(\frac{K+1}{2}\right)\right) \qquad (11)$$

The constant b is then taken as the minimum value given by the Equations (5) and (11).

6 DEVELOPMENT OF DESIGN GUIDANCE

Previous tests at normal temperature, reviewed in Section 4.5, have shown that the load bearing capacity of concrete slabs will be enhanced by membrane forces provide that vertical support is maintained along the slab boundaries. Flat slabs, which only have vertical supports at their corners, do not develop significant tensile membrane forces and therefore benefit little from enhancement due to membrane action.

Therefore, for a composite slab supported on a grillage of steel beams in fire conditions, it is important to divide the slab into rectangular areas, referred to as floor design zones, where vertical support can be maintained on the perimeter of each area. These lines of vertical support are achieved by ensuring that the perimeter beams frame into column positions and are fire protected.

At ambient temperature, the floor is continuous over the boundary of each floor design zone. However, in fire conditions it is likely that cracks will form over the perimeter beams, due to the large thermal curvatures experienced by the slab. This may lead to fracture of the reinforcement, either due to the curvature or due to the combination of bending and membrane stresses. The fracture of the reinforcement in these hogging regions will occur before fracture of the reinforcement in the centre of the floor design zone. Therefore, the floor design zones are considered to have no rotational or transverse restraint along the boundary of the slab.

6.1 Design assumptions

For a composite floor slab, the yield line pattern will depend on the behaviour of the unprotected composite beams, which are continually losing strength as the temperature increases. Unlike ambient conditions the load carrying mechanism of the floor changes with increasing temperature. Initially, the composite slab acts as a one-way spanning element supported on the secondary beams. As these beams lose strength with increasing temperature and the behaviour of the slab tends to the behaviour of a simple supported two-way spanning element, resulting in the formation of the yield line pattern shown in Figure 6.1. By assuming that this ultimate failure condition will occur when the beam strength is low relative to the slab, a conservative estimate of capacity can be obtained relatively simply.

The load bearing capacity of the slab is calculated on the assumption that the composite beams have no strength and is based on the yield line pattern which is compatible with the boundary conditions and which provides the lowest load bearing capacity. This resistance is then enhanced by taking account of the tensile membrane effects based on the estimated deflection of the slab and the modes of failure described in Section 5. The bending resistance of the composite beams are added to this enhanced slab resistance in order to give the total load bearing capacity of the system.

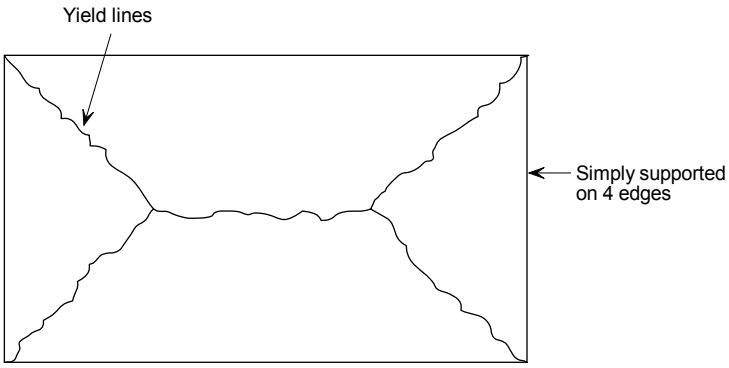

Figure 6.1 *Typical yield line pattern for a rectangular slab simply supported along four edges*

6.2 Failure criterion

Two modes of failure have been witnessed in room temperature and elevated temperature tests, depending on the reinforcement ratio, slab aspect ratio and the reinforcement ductility. Fracture of the reinforcement across the shorter span dominates the failure mode in most of the lightly reinforced slabs, whilst the heavily reinforced slabs and slabs with highly ductile reinforcement may experience compressive failure at the corners of the slab. Both modes of failure are considered by the simple design method as described in Section 5.2

Most tests conducted at elevated temperatures on simply supported concrete slabs have failed due to full depth crack forming across the shorter span (l), as shown in Figure 6.2. The design method presented in Section 5.2 predicts the load bearing capacity for a given deflection. Section 6.2.1 describes the development of an expression for estimating slab deflection just prior to slab failure which is required to calculate the effect of membrane action.

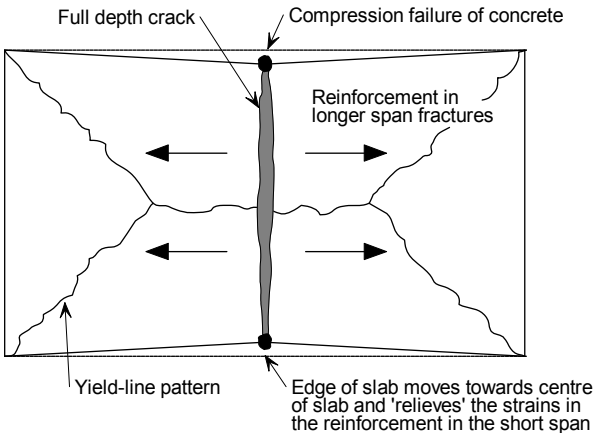

Figure 6.2 *Tensile failure of the slab due to fracture of the reinforcement*

6.2.1 Slab deflection

As the simple design method is based on plastic theory, deflection cannot be calculated using the method. However, in order to calculate the membrane forces a

value of deflection for the slab just prior to failure must be estimated. This estimate of slab deflection will include thermal strains due to the slabs temperature gradient as well as the mechanical strains in the reinforcement.

Thermal effects

Based on the previous investigations, when the maximum deflection of the slab is greater than almost 0.5 times its depth and tensile forces start to build up at the slab centre, any in-plane restraint to the thermal expansion would increase the vertical displacements (i.e. the slab is in the post-buckling phase) and therefore the tensile membrane action. Conservatively, and in order to allow this approach to be used also for the edge slabs, this beneficial effect is ignored and slab is assumed to be unrestrained.

The composite slab in the fire conditions would experience thermal curvature, which, for an unrestrained slab, increases the vertical displacement without inducing any mechanical strains into the mesh reinforcement. If the temperature distribution through the slab is assumed to be linear then the displacements caused by the thermal deflection is calculated as:

$$\frac{d^2w}{dx^2} = \frac{\alpha(T_2 - T_1)}{h}$$

where

w =Vertical displacement

α = Coefficient of thermal expansion

T_2 =Bottom temperature

T_1 = Top temperature

h = Depth of slab

The vertical displacement of the slab due to thermal curvature can be obtained by integrating the above Equation, which gives:

$$w_\theta = \frac{\alpha(T_2 - T_1)l^2}{8h}$$

where

l is the length of the shorter span of the slab

This formulation is based on a constant atmospheric temperature throughout the fire compartment. To the estimated displacement, allowing for real fire conditions where uniform heating is less likely, a reduction factor of 2.0 is applied to the above expression. This results in the design value of vertical displacement due to the thermal curvature given by:

$$w_\theta = \frac{\alpha(T_2 - T_1)l^2}{16h}$$

Mechanical strains in the reinforcement

Assuming that the deflected shape of the slab due to transverse loading is parabolic, the length of the deflected slab is given by the following formulation in which the longer span is (L).

$$L_c = L\left(1 + \frac{8w^2}{3L^2} - \frac{32w^4}{5L^4} + ...\right)$$

where

L_c is the length of the curve,

L is the length of longer span of slab at zero displacement,

w is the vertical displacement of the curve.

For flat curves,

$$L_c = L\left(1 + \frac{8w^2}{3L^2}\right)$$

Hence, the strain in the mesh can be calculated by:

$$\varepsilon = \frac{8w^2}{3L^2}$$

This equation assumes the strain is the same value along the length of the slab. In reality, the slab will experience tension stiffening with strains being concentrated where cracks have occurred. The reinforcement across a crack will also experience a significant increase in the strain, resulting in the eventual fracture of the reinforcement. Therefore, to allow for tension stiffening the component of displacement due to strain in the reinforcement w_ε is based on a conservative value of average strain calculated at a stress equal to half the yield stress at room temperature. The displacement is then given by:

$$w_\varepsilon = \sqrt{\left(\frac{0.5 f_{sy}}{E_s}\right) \frac{3L^2}{8}} \qquad (1)$$

where

E_s is the room temperature elastic modulus of the reinforcement

f_{sy} is the room temperature yield strength of the reinforcement

The displacements due to strain in the reinforcement calculated using Equation (1) have been compared to maximum deflections measured in tests at room temperature. In all the cases considered, the displacement predicted by equation 1 was lower than the maximum displacement recorded in the test, as shown in Table 6.1.

Table 6.1 *Comparison of allowable deflection from Equation (1) and maximum deflections measured in room temperature tests.*

Test	Slab size (m)	Effective Depth (mm)	Reinforcement Diameter (mm)	Bar Spacing (mm)	Steel yield strength (N/mm^2)	Max. test deflection (mm)	Allowable deflection Eqn. (1) (mm)
BRE	9.56x6.46	66.0	6.0	200	580	223	216
Sawczuk & Winnicki	1.6x1.1	26.0	3.0	30.0	263	127*	25
	2.0x1.0	26.0	3.0	60.0	263	76*	31
Hayes & Taylor	0.914x0.914	15.9	9.5	-†	505	50.8*	19.4
	0.914x1.372	15.9	9.5	-†	505	50.8*	29.1
	0.914x1.829	15.9	9.5	-†	505	50.8*	38.8
Taylor, Maher & Hayes	1.829x1.829	43.6	4.8	76.2	376	81	33.5
	1.829x1.829	37.3	4.8	63.5	376	98	33.5
	1.829x1.829	69.0	4.8	122	376	84	33.5
Brothie & Holley	0.381x0.381	14.2	2.3	-†	414	11.6	7.32
	0.381x0.381	31.0	3.4	-†	379	7.45	7.0

*test terminated before fracture of the reinforcement

† Data not reported

Calculation of slab deflection to allow the calculation of membrane forces

The tensile membrane action of the slab is then calculated based on a slab displacement estimated by combining the components due to thermal curvature and strain in the reinforcement, resulting in:

$$w_m = \frac{\alpha(T_2 - T_1)l^2}{16h} + \sqrt{\left(\frac{0.5 f_{sy}}{E_s}\right)\frac{3L^2}{8}} \qquad (2)$$

This equation results in a conservative estimate of load bearing capacity since:

- the estimated vertical displacements due to thermal curvature are divided by two.
- the thermal curvature is calculated based on the shorter span of the slab
- any additional vertical displacements induced by the restrained thermal expansion when the slab is in a post buckled state are ignored
- any contribution from the steel decking is ignored
- the increase of the mesh ductility with the temperature increase is ignored.

6.2.2 Calibration against Cardington fire tests

Bailey & Moore[12] demonstrated that the design method in Section 5.2 provided a reasonable prediction of floor slab capacity when compared to the Cardington Fire Tests. As part on this project a further furnace based fire test has been conducted as described in Section 7.

The above expression for slab deflection was compared to the maximum deflections recorded during the Cardington fire tests. The object was to ensure that the deflections estimated would be conservative when compared to actual slab behaviour just prior to failure. The drawback in using these tests for this purpose was that failure was not reached by the slabs tested therefore the maximum measured deflections do not correspond to failure of the slab. However, it is known

that the results of the comparison will be conservative but the degree of conservatism can not be quantified.

Table 6.2 shows the comparison between the limiting deflection given by equation (2) and the maximum measured deflection from each of the Cardington tests. This comparison includes both thermal and mechanical strains, which are impossible to distinguish in test data.

In all cases, Equation (2) gives deflections which are greater than the measured deflections. In order to ensure that the deflection limit is conservative Bailey and Moore[12] limited the deflection to those recorded in the tests.

Table 6.2 *Comparison of the displacement given by equation (2) against the maximum displacements recorded in the six Cardington fire tests.*

Test	L (m)	l (m)	Deflection due to thermal curvature (mm)	Deflection due to mechanical strain (mm)	Deflection limit Eqn. (2) (mm)	Maximum deflection recorded in test (mm)	Deflection Limit/test deflection
BRE Corner Test	9.0	6.0	135	208	343	269	1.28
British Steel Restrained Beam	9.0	6.0	135	208	343	232	1.50
British Steel 2-D test	14.0	9.0	0*	324	324	293	1.11
BS Corner Test	10.223	7.875	231	237	468	428	1.09
BRE Large Compartment Test	21.0	9.0	303	486	789	557	1.42
BS Office Demo Test	14.6	10.0	373	338	711	641	1.11

*Due to the small area of slab heated in this test the displacement due to thermal curvature was taken as zero.

For mechanical strains, Bailey and Moore introduced an additional limit as shown below.

$$w_\varepsilon = \sqrt{\left(\frac{0.5 f_y}{E}\right)_{reinf} \frac{3L^2}{8}} \quad \text{but } w_\varepsilon \le \frac{l}{30}$$

For thermal deflection they also increased the 'factor of safety' from 2 to 2.4 giving the following conservative expressions for estimating slab deflections:

$$w_m = \frac{\alpha (T_2 - T_1) l^2}{19.2h} + \sqrt{\left(\frac{0.5 f_{sy}}{E_s}\right) \frac{3L^2}{8}} \qquad (3)$$

but not more than $\dfrac{\alpha (T_2 - T_1) l^2}{19.2h} + \dfrac{l}{30}$

Table 6.3 shows the comparison between the limiting deflection given by Equation (3). Given that failure did not occur in any of the tests it was felt that it would be overly conservative to reduce the deflection limit to a point where the

ratio of deflection limit to measured deflection was one for all tests. For the large compartment tests this limit appears to be reasonable.

Table 6.3 *Comparison of the displacement given by equation (3) against the maximum displacements recorded in the six Cardington fire tests.*

Test	L (m)	l (m)	Deflection due to thermal curvature (mm)	Deflection due to mechanical strain (mm)	Deflection limit Eqn. (3) (mm)	Maximum deflection recorded in test (mm)	Deflection Limit/test deflection
BRE Corner Test	9.0	6.0	112	200	312	269	1.16
British Steel Restrained Beam	9.0	6.0	112	200	312	232	1.34
British Steel 2-D test	14.0	9.0	0*	300	300	293	1.02
BS Corner Test	10.223	7.875	193	237	430	428	1.00
BRE Large Compartment Test	21.0	9.0	252	300	552	557	0.99
BS Office Demo Test	14.6	10.0	311	333	644	641	1.00

*Due to the small area of slab heated in this test the displacement due to thermal curvature was taken as zero.

6.3 Design methodology

The design methodology advocated in this document is based on two key principles.

- The risk to life safety of the building occupants, fire fighters and others in the vicinity of the building in the event of a fire should not increase relative to current practice as a result of using the method.
- The fire should be contained within its compartment of origin and the application of the design method should not lead to failure of the compartmentation of the building

The design method is intended to apply to composite steel-concrete floor plates supported on composite or non-composite columns. The structural frame should be braced (non-sway), the connections should be simple nominally pinned connections and the concrete floor slab should be constructed using steel decking not exceeding 80 mm in depth and supported on the top flange of the steel section. The steel beams should be designed to act compositely with the floor slab in accordance with the recommendations of EN 1994-1-1. Excluded from the scope of application are slabs with an exposed concrete soffit including precast concrete slabs and beams with multiple web openings.

In order to apply the simple design method described in Section 5 to a design scenario, the floor plate being considered must be divided into a number of 'floor design zones'. These floor design zones are bounded on their perimeters by beams (normally fire protected) which satisfy the fire resistance requirements specified for the floor plate. Each floor design zone may include a number of internal secondary beams without fire protection which have a much lower fire resistance. The provision of protected beams on the perimeter of the floor slab is intended to result

in slab behaviour in keeping with the assumption that the perimeter of the floor design zone is simply supported.

For periods of fire resistance of 60 minutes or above the perimeter of the floor design zones should correspond to the column gridlines and the perimeter beams should be connected to the columns at either end.

The composite slab may be designed in accordance with EN 1994-1-1 and should also satisfy the minimum insulation thickness recommended by EN 1994-1-2 in fire conditions. Reinforcement of the composite slab should be achieved using a steel mesh. Reinforcement in the ribs of the slab is not considered in the design method. The inclusion of such reinforcement can have a negative as well as a positive effect on the slab performance in fire conditions, as compressive failure in the concrete may result if the slab is over reinforced.

6.3.1 Calculation of load bearing capacity for the slab

The calculation of the yield line capacity of the composite slab and the associated enhancement of this resistance due to large slab deflections is described in detail in Section 5.

6.3.2 Calculation of load bearing capacity for unprotected beams

In fire conditions, the unprotected beams within each floor design zone will add to the tensile resistance of the slab via catenary action. Currently, the design method conservatively assumes that only the bending resistance of these unprotected members contribute to the total slab capacity.

The temperature of the bottom flange of the unprotected beams is calculated using the method given in EN 1994-1-2, 4.3.4.2. The bottom flange and web of the section are assumed to be at uniform temperature for the calculation of moment resistance. The top flange temperature is taken as 80% of this temperature, to allow for the beneficial effect of the composite slab on top flange temperature.

The calculation of the plastic moment resistance of the beam at elevated temperature follows the principles of EN 1994-1-2, 4.3 taking account of the degree of shear connection between the steel section and the concrete.

6.4 Design of fire resisting perimeter beams

The perimeter beams which bound each floor design zone must be designed to achieve the period of fire resistance required by the floor slab. This will ensure that the pattern of yield lines and the associated enhancement due to tensile membrane action which are assumed to occur in the design methodology actually occur in practice. The required moment resistance of the edge beams is calculated by considering alternative yield line patterns that would allow the slab to fold along an axis of symmetry without developing tensile membrane action, as shown by Figure 6.3 and Figure 6.4.

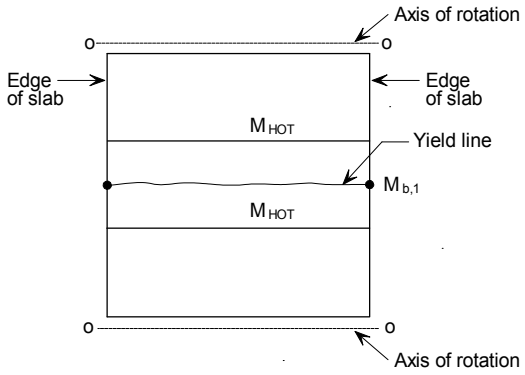

Figure 6.3 *Alternative yield line patterns involving the formation of plastic hinges in the perimeter beams*

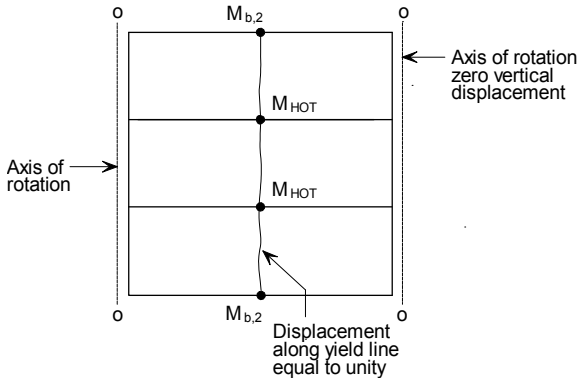

Figure 6.4 *Alternative yield line patterns involving the formation of plastic hinges in the perimeter beams*

Having calculated the required moment capacity of these beams to ensure that they provide sufficient support to allow development of the tensile membrane enhancement of the slab load bearing resistance, a critical temperature for the beams can be calculated and appropriate levels of fire protection can be applied to ensure that this critical temperature is not exceeded during the required fire resistance period.

The design method described in Section 5 assumes that an envelope pattern of yield lines will form in the slab at the ultimate limit state. In order for this to occur, the beams on the perimeter of the floor design zone must have sufficient moment resistance to prevent a beam and slab mechanism occurring at a lower load level.

For a typical floor design zone, as shown in Figure 6.5, two yield line patterns have been considered which include the formation of a plastic hinge in the perimeter beams. The yield lines may occur across the centre of the slab, either parallel to the unprotected beams in the Span 1 direction with plastic hinges forming in the perimeter beams on Sides A and C or perpendicular to the unprotected beams in the

Span 2 direction with plastic hinges forming in the perimeter beams on Side B and D and in the unprotected beams.

Using this pattern of yield lines and equating the internal and external work for the mechanism, the moment resistance of the perimeter beams required to achieve a load bearing capacity equal to that for the floor slab may be determined. The derivation of appropriate design equations is given below.

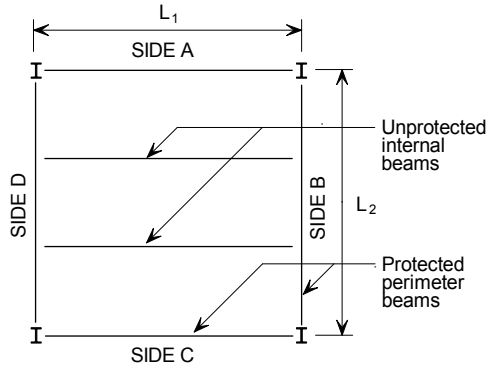

Figure 6.5 *Typical floor design zone*

6.4.1 Unprotected beams with edge beams on both sides

Yield line parallel to unprotected beams

This case considers the required moment resistance of the perimeter beams on Sides B and D of the floor design zone. These beams are also assumed to be at the edge of the slab. A single yield line is assumed to form across the centre of the floor design zone in the Span 1 direction, as shown in Figure 6.6. In keeping with the assumptions of the design method the perimeter of the floor design zone is assumed to be simply supported.

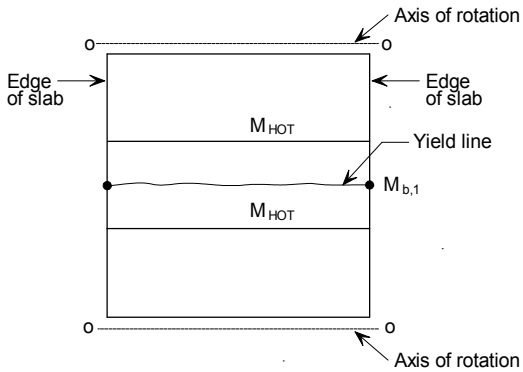

Figure 6.6 *Yield line in parallel to the unprotected beams edge condition on Sides B and D*

Considering a unit displacement along the yield line, the rotation of the yield line can be calculated as follows:

$$\text{Yield line rotation} = 2\frac{1}{L_2/2} = \frac{4}{L_2}$$

The internal work done due to the rotation of the yield line is given by:

$$\text{Internal Work} = \left(ML_{1,\text{eff}} + 2M_{b,1}\right)\frac{4}{L_2} = \frac{4M\,L_{1,\text{eff}}}{L_2} + \frac{8M_{b,1}}{L_2}$$

where

$L_{1,\text{eff}}$ is the effective length of the yield line discounting the effective width of slab assumed to act with the perimeter beams where these are design as composite members.

M is the moment resistance of the slab per unit length of yield line

For a uniform load on the slab, p, the external work due to the displacement is given by:

$$\text{External Work} = \frac{1}{2}pL_1L_2$$

Equating internal and external work gives:

$$pL_1L_2 = \frac{8ML_{1,\text{eff}}}{L_2} + \frac{16M_{\text{b,1}}}{L_2}$$

If the load on the slab is the load bearing capacity determined in accordance with Section 5, the required minimum values of moment resistance for the perimeter beams on Side B and D is given by:

$$M_{\text{b,1}} = \frac{pL_1L_2{}^2 - 8ML_{1,\text{eff}}}{16}$$

where

p is the uniformly distributed load to be supported by the floor design zone in fire conditions.

Yield line perpendicular to unprotected beams

This case considers the required moment resistance of the perimeter beams on Sides A and C of the floor design zone. A single yield line is assumed to form across the centre of the floor design zone in the Span 2 direction, as shown in Figure 6.7. In keeping with the assumptions of the design method the perimeter of the floor design zone is assumed to be simply supported.

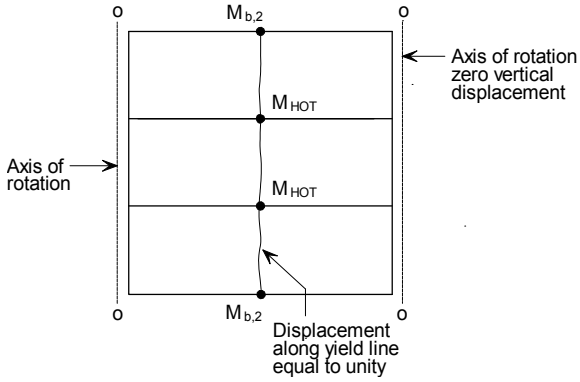

Figure 6.7 *Yield line perpendicular to the unprotected beams edge condition on Sides A and C*

Considering a unity displacement along the yield line the rotation of the yield line can be calculated as follows:

$$\text{Yield line rotation} = 2\frac{1}{L_1/2} = \frac{4}{L_1}$$

The internal work done due to the rotation of the yield line is given by:

$$\text{Internal Work} = \left(ML_{2,\text{eff}} + 2M_{b,2} + nM_{\text{HOT}}\right)\frac{4}{L_1}$$

$$= \frac{4ML_{2,\text{eff}}}{L_1} + \frac{8M_{b,2}}{L_1} + \frac{4nM_{\text{HOT}}}{L_1}$$

where

$L_{2,\text{eff}}$ is the effective length of the yield line discounting the effective width of slab assumed to act with the perimeter beams where these are designed as composite members and the composite unprotected internal beams.

M is the moment resistance of the slab per unit length of yield line

The external work due to the slab displacement is given by:

$$\text{External Work} = \frac{1}{2}pL_1L_2$$

Equating internal and external work gives:

$$pL_1L_2 = \frac{8ML_{2,\text{eff}}}{L_1} + \frac{16M_{b,2}}{L_1} + \frac{8nM_{\text{HOT}}}{L_1}$$

If the load on the slab is the load bearing capacity determined in accordance with Section 5, the required minimum values of moment resistance for the perimeter beams on Side A and C is given by:

$$M_{b,2} = \frac{pL_1^{\,2}L_2 - 8ML_{2,\text{eff}} - 8nM_{\text{HOT}}}{16}$$

Printed 11/07/10~~12/04/10~~

where

p is the uniformly distributed load to be supported by the floor design zone in fire conditions.

6.4.2 Unprotected beams with an edge beam on one side

Yield line parallel to unprotected beams

This case considers the required moment resistance of the perimeter beams on Sides B and D of the floor design zone. In this case the beam on side B is an internal perimeter beam. As the software only deals with an isolated floor plate the calculation of resistance for an internal perimeter beam must assume that the floor design zone is adjacent to an identical area of slab sides where internal beams have been specified. A single yield line is assumed to form across the centre of the floor design zone in the Span 1 direction, as shown in Figure 6.6.

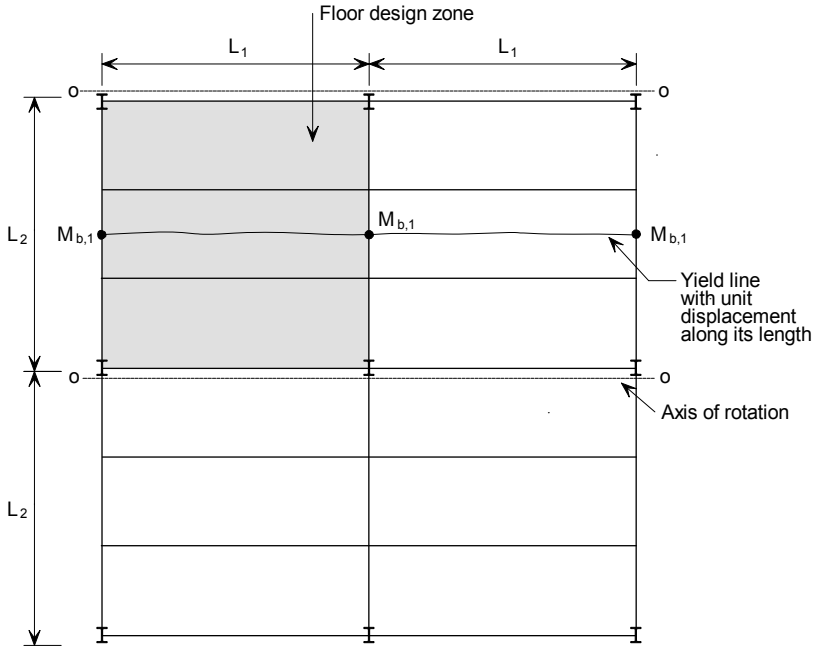

Figure 6.8 *Yield line parallel to the unprotected beams edge condition on Side D*

Considering a unit displacement along the yield line the rotation of the yield line can be calculated as follows:

$$\text{Yield line rotation} = 2\frac{1}{L_2/2} = \frac{4}{L_2}$$

The internal work done due to the rotation of the yield line is given by:

$$\text{Internal Work} = \left(2ML_{1,\text{eff}} + 3M_{b,1}\right)\frac{4}{L_2} = \frac{8M\,L_{1,\text{eff}}}{\mathrm{L}_2} + \frac{12M_{b,1}}{L_2}$$

The external work due to the slab displacement is given by:

$$\text{External Work} = \frac{1}{2} p 2 L_1 L_2$$

Equating internal and external work gives:

$$p L_1 L_2 = \frac{8 M L_{1,\text{eff}}}{L_2} + \frac{12 M_{\text{b,1}}}{L_2}$$

If the load on the slab is the load bearing capacity determined in accordance with Section 5, the required minimum values of moment resistance for the perimeter beams on Side B and D is given by:

$$M_{\text{b,1}} = \frac{p L_1 L_2{}^2 - 8 M L_{1,\text{eff}}}{12}$$

where

$\underline{L}_{1,\text{eff}}$ is the effective length of the yield line discounting the effective width of slab assumed to act with the perimeter beams where these are design as composite members.

M is the moment resistance of the slab per unit length of yield line

p is the uniformly distributed load to be supported by the floor design zone in fire conditions.

Yield line perpendicular to unprotected beams

A single yield line is assumed to form across the centre of the floor design zone in the Span 2 direction, as shown in Figure 6.9.

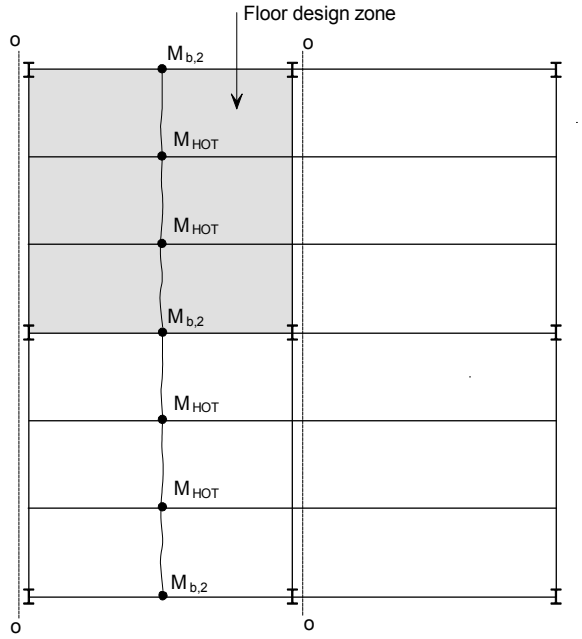

Figure 6.9 *Yield line perpendicular to the unprotected beams edge condition on Side A*

Printed 11/07/10~~12/04/10~~

Considering a unity displacement along the yield line the rotation of the yield line can be calculated as follows:

$$\text{Yield line rotation} = 2\frac{1}{L_1/2} = \frac{4}{L_1}$$

The internal work done due to the rotation of the yield line is given by:

$$\text{Internal Work} = \left(2ML_{2,\text{eff}} + 3M_{b,2} + 2nM_{\text{HOT}}\right)\frac{4}{L_1}$$

$$= \frac{8ML_{2,\text{eff}}}{L_1} + \frac{12M_{b,2}}{L_1} + \frac{8nM_{\text{HOT}}}{L_1}$$

The external work due to the slab displacement is given by:

$$\text{External Work} = \frac{1}{2}pL_1 2L_2$$

Equating internal and external work gives:

$$pL_1L_2 = \frac{8ML_{2,\text{eff}}}{L_1} + \frac{12M_{b,2}}{L_1} + \frac{8nM_{\text{HOT}}}{L_1}$$

If the load on the slab is the load bearing capacity determined in accordance with Section 5, the required minimum values of moment resistance for the perimeter beams on Side A and C is given by:

$$M_{b,2} = \frac{pL_1^{\,2}L_2 - 8ML_{2,\text{eff}} - 8nM_{\text{HOT}}}{12}$$

where

$L_{2,\text{eff}}$ is the effective length of the yield line discounting the effective width of slab assumed to act with the perimeter beams where these are design as composite members and the composite unprotected internal beams.

M is the moment resistance of the slab per unit length of yield line

p is the uniformly distributed load to be supported by the floor design zone in fire conditions.

6.4.3 Floor zone without edge beams

For zones where none of the perimeter beams are edge beams, it is conservative to use the values determined by the expressions in 6.4.2.

6.4.4 Design of edge beams

It is common practice for beams at the edge of floor slabs to be designed as non composite. This is because the costs of meeting the requirements for transverse shear reinforcement are more than the costs of installing a slightly heavier non composite beam. However, for fire design, it is important that the floor slab is adequately anchored to the edge beams, as these beams will be at the edge of floor design zones. For this purpose, if edge beams are designed as non composite, they must have shear connectors at not more than 300 mm centres and U-bars should be provided to tie the edge beam to the composite slab.

6.5 Thermal Analysis

The FRACOF software uses a 2D finite difference heat transfer method to predict the temperature distribution within the composite slab. This method has been used for many years by SCI to predict the temperature distributions in steel and steel-concrete composite cross sections and has been shown to be able to reasonably predict the behaviour of sections in fire resistance tests.

The object to be analysed must defined on a rectangular grid of cells. The method can also analyse the sloping sides of trapezoidal or re-entrant composite slabs by using configuration factors given below.

The thermal properties of steel and concrete used by the FRACOF software are based on the values given by EN1994-1-2.

The thermal actions are calculated on the basis of the net heat flux, $\dot{h}_{net}$ to which the surface of the member is exposed. The net heat flux is determined considering the heat transfer by convection and radiation.

$$\dot{h}_{net} = \dot{h}_{net,c} + \dot{h}_{net,r} \tag{12}$$

The net convective heat flux component is determined as follows:

$$\dot{h}_{net,c} = \alpha_c \left(\theta_g - \theta_m\right) \tag{13}$$

Where

α_c is the coefficient of heat transfer by convection

θ_g is the gas temperature

θ_m is the surface temperature of the member

When carrying out a thermal analysis for a member exposed to the standard temperature –time curve the coefficient of heat transfer by convection on the exposed face is taken as $\alpha_C = 25$ W/m^{2}K.

For nature fire models the coefficient of heat transfer by convection is increased to $\alpha_C = 35$ W/m^{2}K.

On the unexposed side of the slab the net heat flux is based on heat transfer by convection , but the coefficient of heat transfer by convection is taken as $\alpha_C = 9$ W/m^{2}K, to allow for the effects of heat transfer by radiation which are not considered explicitly in the model.

The net radiative heat flux is determined from the following formula

$$h_{net,r} = \Phi \varepsilon_m \varepsilon_f \sigma \left[\left(\theta_r + 273\right)^4 - \left(\theta_m + 273\right)^4\right] \tag{14}$$

Where

Φ is the configuration factor

ε_m is the surface emissivity of the member

ε_f is the emissivity of the fire

σ is the Stephan Boltzmann constant (5,67 x 10^{-8} W/m^{2}K^4)

θ_r is the effective radiation temperature of the fire

θ_m is the surface temperature of the member

The emissivity of the fire is taken as $\varepsilon_f = 1.0$ in accordance with the recommended value in EN1994-1-2. The emissivity of the member may be determined from Table 6.4~~Table 5.1~~.

6.5.1 Configuration Factors

For steel decking profiles the following configuration factors are used to modify the net heat flux incident on each surface. The locations in which the following factors are applied are shown in Figure 6.10~~Figure 5.17~~ for trapezoidal deck profiles and in Figure 6.11~~Figure 5.18~~ for re-entrant deck profiles.

Trapezoidal Profiles

The bottom flange of the trapezoidal profile is assumed to have a configuration factor of 1.0. For the top flange the configuration factor, Φ_{TOP}, is calculated as follows.

$$\Phi_{TOP} = \frac{2\tan^{-1}\left(\frac{h}{2(p-b_1)}\right)}{3.14}$$

Similarily for the sloping web of the trapezoidal profile, the configuration factor, Φ_{SIDE}, is calculated as follows,

$$\Phi_{SIDE} = 0.5\frac{L}{x+y}$$

Re-entrant Deck

The bottom flange of re-entrant steel profiles is assumed to have a configuration factor of 1.0. The configuration factor for the surfaces of the re-entrant dovetail is calculated as follows,

$$\Phi_{INT} = 0.3\frac{L}{x+y}$$

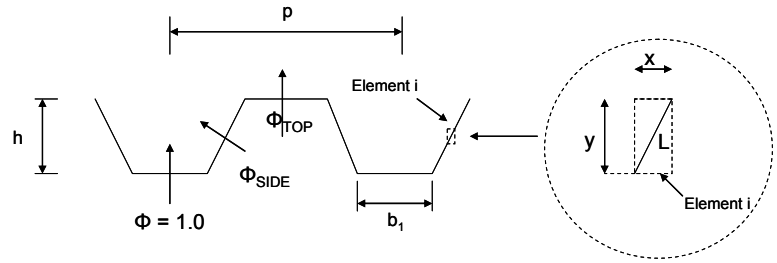

Figure 6.10 *Configuration Factors for trapezoidal decks*

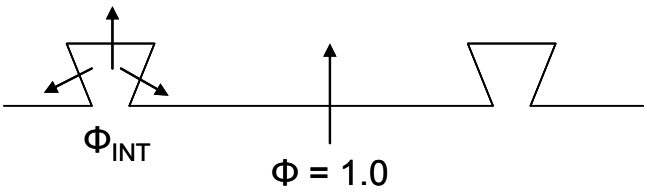

Figure 6.11 *Configuration Factors for re-entrant decks*

6.5.2 Material Properties

The following material properties are used for steel and concrete. These values are based on the recommendations of EN1994-1-2. Table 6.4~~Table 5.1~~ shows the values of surface emissivity, density and moisture content used for steel, normal weight concrete and light weight concrete.

Table 6.4 *Material properties for steel and concrete*

	Steel	NWC	LWC
Emissivity, ε_m	0.7	0.7	0.7
Density, ρ	7850	2300	1850
% moisture by mass	0	4	4

The specific heat capacity of steel, C_a, for all structural and reinforcing steel is given by the following temperature dependant formulae:

$$C_a = 425 + 0.773\theta - 0.00169\theta^2 + 0.00000222\theta^3 \quad \text{(J/kg K)} \quad \text{for } 20°C \le \theta \le 600°C$$

$$C_a = 666 - \frac{13002}{(\theta - 738)} \quad \text{(J/kg K)} \quad \text{for } 600°C \le \theta \le 735°C$$

$$C_a = 545 - \frac{17820}{(\theta - 731)} \quad \text{(J/kg K)} \quad \text{for } 735°C \le \theta \le 900°C$$

$C_a = 650$ (J/kg K) for $900°C \le \theta \le 1200°C$

The following temperature dependant values of specific heat capacity, C_c, are used for normal weight dry concrete with siliceous of calcareous aggregates.

$C_c = 900$ (J/kg K) for $20°C \le \theta \le 100°C$

$C_c = 900 + (\theta - 100)$ (J/kg K) for $100°C \le \theta \le 200°C$

$C_c = 1000 + (\theta - 200)/2$ (J/kg K) for $200°C \le \theta \le 400°C$

$C_c = 1100$ (J/kg K) for $400°C \le \theta \le 1200°C$

As recommended by EN1994-1-2 the following temperature independent value of specific heat capacity is assumed for lightweight concrete.

$C_c = 840$ (J/kg K) for all temperatures

The thermal conductivity of steel is defined using the following temperature dependent relationship.

$\lambda_a = 54 - 0.033(\theta - 20)$ but not less than 27.3 (W/mK)

For normal weight concrete the upper limit of thermal conductivity as defined by EN1994-1-2 has been used. The thermal conductivity for normal weight concrete is determined from the following temperature dependent relationship.

$\lambda_C = 2 - 0.2451(\theta/100) + 0.0107(\theta/100)^2$ (W/mK)

The thermal conductivity of lightweight concrete is also temperature dependent and is given by the following formula.

$\lambda_C = 1 - (\theta/1600)$ but not less than 0.5 (W/mK)

6.5.3 Internal heat transfer by conduction

The thermal analysis computes the conducted heat transfer between a cell and the four cells above, below and to the sides (Figure 6.12). No other cells are involved.

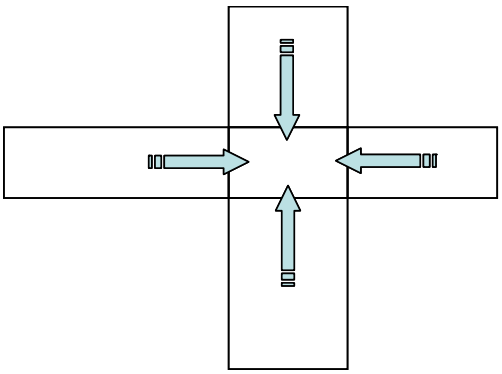

Figure 6.12 *Basis of conductive heat transfer*

The heat transferred per unit time depends on the sizes of the cells, the temperature of each cells and the thermal conductivity of each cell. Each pair of cells are considered in turn and the net heat transferred into or out of a cell is computed. The basic conduction model is illustrated in Figure 6.13.

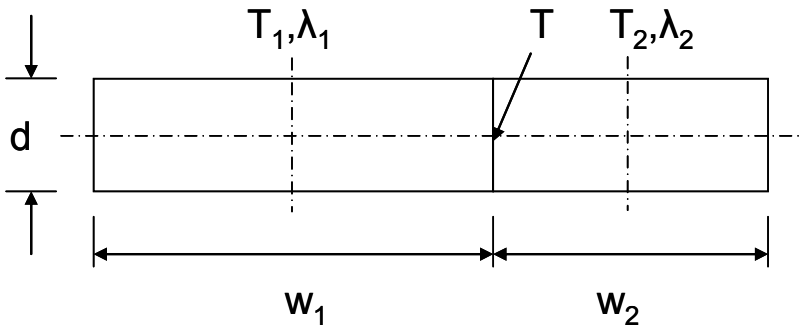

Figure 6.13 *Basic conduction model*

The temperature of each cell is defined at its centre (T_1, T_2). The temperature of the interface between the cells is T. The heat transfer from cell 1 to the interface is the same as the heat transfer from the interface to cell 2. The thermal conductivities of each cell are λ_1 and λ_2.

The heat transfer per unit time from the centre of cell 1 to the interface is:

$$h = \frac{2D\lambda_1}{w_1}(T - T_1)$$

This is equal to the heat transfer per unit time from the interface to the centre of cell 2:

$$h = \frac{2D\lambda_2}{w_2}(T_2 - T)$$

Thus, by eliminating the interface temperature, T:

$$h = \frac{(T_2 - T_1)}{\left(\frac{w_1}{2D\lambda_1} + \frac{w_2}{2D\lambda_2}\right)} \text{ per unit time}$$

This equation is used to compute the heat transfer between all cells. For each cell, the value of:

$$\frac{w}{2D}$$

is precalculated. The value of thermal conductivity will often vary with temperature and is calculated at preset intervals (normally 30 seconds) to speed up computation.

6.5.4 Design temperatures for unprotected steel beams

The design temperature of the unprotected steel beams are calculated based on the simple method given in EN1994-1-2 Section 4.3.4.2.2. The increase in steel temperature during a small time interval is calculated using the following equation.

$$\Delta\theta_{a,t} = k_{shadow}\left(\frac{1}{c_a \rho_a}\right)\left(\frac{A_i}{V_i}\right)\dot{h}_{net}\,\Delta t$$

Where

k_{shadow} is the correction factor for shadow effect

ρ_a is the density of the steel

Δt is the time interval

A_i/V_i is the section factor for part i of the cross section

The FRACOF software calculates the steel temperature for the bottom flange of the section for time increments of 2.5 seconds. The correction factor for the shadow effect is taken as 1.0.

The section factor for the bottom flange is expressed as a function of flange thickness, e_1, as follows

$$A_i/V_i = \frac{2000}{e_1}$$

The material properties are given in Section 6.5.2~~5.4.2~~.

The net heat flux is calculated as shown in Equation 12, with the convective and radiative components calculated as shown by Equations 13 and 14 respectively. When calculating the radiative heat flux using Equation 14 the configuration factor should be taken as 1.0.

7 FIRE RESISTANCE TEST OF A FULL SCALE COMPOSITE FLOOR SYSTEM

7.1 Scope

As described in the Section 5, the simple design method was developed mainly on the basis of full scale natural fire tests in which floors were subjected to fully developed compartment fires. The design concept could also be applied in principle to fire design using the standard temperature-time curve. However, several questions require further investigation, such as the influence of:

- long duration fires (up to 120 minutes)
- different construction details
- the effect of higher values of design actions

These considerations resulted in a furnace fire test being undertaken as part of the FRACOF project. This latter was intended to provide experimental evidence about the behaviour of composite steel and concrete floors exposed to the standard temperature-time curve and to enlarge the application of the design concept based on membrane action. In addition, in order to investigate the fire resistance of connections between concrete slab and steel members at the edge parts of composite floor subjected to large deflection under membrane action, another furnace fire test was carried out in the framework of COSSFIRE project. The tests were conducted on two different full scales composite steel and concrete floor specimens in accordance with EN1365-2. The observed fire performance of these floor systems during the tests was extremely satisfactory and revealed a solid robustness of such type of structure systems in fire situation.

7.2 FRACOF Test

7.2.1 Test specimen

The arrangement of the test specimen is shown in Figure 7.1. The composite steel and concrete floor was composed of four secondary beams, two primary beams, four short columns and a 155 mm thick floor slab.

The test specimen was designed to achieve 120 minutes fire resistance. The beams framing into the column positions were fire protected and the secondary beams in the centre of the floor slab were left unprotected. The load bearing capacity of the test specimen was calculated in accordance with the simple design method, treating the test specimen as a floor design zone, see Section 6. This design showed that locating a steel reinforcing mesh with an area of 256 mm^2/m in both directions 50 mm below the top surface of the slab would provide adequate load bearing capacity. The simple design method predicted that the test specimen would have a load bearing capacity of 7.58 kN/m^2, following 120 minutes exposure to the standard temperature-time curve. The thickness of the slab was selected in order to fulfil the insulation requirements for 120 minutes fire resistance in accordance with the guidance given in EN 1994-1-2[(33)].

The steel beams were connected to the concrete slab with headed studs. Beam to column joints were made using flexible endplates (to the flanges of the column) and double angle cleats (to the column web). Beam to beam joints were fabricated from double angle cleats (Figure 7.2). The composite steel and concrete slab was

constructed with 0.75mm thick COFRAPLUS60 steel decking which has a trapezoidal profile. This steel decking is commonly used in the French market. This deck has a small volume of concrete in the ribs and is therefore likely to heat up more quickly in a fire than other decks with a similar geometry.

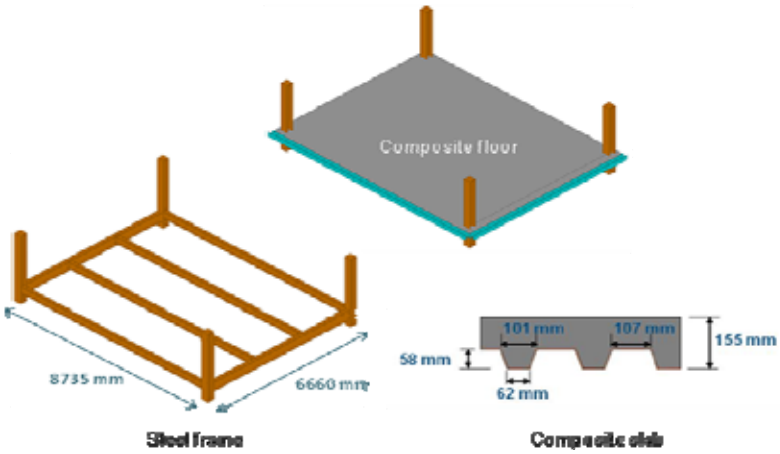

Figure 7.1 *Fire test set-up*

The dimensions of the test specimen were:

- span of secondary beam: 8.735 m
- span of primary beam: 6.66 m
- span of composite slab: 2.22 m
- total length of each steel column: 2.5 m, with 0.8 m below composite slab

The following characteristic values of actions were considered in the design of the structural members for this floor:

- Permanent action: self weight of the structure plus 1.25 kN/m² for non-structural elements.
- variable action: 5.0 kN/m²

For room temperature design, the following combination of actions was considered in accordance with EN1990.

$$\sum \gamma_{G,j,\text{sup}} G_{k,j,\text{sup}} + \gamma_{Q,1} Q_{k,1}$$

Where

$\gamma_{Gj,\text{sup}}$ is the partial factor for permanent action, j (taken as 1.35)

$G_{k,j,\text{sup}}$ is the permanent action, j

$\gamma_{Q,1}$ is the partial factor for the leading variable action (taken as 1.5)

$Q_{k,1}$ is the leading variable action.

On the basis of the above loading, the cross sections of all steel members and the shear connection of the composite beams was verified in accordance with the requirements of EN 1994-1-1[34] for room temperature design of composite structures. The steel joints were designed according to the requirements of EN 1993-1-8[35]. The following section sizes were selected for the main structural members:

- secondary beams: IPE300 with the steel grade of S235
- primary beams: IPE400 with the steel grade of S355
- columns: HEB260 with the steel grade of S235

Normal weight Grade C30/37 concrete was used for the floor slab.

(a) Beam to column joints with flexible end plates and double angle web cleats

(b) Beam to beam joints with double angle web cleats

Figure 7.2 *Steel member joints*

Actual material properties of the steel and concrete were measured at room temperature. Nominal and measured values are given in Table 7.1.

Table 7.1 *Material properties of tested elements*

Type of material	Mechanical property items			
Secondary Beams Grade S235	Yield stress (MPa)		Ultimate tensile strength (MPa)	Measured maximum elongation
	Nominal	Measured	Measured	31.6 %
	235	311	446	
Primary Beams Grade S355	Yield stress (MPa)		Ultimate tensile strength (MPa)	Measured maximum elongation
	Nominal	Measured	Measured	29.9 %
	355	423	549	
Steel Reinforcing mesh Grade B500A	Yield stress (MPa)		Ultimate tensile strength (MPa)	Measured maximum elongation
	Nominal	Measured	631	15.5 %
	500	594		
Concrete C30/37	Compressive strength (MPa)			
	Characteristic value		Measured value	
	30		36.7	

The shear connectors were studs with a diameter of 19 mm and a height of 125 mm, the distribution of which is shown in Figure 7.3.

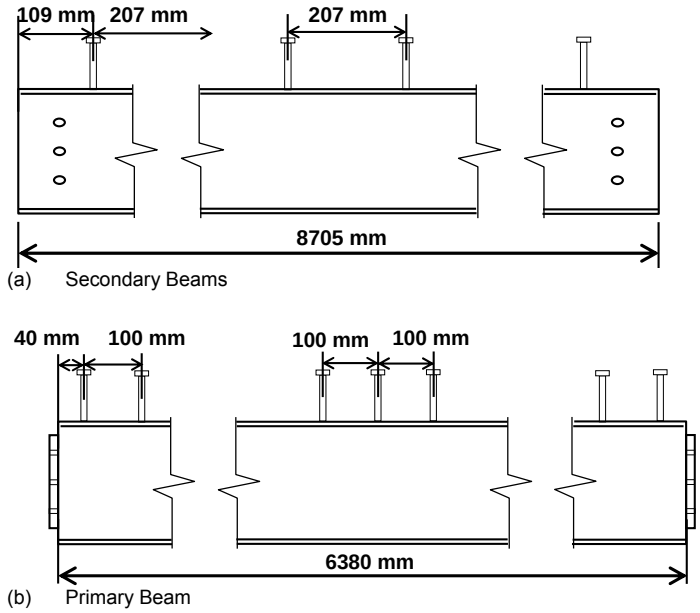

Figure 7.3 *Distribution of shear connectors for steel beams*

The reinforcing steel mesh was located at 50 mm from the top of the slab. The mesh was formed of 7 mm diameter bars, with a steel grade of S500, spaced at 150mm centres in both directions. Additional 10 mm diameter reinforcing bars were used for the edge steel and concrete composite connection (see Figure 7.4).

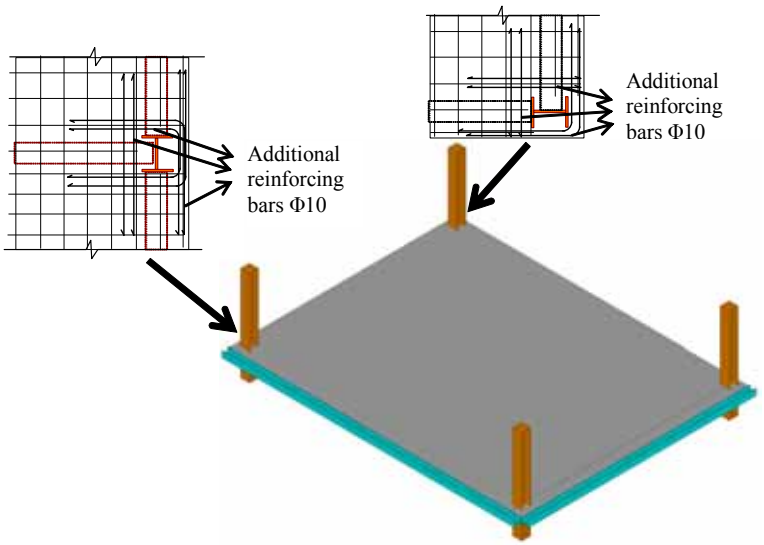

Figure 7.4 *Connection configurations investigated in the fire test*

7.2.2 Test methodology

During the fire test, the mechanical loading on the floor was applied with fifteen sand bags uniformly distributed over the floor (see Figure 7.5). Each sand bag weighed exactly 15.0 kN, equivalent to a uniform load of 3.87 kN/m². This value is slightly higher than a design value of 3.75 kN/m² for the Eurocode combination of actions for office buildings in a fire situation, using the recommended value of 0.5 for the combination factor, ψ_1.

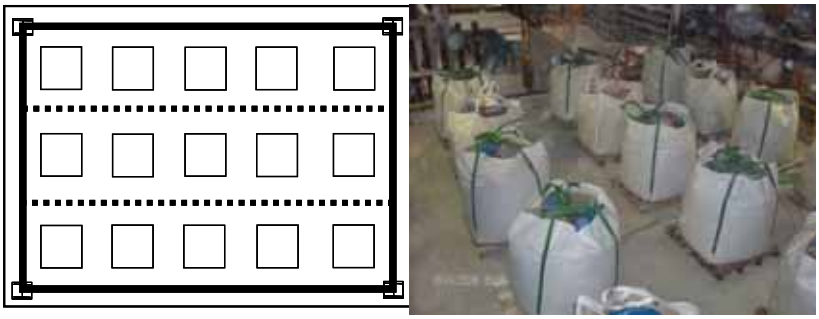

Figure 7.5 *Loading of the floor with sand bags*

In conformance with the simple design method described in Section 5 for this type of floor, the two secondary beams and the composite slab were unprotected. However, all the boundary beams on the perimeter of the floor design zone (all beams connected directly to the columns) and all of the columns were fire protected to ensure that they maintained their structural stability in the fire situation. All the joints were also protected. The fire protection material used was two layers of mineral fibres blanket [25 mm-128 kg/m^3]. The reinforcing steel mesh at two sides of the slab was welded to two steel beams placed along the edge

of the slab as shown in Figure 7.4. These beams were in turn fixed to the furnace structure in order to simulate the continuity condition of the composite floor.

A total of 194 measurement locations were used to record the behaviour. The main measurements were the temperature and the deflected shape of the floor. Approximately 170 thermocouples were used to monitor the temperature of the steel frame (see Figure 7.6 and Figure 7.7) and the temperature distribution of the slab (see Figure 7.8 and Figure 7.9). Seven displacement transducers were installed to measure the vertical deflection of the floor (see Figure 7.10). Two other transducers were used to measure the horizontal movement of the floor. A special high temperature video camera was put inside the furnace to record visually the floor deformations with time.

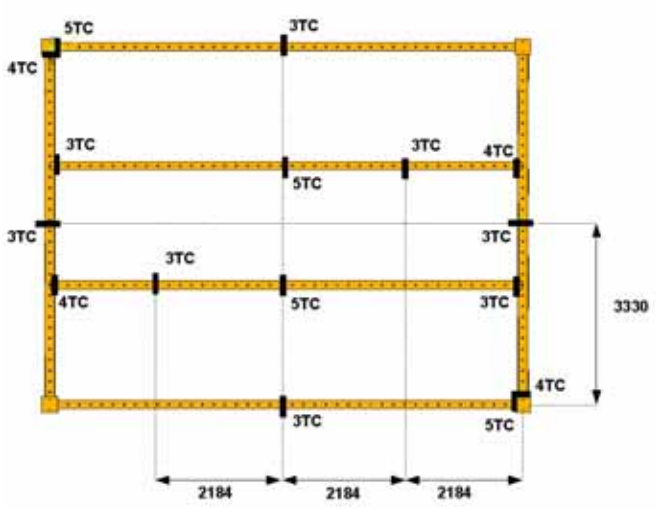

Figure 7.6 *Location of thermocouples on the steel frame*

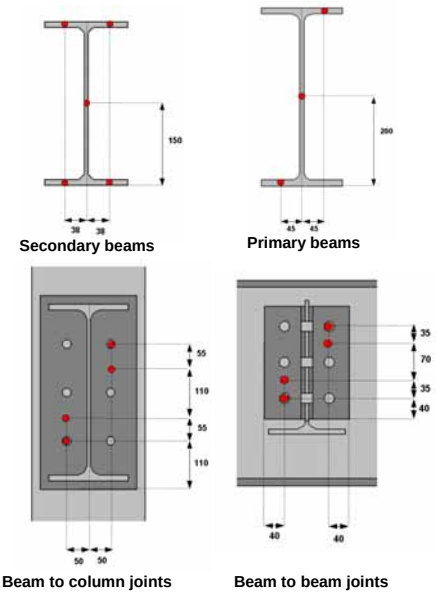

Figure 7.7 *Location of thermocouples on each instrumented steelwork cross section*

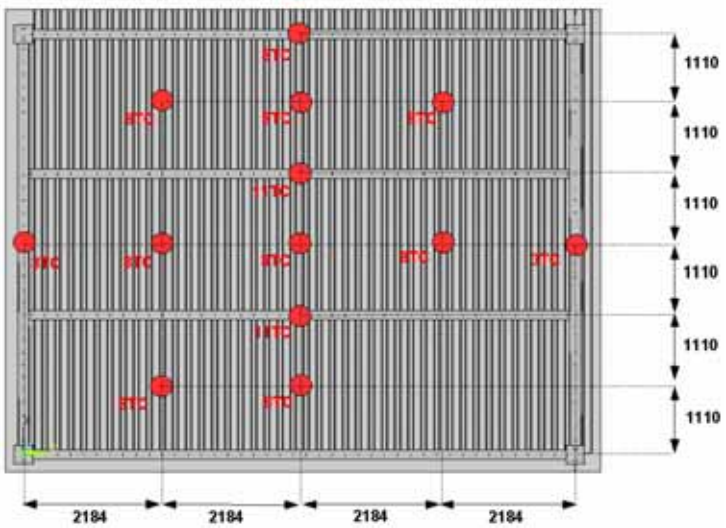

Figure 7.8 *Locations and numbers of thermocouples in the composite slab*

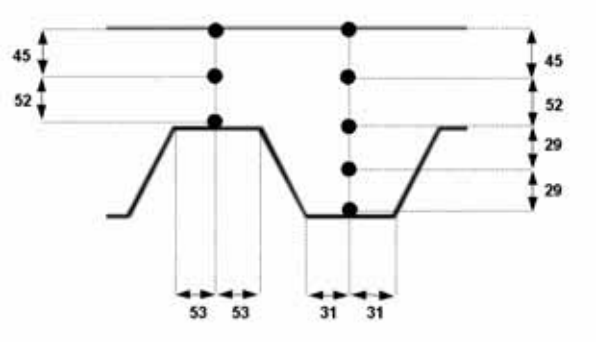

Figure 7.9 *Typical cross section through composite slab showing thermocouple locations*

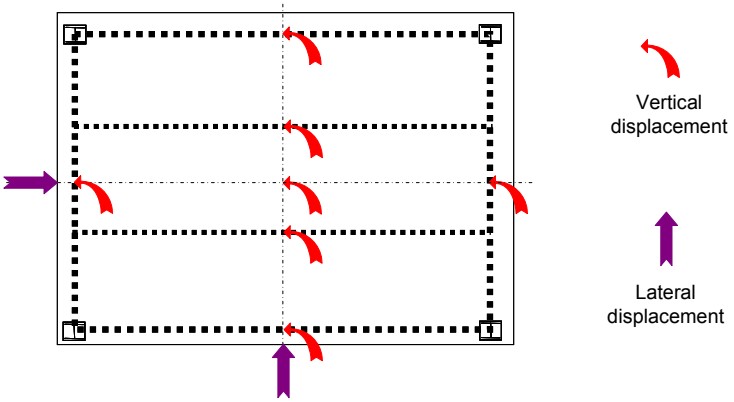

Figure 7.10 *Location of displacement transducers*

7.2.3 Results

The test lasted for more than 120 minutes and the fire was stopped following integrity failure of the floor. However, the recording of specimen's behaviour continued until 900 minutes, allowing the performance of the floor during the cooling phase to be monitored.

Temperature variation in structure

During the test, the furnace temperature was controlled with plate thermocouples in accordance with the recommendations of EN1363-1. These plate thermocouples were located just below the floor and the recorded temperatures from these instruments showed that the furnace temperature was controlled within the tolerances permitted by the fire testing standard EN1363-1 (see Figure 7.11).

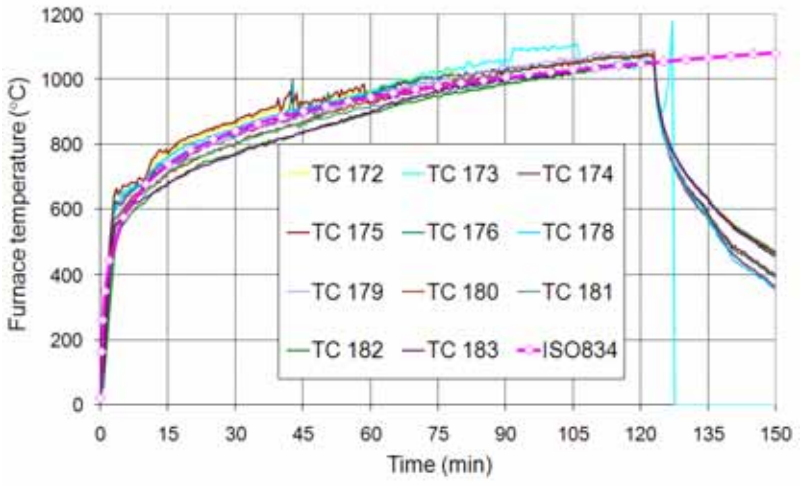

Figure 7.11 *Furnace temperature versus standard temperature-time curve*

Measurements of the temperature at the mid-span of the composite beams were taken on the bottom flange, the web and upper flange of each section. A summary of the temperatures recorded in the beams is presented in Figure 7.12 and Figure 7.13. The unprotected steel beams reached a maximum temperature of 1040°C. In contrast, the protected steel beams reached a maximum temperature of 300°C; this temperature is lower than would be expected in practice, due to the reduced exposure of these members located at the edge parts of the furnace.

A summary of the temperatures recorded in the composite slab is presented in Figure 7.14. The temperatures of points A and B where not recorded because the thermocouples fixed to steel sheet failed early in the test, probably due to debonding between the steel sheet and the concrete once exposed to fire. Debonding of the steel sheet was observed over a large proportion of the soffit of the composite slab. The temperature recorded at the unexposed side of the composite slab is shown in Figure 7.15. The temperature rise at the unexposed face of the composite slab after 120 minutes of fire was slightly above 100°C, which is less than the upper limit of 140°C that defines the insulation criterion.

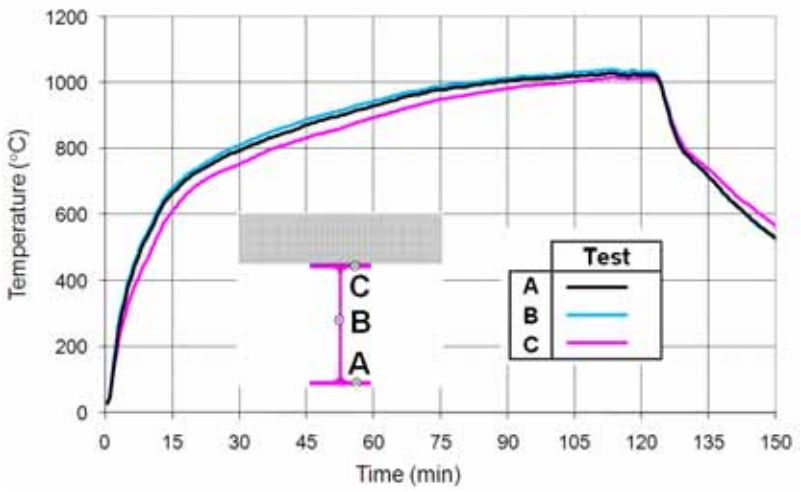

Figure 7.12 *Heating of unprotected steel beams*

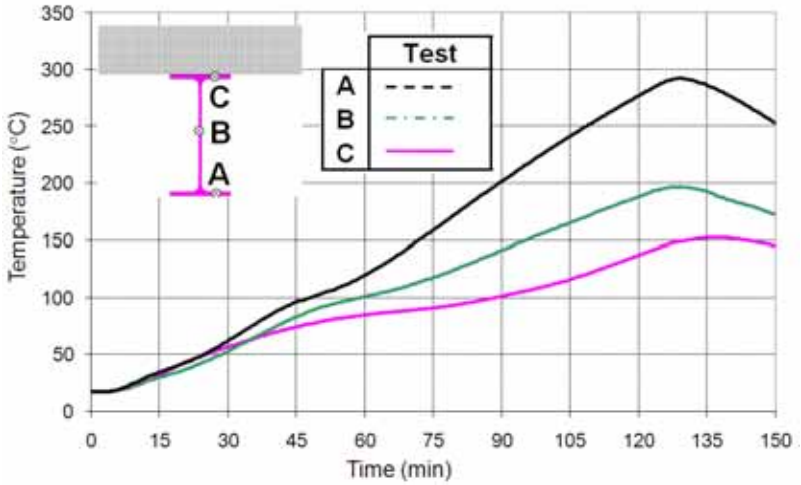

Figure 7.13 *Heating of protected steel beams*

Printed 11/07/10~~12/04/10~~

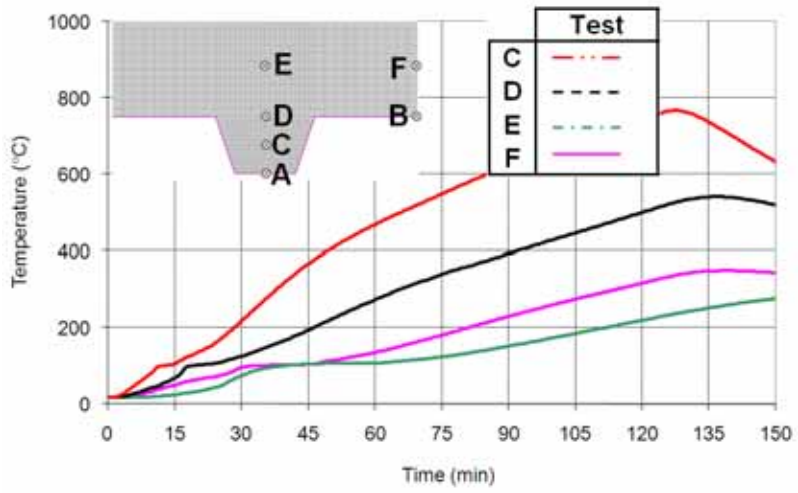

Figure 7.14 *Heating of composite slab*

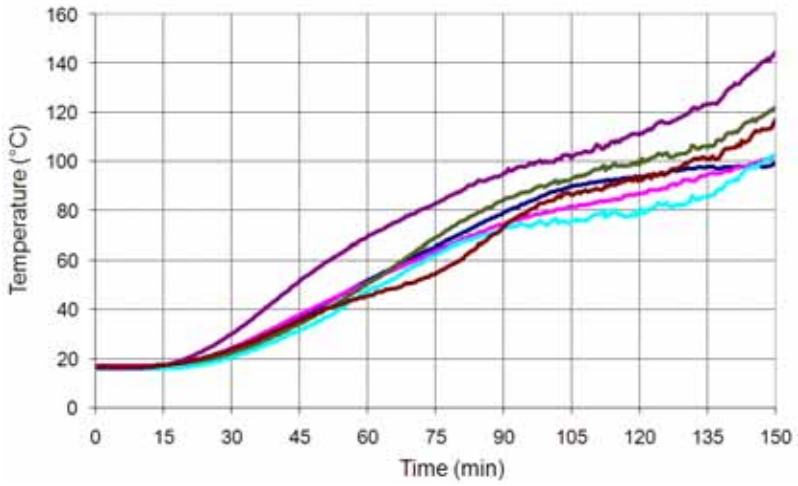

Figure 7.15 *Temperatures recoded at unexposed side of the composite slab*

Displacement variation of the structural members

Figure 7.16 shows the vertical displacements of the floor over the whole period of test. The decrease of deflection after about 120 minutes corresponds to the time when the burners of the furnace were switched off. A more detailed illustration of these displacements, mainly during the heating phase of the test, is given in Figure 7.17. It can be observed that the maximum deflection of the floor is about 450 mm and the deflections measured at the two unprotected secondary beam positions were approximately 420 mm, less than one twentieth of their span. During the cooling phase, the deflection increased slightly and reached a maximum

value at about 135 minutes. Although the furnace temperature had dropped from 1050°C to only 600°C (see Figure), heat was still being conducted through the thickness of the composite slab and at this time the maximum temperature of the mesh was reached (see Figure 7.14).

The fire protected beams located on the perimeter of the test specimen only reached a temperature of 300°C. As steel retains 100% of its room temperature yield stress at 300°C, the deflection of these beams is lower than expected, with a maximum of 100mm deflection measured at the mid span of secondary beams. In practice it would be reasonable to assume that the critical temperature for these beams would be between 500°C and 600°C with a deflection in excess of span/30.

If more attention is paid to the evolution of the deflection of the floor, one can find that it increased very rapidly during the first 20 minutes of fire and then increased with nearly a constant speed. If this deflection is related to the heating of unprotected beams, it can be found also that these beams were heated gradually up to about 700 °C. Obviously their flexural load bearing capacity with this level of heating would no longer allow them to bear the applied load alone. In consequence, the membrane effect of the floor was progressively activated, to maintain the global stability of the floor. This tensile membrane effect was also clearly illustrated through the measurement of the lateral displacement at the edge of the floor, shown in Figure 7.18. Once again, one can find that following 15 minutes of fire, the edge part of the floor moved inwards due to the tensile membrane effect. The sudden increase of this displacement at around 105 minutes could be explained by the important failure of reinforcing steel mesh in the central part of the floor (for more details, see Section 7.4.3).

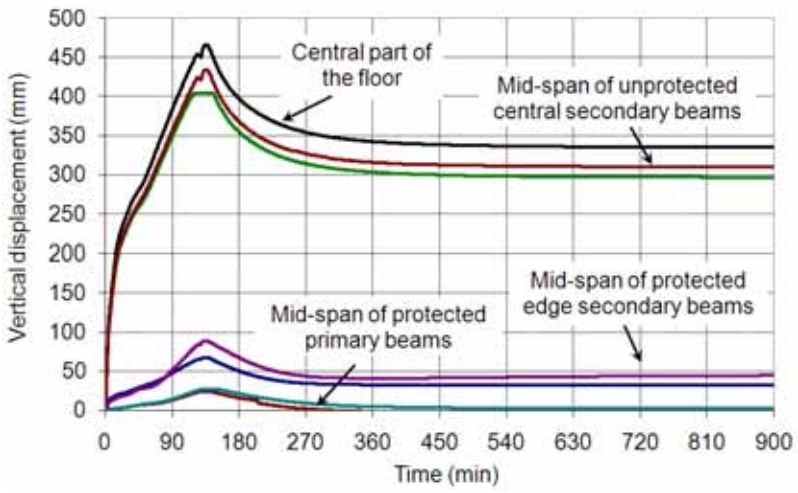

Figure 7.16 *Deflection of the floor recorded during the whole period of test*

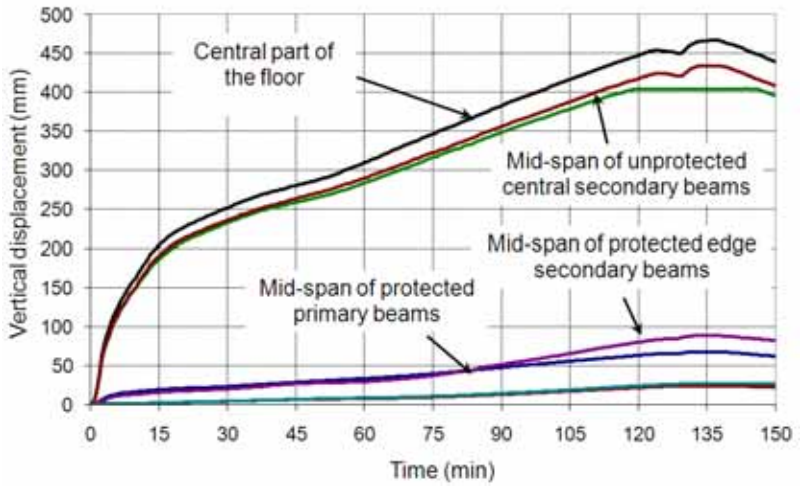

Figure 7.17 *Deflection of the floor recorded during the heating period of test*

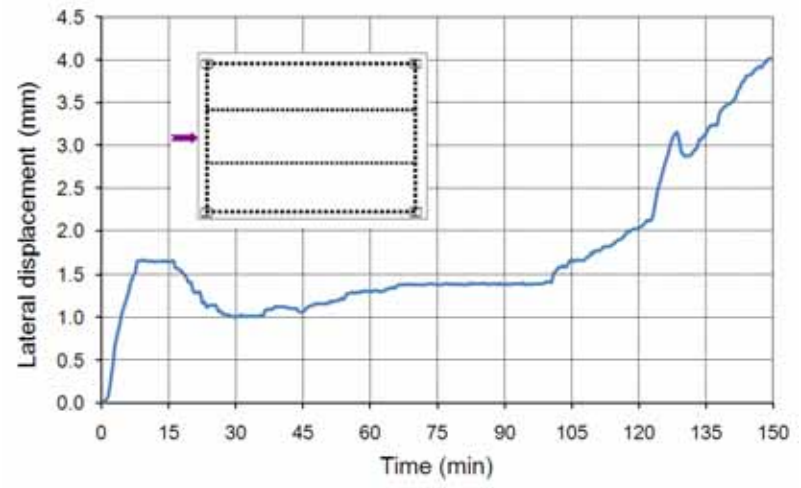

Figure 7.18 *Lateral displacement at the edge of the floor recorded during the heating period of test*

Behaviour of composite slab observed during the test

The main observations regarding cracking of the concrete slab were:

- Small cracks occurred in the concrete, particularly around steel columns and continuous edges of the slab, at an early stage of the fire test, as shown in Figure 7.19(a).
- There was some enlargement of these cracks during the heating phase of the test, but this did not significantly influence the integrity performance of the floor (see Figure 7.19(b)).

- A more significant crack occurred in the central part of the floor after 105 minutes of fire exposure, as shown in Figure 7.20.

Investigation of the central crack after the test showed that the crack was caused by the failure of a welded joint between two steel reinforcing meshes, as shown in Figure 7.21. As the simple design method relies on being able to stress the reinforcement to it ultimate failure load across the centre of the slab, full tension laps must be provided at all joints between sheets of mesh reinforcement. This type of failure can be avoided if construction details in accordance with EN 1992-1-1[36] are adopted.

As the test specimen did not reach the point of collapse during the test, the occurrence of such an important crack and failure of steel reinforcing mesh in the longitudinal direction at the central part of the floor did not affect its load bearing capacity.

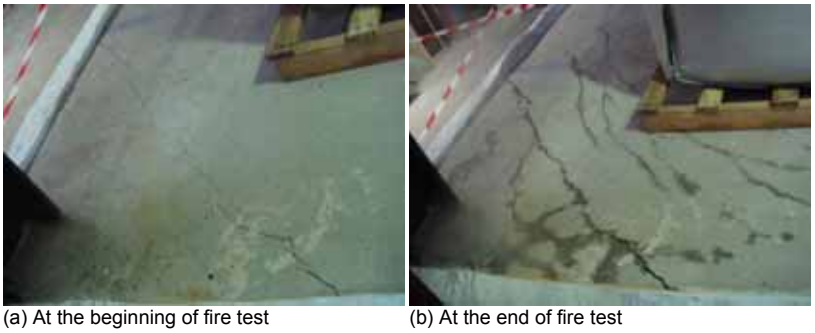

(a) At the beginning of fire test (b) At the end of fire test

Figure 7.19 *State of slab around steel column*

(a) State of the cracking at central part of the floor (b) State of the cracking after cooling

Figure 7.20 *State of slab at central part of the floor during and after the test*

(a) Welded reinforcement joint prior to the concrete casting

(b) State of the reinforcement joint at the location of the crack after cooling

Figure 7.21 *Joint of reinforcing steel meshes before and after test*

7.2.4 Comments on the test results

The test results have demonstrated the adequate performance of a composite floor slab designed in accordance with the simple design method. The remarks derived from test results regarding the fire performance of the floor are:

- even with unprotected secondary steel beams of a span of 8.735 m, the load bearing criterion (R) was fulfilled for a period of more than 120 minutes,
- the integrity criterion (E) and the insulation criteria (I) were fulfilled for a period of 105 minutes. Failure was due to the formation of a crack across the composite slab due to premature failure of reinforcing steel mesh, see Section 0.0.0~~7.4.3~~.
- the whole floor remained structurally very robust under a long duration fire, despite the failure of steel mesh reinforcement in the concrete slab,
- it must be ensured that the reinforcing mesh is properly overlapped to activate the membrane action / to ensure continuity of load transfer, especially in the region of unprotected beams and around columns
- the concrete cracking at the edge of the floor was very limited and had no influence on the integrity and insulation performance of the floor,
- the floor behaved satisfactorily during the cooling phase of fire.
- the steel joints were all adequately protected and their maximum heating was limited to around 500°C. All joints between steel members performed very well during both heating and cooling phases.

7.3 COSSFIRE Fire test programme

7.3.1 Test specimen

In the scope of COSSFIRE project, another specific composite floor as shown in **Chyba! Nenalezen zdroj odkazů.**~~Figure 7.22~~ was fire tested. For this floor, the cross sections of steel beams and steel columns are respectively in IPE270 and HEB200. The nominal steel grade of all these structural members is S235. The design of this floor system was undertaken in accordance with the requirements of EN1994-1-1[34] for room temperature design of composite structures with a permanent load of 1.25 kN/m² in addition to self weight of the structure and a live load of 5.0 kN/m². The fire test was conducted with a load of 3.93 kN/m² which corresponds approximately to 100% of various permanent actions and 50% of live actions according to Eurocode load combination in fire situation for office buildings. As far as steel joints are concerned, they are designed according to the requirements of EN1993-1-8[35].

The composite slab was made of normal-weight in-situ concrete with a concrete quality of C30/37. The total depth of the slab was 135 mm and the profiled steel sheet is COFRAPLUS60 (trapezoidal). With respect to shear connectors, they were all in headed studs with a diameter of 19 mm and a height of 125 mm and their distributions over steel beams are respectively one stud every 207 mm for secondary beams and one stud every 300 mm for main beams. The reinforcing steel mesh located at 35 mm from the top of the slab is in grade S500 and has a diameter of 7 mm. Its grid size is 150 mm x 150 mm.

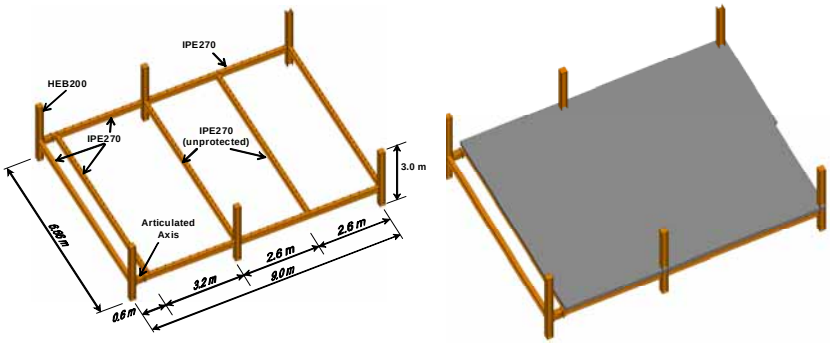

a- View over the steel frame b- View over the composite floor

Figure 7.22 *Fire test set-up*

The real mechanical properties of used materials in this test are summarised in Table C.1 given below.

Table 7.2 *Material properties of COSSFIRE tested elements*

Item	Value
Steel grade of main beams	320 MPa
Steel grade of secondary beams	320 MPa
Steel grade of reinforcing steel	590 MPa
Compressive strength of concrete	38.0 MPa

In compliance with the existing simple engineering design method of such a type of floor under membrane action, the two intermediate secondary beams and the composite slab are unprotected. However, all the boundary beams of the floor are fire protected for a fire rating of 120 minutes. The steel columns were also protected except the protection around the joints which was intentionally reduced so that the heating of the joint components was important enough during heating phase in order to investigate the impact of such heating on their behaviour during cooling phase.

In order to investigate the behaviour of connections between concrete slab and steel members at the edge parts of composite floor in fire, six edge connection configurations were adopted with this floor, as shown in **Chyba! Nenalezen zdroj odkazů.** ~~Figure~~ 7.23.

The mechanical load during fire was applied with help of twenty sand bags uniformly distributed over the floor. Each of these sand bags weighs exactly 11.0 kN, leading together with wood pallet and lightweight concrete blocks to an equivalent uniform load of 3.93 kN/m². As far as thermal load is concerned, the ISO standard fire curve was imposed until the moment that the collapse of the floor begin to occur. However, the recording of test results was maintained during the cooling phase in order to know the behaviour of the floor during the whole period of fire.

Figure 7.23 *Different steel and concrete composite connection configurations*

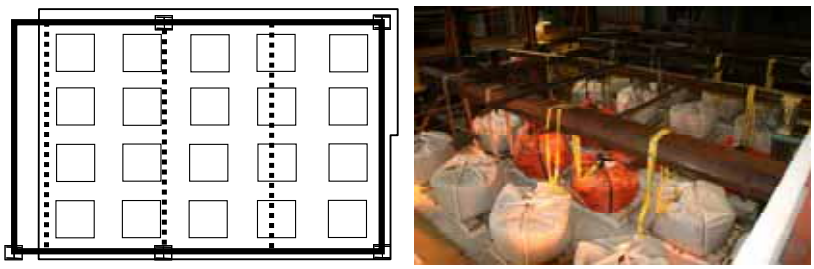

Figure 7.24 *Loading conditions of steel and concrete composite floor exposed to fire*

7.3.2 Measurement of test results

The main measurements of the test are related to temperature and the deflection of the floor. A total of 203 thermocouples of which 66 thermocouples on steel members (Figure 7.25), 80 thermocouples on connections (Figure 7.26) and 57 thermocouples in composite slab (see figures 7.27& 7.28) were used to record both the gas and specimen's temperatures. In addition, 20 displacement transducers of which 16 vertical displacement transducers were installed to measure the deflection of the floor (Figure 7.29). The four remained transducers were used to measure the horizontal movement of the floor. In addition, a special video camera was put inside the furnace which has recorded visually the floor deflections versus time.

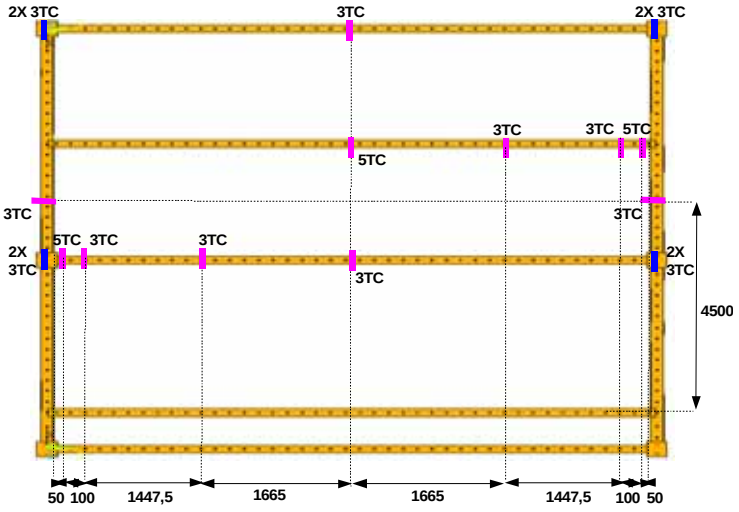

Figure 7.25 *Location of thermocouples on the steel frame*

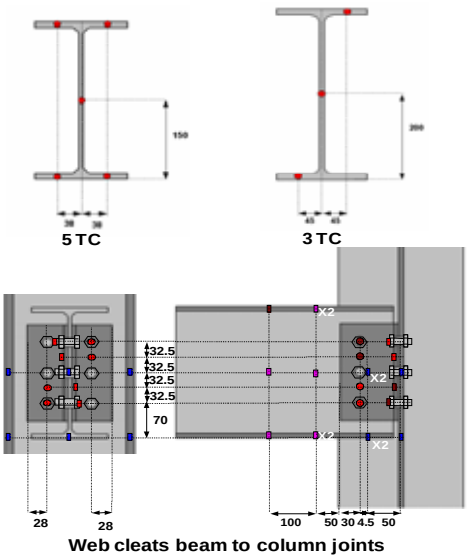

Figure 7.26 *Location of thermocouples on each instrumented steelwork cross section*

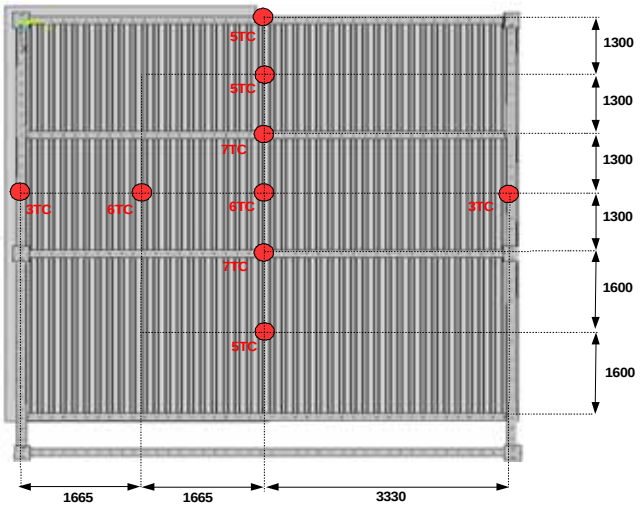

Figure 7.27 *Locations and numbers of thermocouples in the composite slab*

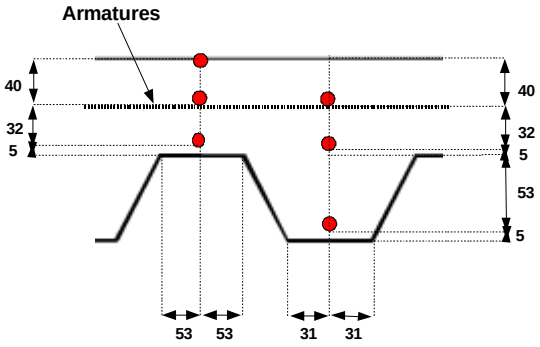

Figure 7.28 *Typical cross section through composite slab showing thermocouple locations*

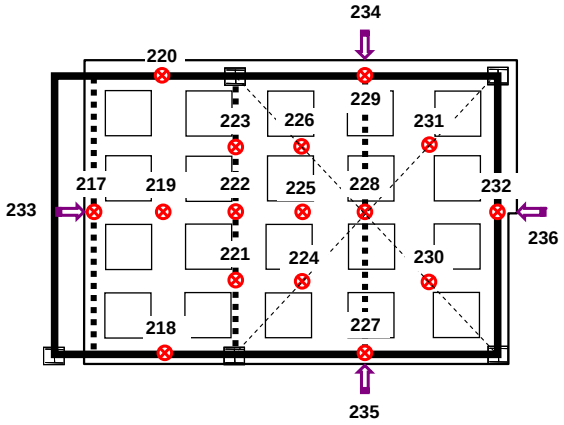

Figure 7.29 *Location of displacement transducers*

7.3.3 Principal experimental results

During the heating phase of this test, the ISO-834 fire curve was followed (Figure 7.30) which lasted for more than 120 minutes until the apparent collapse of one edge secondary beam linked to main beams (see D6 of Figure 7.36). After that, all burners were turned off and the furnace was cooled down naturally. As far as the heating of steel beams is concerned, it varied a lot according to the protection condition. In fact, the unprotected steel beams located at the middle of the floor were heated up to more than 1000 °C (Figure 7.31). On the contrary, the protected steel beams were heated up in general to around 550 °C (Figure 7.32) except one of the edge protected secondary beams which was significantly hotter than all other protected beams, certainly due to defective fire protection during test (Figure 7.33).

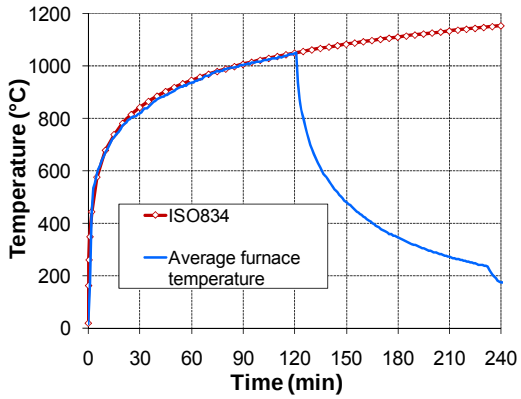

Figure 7.30 *Furnace temperature versus ISO fire curve*

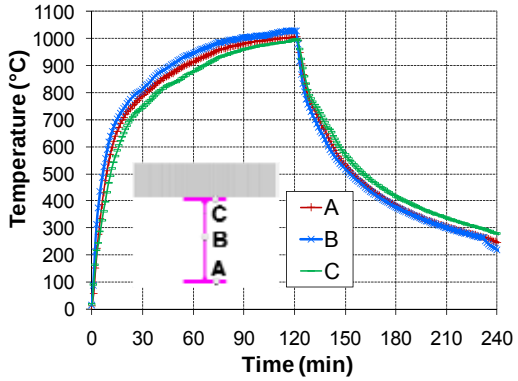

Figure 7.31 *Heating of unprotected secondary beams*

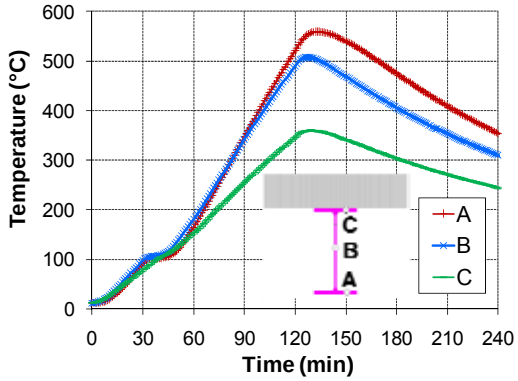

Figure 7.32 *Heating of one protected main beams*

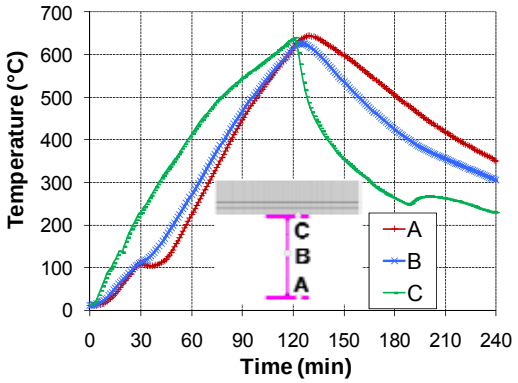

Figure 7.33 *Heating of collapsed edge beam*

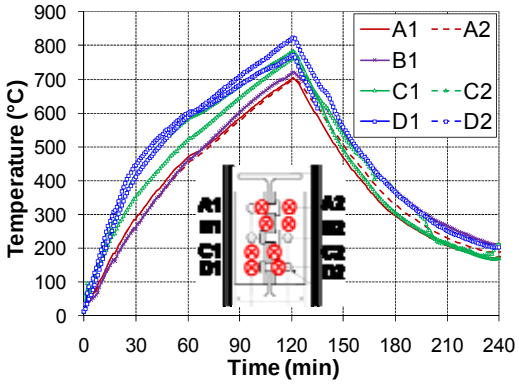

Figure 7.34 *Heating of collapsed edge beam*

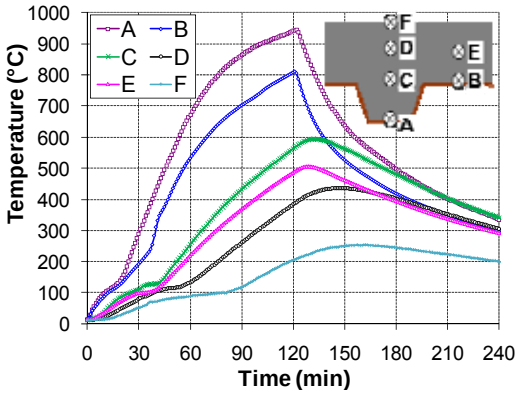

Figure 7.35 *Heating of collapsed edge beam*

Printed 11/07/10~~12/04/10~~

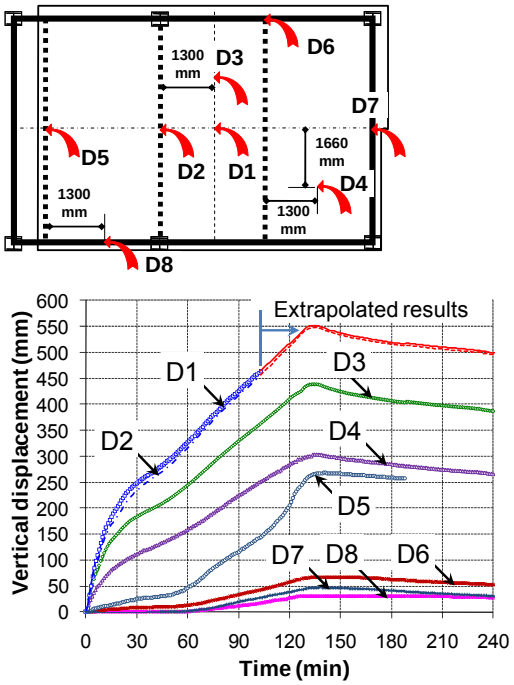

Figure 7.36 *Measured vertical displacements of the floor during the test*

As the steel joints in this test were not fully protected, some bolts of joints were heated up to more than 800 °C (Figure 7.34). From the temperature measurement in composite slab during the test, it can be found that the maximum temperatures at 5 mm from the exposed side of the composite slab were about 950 °C (Figure 7.35) and the reinforcing steel mesh was heated to about 500 °C. Moreover, the temperature measured at the unexposed side of the composite slab was more than 200 °C after more than 120 minutes of fire exposure which was beyond the insulation criteria.

During the test, the fire was stopped when it was observed that one edge beam was collapsing at around 120 minutes (see D6 in **Chyba! Nenalezen zdroj odkazů.**~~Figure~~ 7.36). As far as the global deflection of the floor is concerned, it increased significantly at the beginning until 30 minutes of fire and slowed down since. At 120 minutes of ISO standard fire, the total deflection of the floor could be more than 500 mm. Once the heating was stopped, the deflection of the floor continued to increase for a while (about 15 minutes) before decreasing definitely and slowly. Finally, the deflection recovery of the floor was about 100 mm.

7.3.4 Observation of the fire tests

From measured global deflection of the floor, it is fund that it increased very possibly to more than 500 mm after 120 minutes. However, the floor behaved still very well and there was no sign of failure in the central part of the floor. In fact, the fire was stopped due to an excessive deflection of the mostly heated secondary edge beam (Figure 7.37). A closer observation of this edge beam reveals that an important concrete crushing occurred at its mid-span, which means that this beam was really collapsing. Nevertheless, this failure did not lead to the collapse of the global floor owing apparently to load redistribution under membrane effect (see figure 7.38).

Local buckling of the unprotected secondary beam connected to central steel beams near joints is observed in its lower flange and web (see figure 7.39). However, the most remarkable feature from this test regarding the steel joints is that they all performed very well during both heating and cooling phases. Also, for unprotected secondary beams connected to steel main beams near joint, no local buckling can be found (Figure 7.40). In addition, no failure of the edge connections between concrete slab and steel members is observed.

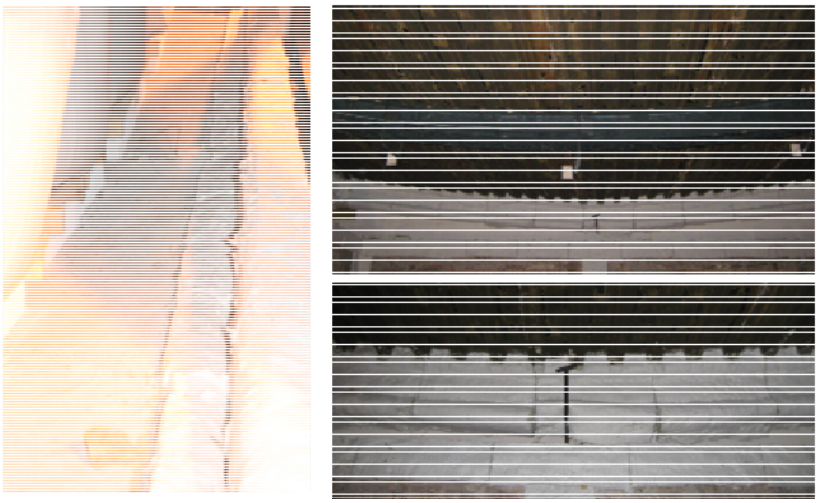

Figure 7.37 *Collapse of edge beam*

Figure 7.38 *Tested floor during and after the fire*

Figure 7.39 *Local buckling of unprotected secondary beams connected to*

column

Figure 7.40 *No local buckling of unprotected secondary beams connected to main beams*

Figure 7.41 *Cracking of concrete at corner parts of the floor*

Figure 7.42 *Cracking of concrete around central columns*

Figure 7.43 *Overlapping of reinforcing steel mesh in composite slab*

Another important feature to be mentioned here is the cracking of the composite floor around columns which could have a direct influence on fire performance of the floor. The main observed results in this respect are as follows:

- Concerning cracking of concrete at corner parts of the floor, it remained small and without any negative impact on integrity criteria (see figure 7.41).
- As for cracking of concrete around central columns, the important deflection of unprotected beam beneath created a large movement of slab toward inside and possible negative impact on integrity criteria can occur due to the opened crack in front of the column (see figure 7.42).
- There was no significant crack of concrete slab in the central part of the floor, which means that the reinforcing steel mesh behaved appropriately under membrane action even under a heating up to 500 °C. Such a good behaviour was without any doubt due to the appropriate overlapping of reinforcing steel meshes (see figure 7.43).
- The constructional details of putting reinforcing steel mesh behind the studs of edge beams are proved to be very efficient in case of membrane action of composite floor which could provide a beneficial lateral restraints to the floor slab.
- The residual loadbearing capacity of the floor remains adequate and is important enough despite significant deflection of the floor.

8 PARAMETRIC NUMERICAL STUDIES

8.1 Scope

The full scale standard fire resistance test has confirmed once again the excellent performance of the composite flooring system due to the presence of tensile membrane action in the slab as observed and described by Bailey & Moore[12,13]. Nevertheless, it is still necessary to extend the verification of the simple design method to its full application domain. With current knowledge in fire safety engineering, such verification can be achieved by means of a numerical parametric study on the basis of advanced calculation models, in which several specific features, such as deflection limit of the floor and elongation of reinforcing steel can be checked easily. However, before the parametric study in this project was carried out, the advanced numerical model had to be validated against the fire test.

8.2 Verification of numerical model

8.2.1 General

In order to provide a valid numerical model to simulate the fire behaviour of composite floors, numerical investigation of the full scale fire test described in Section 7 was performed using the computer software package ANSYS. The numerical model was composed of two different parts, one for heat transfer analysis and one for structural analysis.

8.2.2 Structural Analysis

The structural analysis was based on a hybrid structural model that took account of the steel beams; steel sheet; concrete rib and reinforcing steel mesh (see Figure 8.1). In this structural model, the following three types of finite elements were used:

- 3D non-linear line element - BEAM24,
- 3D non-linear multi-layer shell element - SHELL91
- 3D linear line element – PIPE16.

The composite floor was represented by shell elements for the solid part of the composite slab as well as reinforcing steel mesh. Beam-column elements were used for the steel members, the steel sheet and the ribs of the composite slab. Link elements were used for the shear connection between the steel beams and the composite slab.

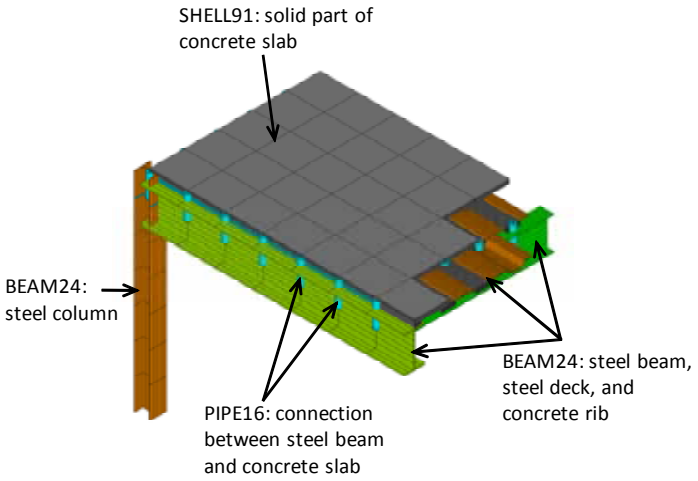

Figure 8.1 *Detail of the structural modelling*

8.2.3 Heat transfer analysis

In the heat transfer analysis, the heating of all the structural members was predicted with help of 2D models using the typical cross section of each structural member. As the validation of the numerical model concerns mainly the structural behaviour, the thermal properties of insulation material were adjusted in order to simulate the heating of protected steel members recorded during the fire test. For the steel and concrete elements, their thermal properties are those given in EN1994-1-2[(33)]. A comparison of calculated temperatures with test temperatures for different structural members is illustrated by Figure 8.2 to Figure 8.5.

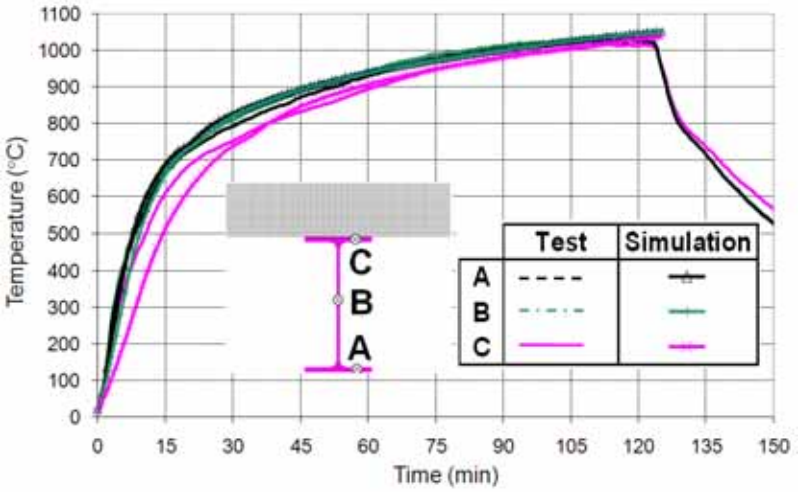

Figure 8.2 *Temperature comparison between test and numerical calculation - unprotected steel beams*

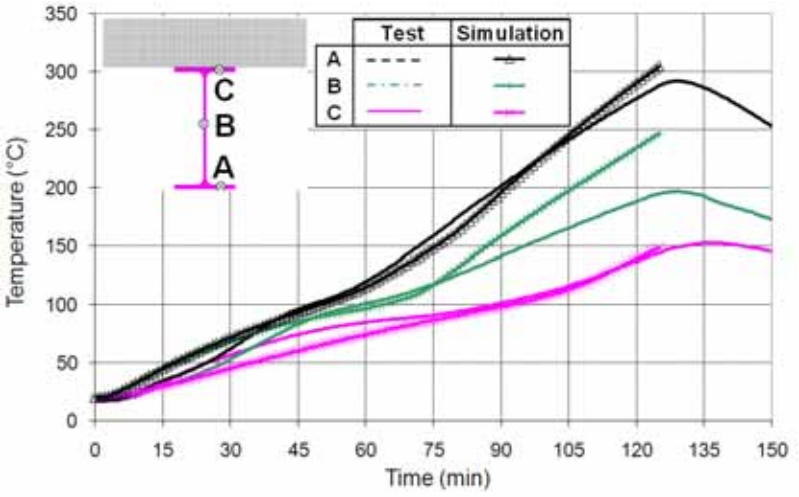

Figure 8.3 *Temperature comparison between test and numerical calculation - Protected secondary beams*

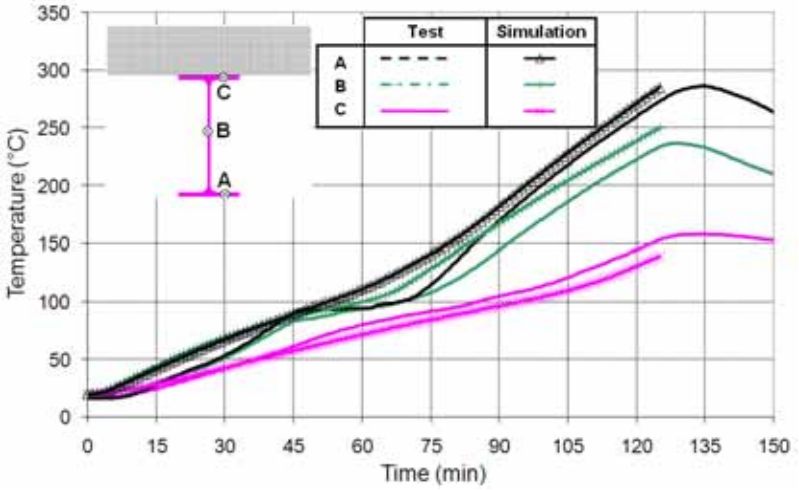

Figure 8.4 *Temperature comparison between test and numerical calculation - Protected main beams*

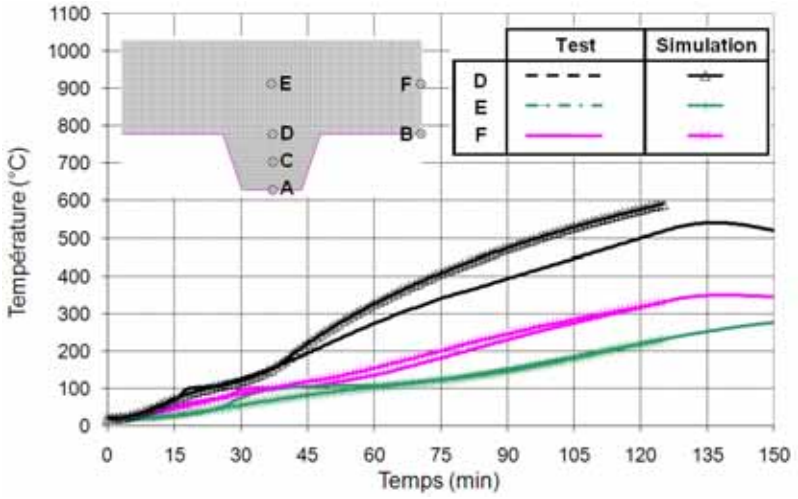

Figure 8.5 *Temperature comparison between test and numerical calculation - composite slab*

8.2.4 Mechanical behaviour of structural members

The structural behaviour of the floor was analysed based on the temperatures given by the heat transfer model and the structural model shown in Figure 8.1.

It can be observed easily from this model that the central part of the floor was heated much more than the boundary structural members. The simulated structural behaviour of the floor is shown in Figure 8.7, which gives the deformed shape predicted by the numerical model following 120 minutes exposure to the standard temperature-time curve.

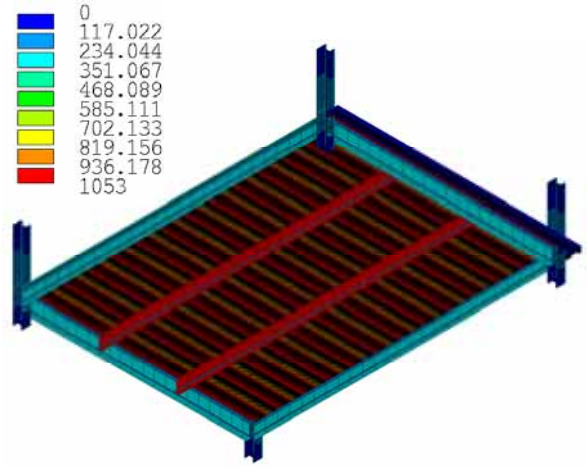

Figure 8.6 *Global structural model and attributed temperature field at 120 minutes of ISO fire*

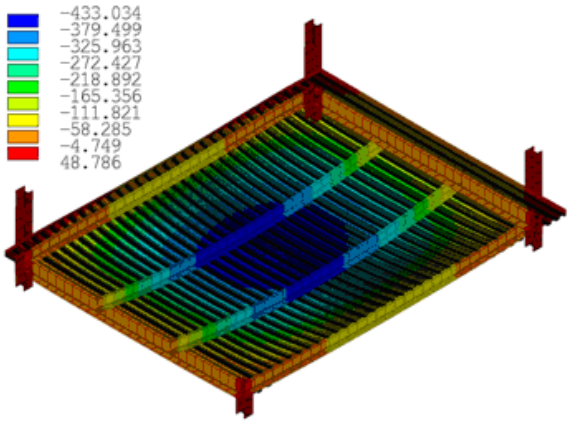

Figure 8.7 *Simulated deformed shape of the floor*

A comparison between the vertical displacement of the floor calculated using the numerical model and the measured displacements of the test specimen is shown in Figure 8.8. It can be observed that globally the numerical modelling predicts results very close to the experimental ones. However, a slight discrepancy occurs in the deflection of the unprotected beams after 50 minutes, resulting in some divergence between the measured deflections and those predicted by the numerical analysis. This phenomenon was attributed to the loss of continuity in the reinforcing mesh during the test, which resulted in a higher value of deflection for the unprotected beams. Despite this small difference, the validity of the numerical model as well as its capacity to predict fire behaviour was demonstrated.

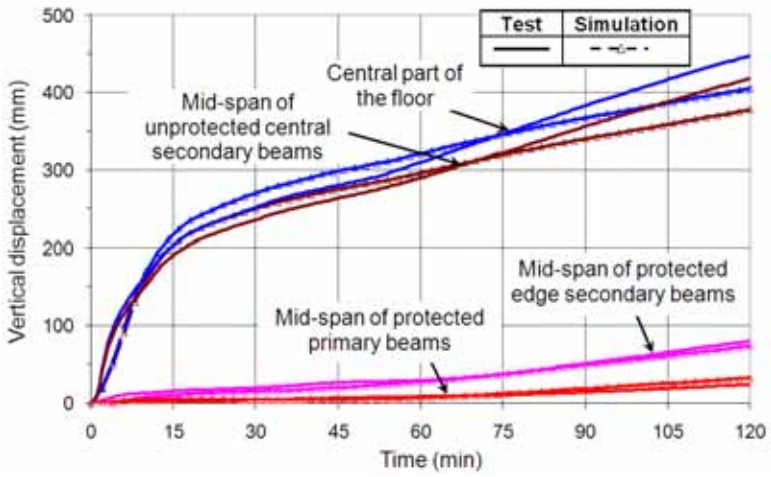

Figure 8.8 *Comparison of the predicted deflection of the floor recorded during the heating period of test*

8.3 Parametric numerical study using standard temperature-time curve

8.3.1 Input data for parametric study

A parametric study was used to extend the investigation of the simple design method to its full application domain. However, a full parametric study would require a great number of numerical simulations, which would necessitate a huge computation cost. Consequently the scope of the parametric study was limited to the following key parameters:

- Grid size of the floor,
- Degree of utilisation
- Fire duration

It must be pointed out that this parametric study is focused only on the behaviour of steel and concrete composite floors exposed to the standard temperature-time curve.

A preliminary numerical calculation was undertaken for a composite floor with an area of 18 m by 18 m, comprising two bays of 9 m span in each direction, (see Figure 8.9(a)). The main aim of this preliminary analysis was to determine the appropriate boundary conditions, in particular the restraint conditions of the slab to be adopted if the model is limited to one bay in the parametric study. As shown in Figure 8.9(b), the predicted deflection of the corner grid with two continuous edges is the most important among all four grids (the other three grids are with three or four continuous edges). In consequence, all numerical simulations in the parametric study simulated the restraint conditions appropriate to a corner bay with two edges laterally restrained, to simulate continuity of the slab.

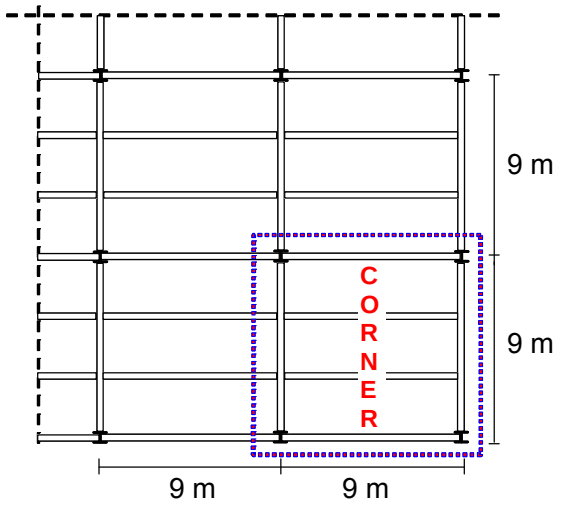

(a) Structure grid of a real building

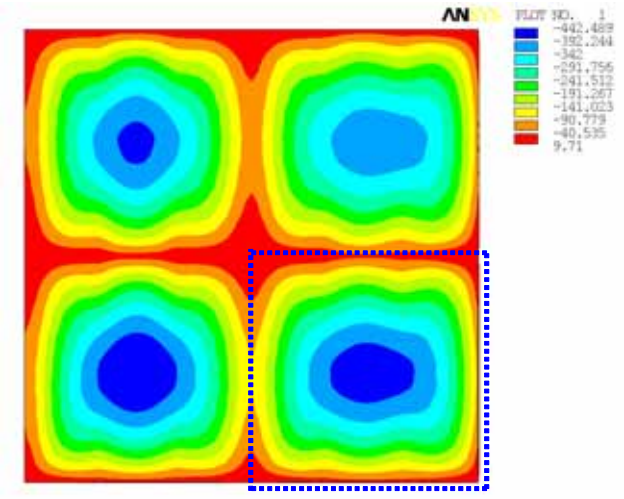

(b) ANSYS model

Figure 8.9 *Numerical calculation of four floor grids*

Seven bay sizes were investigated in the parametric study: 6 × 6 m, 6 × 9 m, 6 × 12 m, 9 × 9 m, 9 × 12 m, 9 × 15 m and 7.5 × 15 m (Figure 8.10. All these cases were modelled with simulated continuity of the composite slab on two edges. All boundary beams were assumed to be protected but all internal secondary beams were assumed to be unprotected.

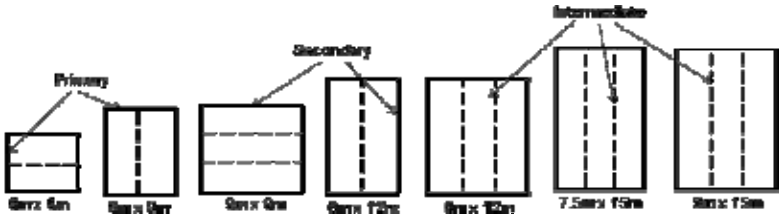

Figure 8.10 *Floors considered in the parametric numerical study*

Three different intensities of variable action were considered in the study, as shown in Table 8.1. These values of variable action correspond to those commonly used in room temperature design in the French building market. Nevertheless, if different load values were used, there would be no influence on the simple design method because the applied load is only an input data given by design engineers. In the parametric study, only Case 1 and Case 3 were investigated numerically. Case 2 was considered to be covered as it is an intermediate value between Case 1 and Case 3.

Table 8.1 *Value of permanent and variable actions considered.*

Case	Permanent action G	Variable action Q
1	Self weight + 1.25 kN/m²	2.5 kN/m²
2	Self weight + 1.25 kN/m²	3.5 kN/m²
3	Self weight + 1.25 kN/m²	5.0 kN/m²

Four standard fire durations, that is 30, 60, 90 and 120 minutes, were investigated. The depth of the composite slab in each case was based on the minimum depth required to fulfil the insulation criteria for these fire durations. Based on the use of a 60mm deep trapezoidal steel deck profile this resulted in composite slabs 120, 130, 140 and 150 mm deep. The geometry of the trapezoidal profile is based on the COFRAPLUS 60 product, the most commonly used deck profile on the French market. This steel deck has narrow ribs relative to other profiles, resulting in a more onerous temperature profile and lower mechanical resistance. Therefore, if the simple design method is verified with this steel decking, the conclusion could be conservatively applied to any other types of steel decking.

With the combination of all above parameters, a total of 112 numerical simulations were conducted.

Prior to the analysis of the fire behaviour of the different floor grids, preliminary designs were carried out in accordance with EN 1994-1-1[34], to determine the size of structural members of all the composite floors. In these designs, all steel beams were considered to be connected to the composite slab with headed studs. As far as the material properties used in these designs are concerned, the quality of concrete was assumed to be C30/37 with a compressive strength of 30 MPa. The reinforcing steel mesh was steel grade B500. The steel grade of the beams was mainly S235.

An important parameter for the fire performance of composite floor designed with the simple design method is the size of reinforcing steel mesh used in the composite slab. As the parametric study was to verify the simple design method, the size of all reinforcing steel mesh was derived directly from this simple design method. In addition, the axis distance (i.e. distance between the axis of longitudinal

reinforcement and the unexposed side of concrete slab) was taken as 45 mm in all cases.

The heating of the fire protected boundary beams and columns will also influence the performance of the floor slab. In the parametric study, the thermal properties of the fire protection were modelled such that the temperature of these members at the expected fire duration was in general around 550 °C. However, if this heating was reached before the expected fire duration, the heating of the corresponding steel beam was then maintained to 550 °C for all instants following that when this heating was reached.

Details of the size of steel beams and mesh considered for each case are given in Table 8.2 to Table 8.5 The table also includes the degree of shear connection of the composite beams and the steel grade if it is different from S235. B1, B2, S and DC mean respectively primary beams, secondary beams, area of the reinforcing mesh in mm^2/m and degree of shear connection of composite beams. In addition, Span 1 indicates the length of secondary beams and Span 2 that of primary beams. For each case, two simulations were conducted, one with the existence of mechanical link between slab and columns (for example, through additional reinforcing bars) and another one without this link.

Table 8.2 *Parameters selected for floors designed for 30 minutes fire resistance*

R 30 Depth = 120 mm		**Span1 [m]**							
Span2 [m]	**Load [kN/m²]**	**6**		**9**		**12**		**15**	
6	**2.5+1.25**	B1	IPE300 DC: 0.9	B1	IPE360 DC: 1.0	B1	IPE450 DC: 1.0		
		B2	IPE240 DC: 0.8	B2	IPE360 DC: 0.7	B2	IPE450 DC: 0.7		
		S	84	S	99	S	142		
	5.0+1.25	B1	IPE360 DC: 0.9	B1	IPE450 DC: 1.0	B1	IPE500 DC: 1.0		
		B2	IPE270 DC: 0.7	B2	IPE400 DC: 0.6	B2	IPE500 DC: 0.6		
		S	99	S	142	S	142		
7.5	**2.5+1.25**							B1	IPE600 DC: 1.0
								B2	IPE550 DC: 0.7
								S	142
	5.0+1.25							B1	IPE600 -S355 DC: 1.0
								B2	IPE600 DC: 0.7
								S	142
9	**2.5+1.25**			B1	IPE550 DC: 0.6	B1	IPE600 DC: 0.8	B1	IPE600 DC: 1.0
				B2	IPE360 DC: 0.7	B2	IPE450 DC: 0.7	B2	IPE500 DC: 0.7
				S	99	S	142	S	142
	5.0+1.25			B1	IPE550 -S355 DC: 0.6	B1	IPE600 -S355 DC: 0.8	B1	IPE600 -S355 DC: 1.0
				B2	IPE400 DC: 0.6	B2	IPE500 DC: 0.6	B2	IPE600 DC: 0.7
				S	142	S	142	S	142

Printed 11/07/10~~12/04/10~~

Table 8.3 *Parameters selected for floors designed for 60 minutes fire resistance*

R 60 Depth = 130 mm		**Span1 [m]**							
Span2 [m]	**Load [kN/m²]**	**6**		**9**		**12**		**15**	
6	**2.5+1.25**	B1	IPE300 DC: 0.8	B1	IPE360 DC: 0.9	B1	IPE450 DC: 1.0		
		B2	IPE240 DC: 0.8	B2	IPE360 DC: 0.8	B2	IPE450 DC: 0.7		
		S	115	S	193	S	284		
	5.0+1.25	B1	IPE360 DC: 0.8	B1	IPE450 DC: 0.9	B1	IPE500 DC: 1.0		
		B2	IPE270 DC: 0.7	B2	IPE400 DC: 0.6	B2	IPE500 DC: 0.5		
		S	151	S	227	S	347		
7.5	**2.5+1.25**							B1	IPE600 DC: 1.0
								B2	IPE550 DC: 0.7
								S	347
	5.0+1.25							B1	IPE600-S355 DC: 1.0
								B2	IPE600 DC: 0.6
								S	433
9	**2.5+1.25**			B1	IPE550 DC: 0.5	B1	IPE600 DC: 0.7	B1	IPE600 DC: 0.9
				B2	IPE360 DC: 0.8	B2	IPE450 DC: 0.7	B2	IPE550 DC: 0.7
				S	166	S	245	S	311
	5.0+1.25			B1	IPE550 -S355 DC: 0.5	B1	IPE600 -S355 DC: 0.7	B1	IPE750 x 173 DC: 0.9
				B2	IPE400 DC: 0.6	B2	IPE500 DC: 0.5	B2	IPE600 DC: 0.6
				S	210	S	297	S	393

Printed 11/07/10~~12/04/10~~

Table 8.4 *Parameters selected for floors designed for 90 minutes fire resistance*

R 90 Depth = 140 mm		**Span1 [m]**							
Span2 [m]	**Load [kN/m²]**	**6**		**9**		**12**		**15**	
6	**2.5+1.25**	B1	IPE300 DC: 0.7	B1	IPE360 DC: 1.0	B1	IPE450 DC: 1.0		
		B2	IPE240 DC: 0.7	B2	IPE360 DC: 0.8	B2	IPE450 DC: 0.7		
		S	119	S	187	S	291		
	5.0+1.25	B1	IPE360 DC: 0.7	B1	IPE450 DC: 1.0	B1	IPE500 DC: 1.0		
		B2	IPE270 DC: 0.7	B2	IPE400 DC: 0.6	B2	IPE500 DC: 0.6		
		S	146	S	233	S	355		
7.5	**2.5+1.25**							B1	IPE600 DC: 0.9
								B2	IPE550 DC: 0.7
								S	393
	5.0+1.25							B1	IPE600 -S355 DC: 0.9
								B2	IPE600 DC: 0.6
								S	473
9	**2.5+1.25**			B1	IPE550 DC: 0.5	B1	IPE600 DC: 0.6	B1	IPE600 -S355 DC: 0.7
				B2	IPE360 DC: 0.8	B2	IPE450 DC: 0.7	B2	IPE550 DC: 0.7
				S	177	S	252	S	340
	5.0+1.25			B1	IPE550-S355 DC: 0.5	B1	IPE600 -S355 DC: 0.6	B1	IPE750 x 173 DC: 0.7
				B2	IPE400 DC: 0.6	B2	IPE500 DC: 0.6	B2	IPE600 DC: 0.6
				S	215	S	311	S	433

Table 8.5 *Parameters selected for floors designed for 120 minutes fire resistance*

R 120 Depth = 140 mm		Span1 [m]							
Span2 [m]	**Load [kN/m²]**	**6**		**9**		**12**		**15**	
6	**2.5+1.25**	B1	IPE300 DC: 0.6	B1	IPE360 DC: 1.0	B1	IPE450 DC: 1.0		
		B2	IPE240 DC: 0.7	B2	IPE360 DC: 0.8	B2	IPE450 DC: 0.7		
		S	132	S	204	S	318		
	5.0+1.25	B1	IPE360 DC: 0.6	B1	IPE450 DC: 1.0	B1	IPE500 DC: 1.0		
		B2	IPE270 DC: 0.7	B2	IPE400 DC: 0.6	B2	IPE500 DC: 0.6		
		S	161	S	252	S	393		
7.5	**2.5+1.25**							B1	IPE600 DC: 0.8
								B2	IPE550 DC: 0.7
								S	417
	5.0+1.25							B1	IPE600 -S355 DC: 0.8
								B2	IPE600 DC: 0.6
								S	503
9	**2.5+1.25**			B1	IPE550 DC: 0.4	B1	IPE550-S355 DC: 0.6	B1	IPE600 -S355 DC: 0.7
				B2	IPE360 DC: 0.8	B2	IPE450 DC: 0.7	B2	IPE550 DC: 0.7
				S	193	S	277	S	377
	5.0+1.25			B1	IPE550 -S355 DC: 0.4	B1	IPE600-S355 DC: 0.6	B1	IPE750 x 173 DC: 0.7
				B2	IPE400 DC: 0.6	B2	IPE500 DC: 0.6	B2	IPE600 DC: 0.6
				S	252	S	340	S	457

8.3.2 Input data for parametric study

The results from the parametric study have been used to investigate the following two issues, which are significant to the application of the simple design method in practice.

- maximum deflection of floor
- maximum mechanical elongation of reinforcing steel mesh

Maximum deflection of floor

As described for the simple design method (Section 5) and demonstrated during the fire test (see Section 7), large deflection of the floor could occur before the point of structural collapse is reached. As the resistance of the slab relies on tensile membrane action of the floor slab, this large deflection is required to activate this load carrying mechanism. However, large deflections of the floor can also lead to loss of integrity performance due to concrete cracking, high strains in the reinforcement and the possible modification of loading condition if the floor becomes too sloping. Regulatory authorities are also concerned by design methods which result in deflections much larger than those experienced in traditional fire

tests, although these are not really relevant to the design method discussed in this publication. Also the simple design method assumes that the beam on the perimeter of each floor design zone remains rigid. In reality the surrounding beams deflect once subjected to fire. The parametric study therefore pays special attention to deflections in order to address these issues.

In the simple design method, a maximum allowable value of deflection has been assumed (see Section 6.2.1) to predict the ultimate load-carrying capacity of the floor. Therefore, the first step of the current investigation is to check whether this maximum allowable deflection is consistent with deflection predicted by the advanced calculation method. As a result, a comparison between deflection calculated in the numerical analysis and maximum allowable deflections according to the simple design method was carried out and the results are illustrated in Figure 8.11 (with mechanical link between slab and columns) and Figure 8.12 (without mechanical link between slab and columns). Due to the fact that the simple design method assumes the vertical restrained peripheral supports and advanced calculations takes account of flexible peripheral steel beams, the comparison between them was made with total deflection of floor under fire situation deducted of the deflection of peripheral beams.

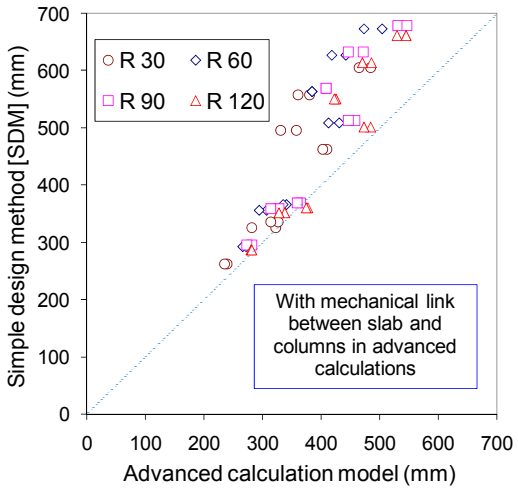

Figure 8.11 *Comparison of the deflection predicted by the advanced calculation model with maximum allowable deflection according to the simple design method (SDM) with mechanical link between slab and columns*

It can be found from the comparison that the maximum allowable deflection used in the simple design method is systematically greater than the maximum deflection predicted in numerical analysis. The scatter between them seems to increase as a function of floor panel size. In fact, the physical meaning of this finding is that the simple design method predicts lower load bearing capacity of the floor than the advanced calculation model under the same deflection value. From this point of view, the simple design method can be considered as conservative.

Traditionally, certain national fire regulations define the deflection value of span/30 as the failure criterion of a single structural member in bending (beams and slabs) tests under ISO fire condition[38]. In the case of composite floors comprising primary beams, secondary beams and slabs, one can propose that the total deflection limit of the floor shall be the sum of the allowable deflections of each of

the structural members as illustrated in Figure 8.13 instead of that with each deflection considered individually because these structural members are assembled together.

Consequently, whatever the beam distribution is, the deflection limit shall be at least (span1+span2)/30, where span 1 is the length of the secondary beams and span 2 is the length of the primary beams.

For this failure criterion, it is then interesting to check the fire rating of the floor. A comparison is illustrated in Figure 8.14, which gives the ratio between the fire duration to reach above deflection criterion according to the advanced numerical model, and the fire rating predicted by the Simple Design Method. In all cases, this ratio is greater than 1.0, which means that if the above deflection is adopted as the failure criterion, the fire rating will be greater than that given by the simple design method. Therefore, the application of the simple calculation will satisfy automatically the above deflection criterion.

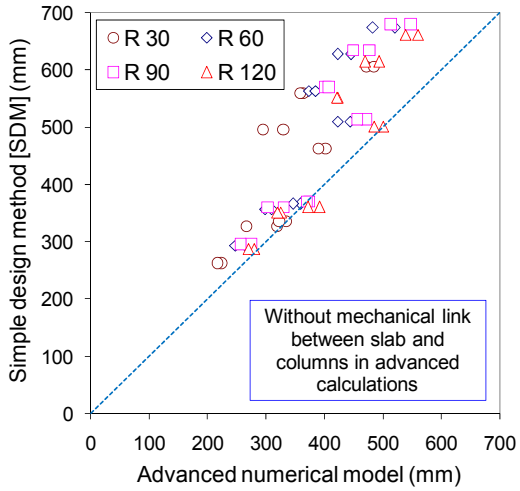

Figure 8.12 *Comparison of the deflection predicted by the advanced calculation model with maximum allowable deflection according to the simple design method (SDM) without mechanical link between slab and columns*

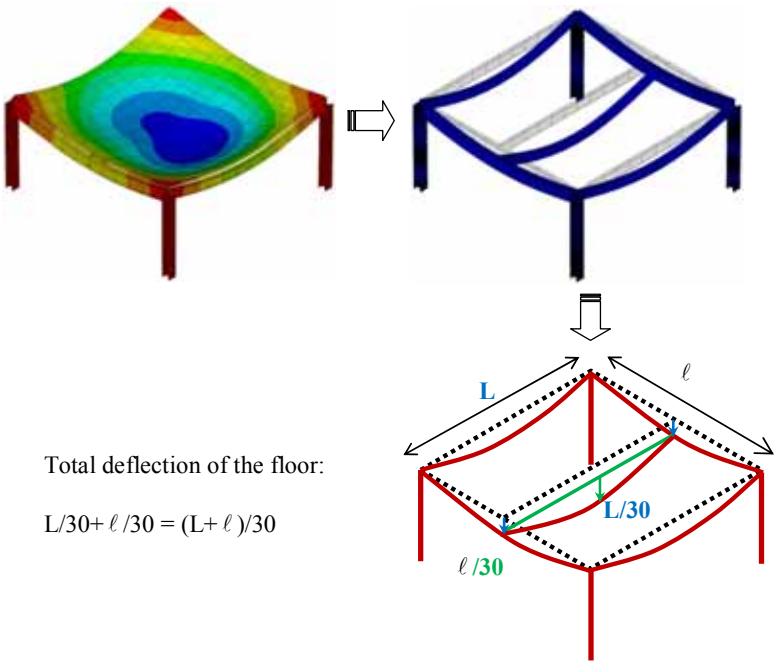

Total deflection of the floor:

$L/30 + \ell/30 = (L + \ell)/30$

Figure 8.13 *Total deflection limit according to the criterion of span/30*

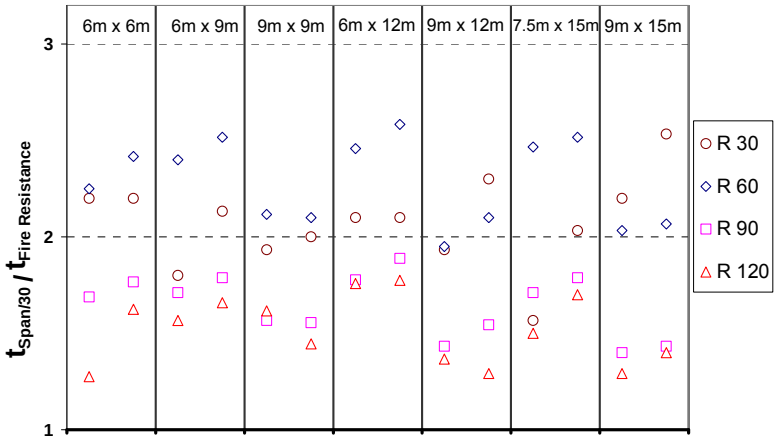

Figure 8.14 *Ratio between the time when the predicted deflection reaches span/30 and the fire resistance predicted according to the simple design method*

The European standard for fire resistance tests[32], defines the following deflection limits for assessing the load bearing criterion of elements subject to bending. The load bearing failure for this type of structural element is deemed to occur if the measured deflection exceeds the limiting deflection or the limiting rate of deflection given below:

Limiting deflection, $D = \frac{L^2}{400d}$ mm; and,

Limiting rate of deflection, $\frac{dD}{dt} = \frac{L^2}{9000d}$ mm/min

where:

L is the clear span of the test specimen, in millimetres

d is the distance from the extreme fibre of the cold design compression zone to the extreme fibre of the cold design tension zone of the structural section, in millimetres.

It must be kept in mind that the criterion with respect to the rate of deflection is not applied until a deflection of span/30 has been exceeded. That is the reason why this criterion is not taken into account, since it is already included in the previous deflection criterion based on Span/30. The same principle as considered with the criterion of Span/30 can be applied to get the maximum allowable deflection limit of the floor.

Elongation of the steel reinforcing mesh

In addition to the deflection of the floor, the elongation of reinforcing steel is the second feature that is investigated in detail in this parametric study. The simple design method is based on plastic analysis for the load bearing capacity of the floor system allowing for an enhancement due to tensile membrane action. As discussed in Section 6 failure of the slab could occur due to the fracture of the mesh across the short span of the slab. Moreover, this fracture could occur equally at the edge parts of the floor where the continuity of the slab exists.

This parametric study provided the opportunity to investigate the strain in the reinforcement predicted by the advanced calculation model when the target fire resistance is reached. Knowing the elongation of the reinforcement at fracture a conclusion can than be drawn as to the margin of safety against mesh fracture provided by the simple method.

As the reinforcing steel mesh is put over the whole area of the floor, and is continuous across all beams including protected boundary beams, significant tensile strain will also occur over the protected beams and around columns.

If the elongation becomes too great, fracture of the reinforcement could occur, which may lead to loss of integrity and insulation performance of the floor before load bearing failure is reached. However, the question arises about the criterion to be applied to elongation capacity of reinforcing steel. EN 1992-1-2[35] implies that for plastic design the minimum elongation capacity at ultimate stress for reinforcing steel must be at least 5%. Therefore, this value is taken as the elongation criterion in this parametric study for reinforcing steel mesh.

The results of this parametric study related to maximum deflection of the floors obtained for all fire resistance durations and the maximum elongation of

reinforcing steel along two orthogonal directions (parallels respectively to primary and secondary beams) are summarised in Table 8.10 to Table 8.13. In these tables, SDM means simple design method and Spans means (Span 1 + Span 2). From these tables, it can be found that in all cases, the maximum allowable deflection used to evaluate the load-bearing capacity in the simple design method always exceeds the predictions of the advanced numerical model. With respect to the maximum elongation of reinforcing steel, it can be observed that the maximum values obtained with the advanced numerical model for any fire duration are always lower than 5%, which once again is very satisfactory.

Table 8.6 *Deflection of the floor and elongation of reinforcing steel for fire duration R30 (with mechanical link between slab and columns)*

Load [kN/m²]	Span1 L [m]	Span2 ℓ [m]	ANSYS [mm]		SDM [mm]	$\frac{L+\ell}{30}$ [mm]	$\frac{L^2}{400\,d}$ [mm]	Elongation Span1 [%]	Elongation Span2 [%]
			Total add.	Slab					
2.5+1.25	6	6	248	239	262	400	500	2.8%	3.0%
5.0+1.25	6	6	240	235	262	400	462	2.9%	2.7%
2.5+1.25	9	6	359	322	326	500	609	2.8%	2.4%
5.0+1.25	9	6	312	282	326	500	563	3.0%	2.3%
2.5+1.26	9	9	359	331	495	600	844	3.4%	2.6%
5.0+1.25	9	9	389	358	495	600	779	3.0%	2.4%
2.5+1.25	12	6	379	326	335	600	789	3.1%	2.3%
5.0+1.25	12	6	361	314	335	600	726	3.0%	2.5%
2.5+1.25	12	9	443	381	558	700	987	3.2%	2.3%
5.0+1.25	12	9	416	361	558	700	907	3.0%	2.6%
2.5+1.25	15	7.5	480	410	462	750	1049	3.1%	3.8%
5.0+1.25	15	7.5	461	403	462	750	977	3.0%	4.0%
2.5+1.25	15	9	539	465	605	800	1234	3.2%	3.1%
5.0+1.25	15	9	578	485	605	800	1063	3.5%	4.4%

Table 8.7 *Deflection of the floor and elongation of reinforcing steel for fire duration R60 (with mechanical link between slab and columns)*

Load [kN/m²]	Span1 L [m]	Span2 ℓ [m]	ANSYS [mm]		SDM [mm]	$\frac{L+\ell}{30}$ [mm]	$\frac{L^2}{400\,d}$ [mm]	Elongation Span1 [%]	Elongation Span2 [%]
			Total add.	Slab					
2.5+1.25	6	6	288	271	293	400	486	3.6%	3.1%
5.0+1.25	6	6	280	266	293	400	450	3.7%	2.9%
2.5+1.25	9	6	348	307	356	500	597	3.5%	2.8%
5.0+1.25	9	6	334	294	356	500	552	3.4%	2.6%
2.5+1.26	9	9	434	385	563	600	827	3.9%	2.9%
5.0+1.25	9	9	429	384	563	600	764	3.6%	2.8%
2.5+1.25	12	6	409	341	366	600	776	3.3%	2.4%
5.0+1.25	12	6	397	335	366	600	714	3.1%	2.5%
2.5+1.25	12	9	527	442	627	700	970	3.7%	2.7%
5.0+1.25	12	9	499	419	627	700	893	3.4%	2.7%
2.5+1.25	15	7.5	524	431	509	750	1034	3.1%	3.7%
5.0+1.25	15	7.5	492	413	509	750	963	2.8%	3.4%
2.5+1.25	15	9	607	505	673	800	1125	3.6%	3.4%
5.0+1.25	15	9	571	474	673	800	1048	3.3%	3.1%

Table 8.8 *Deflection of the floor and elongation of reinforcing steel for fire duration R90 (with mechanical link between slab and columns)*

Load [kN/m²]	Span1 L [m]	Span2 ℓ [m]	ANSYS [mm]		SDM [mm]	$\frac{L+\ell}{30}$ [mm]	$\frac{L^2}{400\,d}$ [mm]	Elongation Span1 [%]	Elongation Span2 [%]
			Total add.	Slab					
2.5+1.25	6	6	306	282	295	400	474	2.7%	2.6%
5.0+1.25	6	6	294	274	295	400	439	2.8%	2.3%
2.5+1.25	9	6	379	328	359	500	585	2.7%	2.5%
5.0+1.25	9	6	364	314	359	500	542	2.7%	2.2%
2.5+1.26	9	9	471	408	569	600	810	3.3%	2.2%
5.0+1.25	9	9	468	409	569	600	750	3.1%	2.2%
2.5+1.25	12	6	448	365	369	600	763	2.5%	2.6%
5.0+1.25	12	6	436	360	369	600	703	2.2%	2.4%
2.5+1.25	12	9	579	472	633	700	953	3.0%	2.4%
5.0+1.25	12	9	548	447	633	700	879	2.7%	2.3%
2.5+1.25	15	7.5	579	458	513	750	1019	2.6%	3.1%
5.0+1.25	15	7.5	550	446	513	750	950	1.9%	2.9%
2.5+1.25	15	9	670	532	679	800	1109	2.6%	3.1%
5.0+1.25	15	9	668	547	679	800	1034	2.3%	2.5%

Table 8.9 *Deflection of the floor and elongation of reinforcing steel for fire duration R120 (with mechanical link between slab and columns)*

Load [kN/m²]	Span1 L [m]	Span2 ℓ [m]	ANSYS [mm]		SDM [mm]	$\frac{L+\ell}{30}$ [mm]	$\frac{L^2}{400\,d}$ [mm]	Elongation Span1 [%]	Elongation Span2 [%]
			Total add.	Slab					
2.5+1.25	6	6	360	281	287	400	462	3.1%	2.6%
5.0+1.25	6	6	305	281	287	400	429	3.2%	2.7%
2.5+1.25	9	6	398	339	351	500	574	3.0%	2.7%
5.0+1.25	9	6	386	328	351	500	532	3.0%	2.6%
2.5+1.26	9	9	500	426	551	600	794	3.9%	2.7%
5.0+1.25	9	9	492	422	551	600	736	3.6%	2.6%
2.5+1.25	12	6	476	377	360	600	750	2.8%	3.1%
5.0+1.25	12	6	464	374	360	600	692	2.4%	3.0%
2.5+1.25	12	9	616	487	614	700	938	3.6%	2.8%
5.0+1.25	12	9	626	470	614	700	865	3.4%	2.8%
2.5+1.25	15	7.5	625	485	501	750	1004	2.6%	3.6%
5.0+1.25	15	7.5	592	473	501	750	938	2.2%	3.4%
2.5+1.25	15	9	705	545	661	800	1093	3.2%	3.3%
5.0+1.25	15	9	676	530	661	800	1020	2.7%	3.2%

The results given in these tables from the parametric investigation with the advanced calculation model ANSYS are based on the assumption that the composite slab is linked to all steel columns with additional reinforcing steel bars. Certainly, this constructional detail can reduce the deflection of the floor but in reality this is not always possible, especially for edge beams. It will be then very important to know if this constructional detail is applied what will be the impact on the global behaviour of the floor. A second series of studies was made without this constructional detail and the results are presented in the same way in tables Table 8.10 to Table 8.13. Certainly the maximum deflections are slightly higher than previously. However, they remain nearly always lower than those estimated according to different traditional criteria. Moreover, the maximum elongation of reinforcing steel mesh for all floors is lower than 5% for all given fire ratings.

Table 8.10 *Deflection of the floor and elongation of reinforcing steel for fire duration R30 (without mechanical link between slab and columns)*

Load [kN/m²]	Span1 L [m]	Span2 ℓ [m]	ANSYS [mm]		SDM [mm]	$\frac{L+\ell}{30}$ [mm]	$\frac{L^2}{400\,d}$ [mm]	Elongation Span1 [%]	Elongation Span2 [%]
			Total add.	Slab					
2.5+1.25	6	6	305	224	262	400	500	2.8%	2.4%
5.0+1.25	6	6	285	218	262	400	462	3.0%	2.2%
2.5+1.25	9	6	363	274	326	500	609	2.9%	2.2%
5.0+1.25	9	6	330	267	326	500	563	3.0%	2.1%
2.5+1.26	9	9	406	295	495	600	844	3.2%	2.2%
5.0+1.25	9	9	394	330	495	600	779	3.1%	2.4%
2.5+1.25	12	6	415	335	335	600	789	3.4%	2.1%
5.0+1.25	12	6	392	323	335	600	726	3.0%	2.2%
2.5+1.25	12	9	464	364	558	700	987	3.3%	2.2%
5.0+1.25	12	9	442	359	558	700	907	3.0%	2.5%
2.5+1.25	15	7.5	490	402	462	750	1049	3.2%	3.0%
5.0+1.25	15	7.5	463	390	462	750	977	2.8%	3.1%
2.5+1.25	15	9	569	472	605	800	1234	3.0%	3.6%
5.0+1.25	15	9	578	485	605	800	1063	3.1%	4.0%

Table 8.11 *Deflection of the floor and elongation of reinforcing steel for fire duration R60 (without mechanical link between slab and columns)*

Load [kN/m²]	Span1 L [m]	Span2 ℓ [m]	ANSYS [mm]		SDM [mm]	$\frac{L+\ell}{30}$ [mm]	$\frac{L^2}{400\,d}$ [mm]	Elongation Span1 [%]	Elongation Span2 [%]
			Total add.	Slab					
2.5+1.25	6	6	348	264	293	400	486	3.7%	2.6%
5.0+1.25	6	6	325	248	293	400	450	3.7%	2.6%
2.5+1.25	9	6	400	310	356	500	597	3.5%	2.5%
5.0+1.25	9	6	380	298	356	500	552	3.6%	2.5%
2.5+1.26	9	9	493	373	563	600	827	3.5%	2.5%
5.0+1.25	9	9	481	385	563	600	764	3.2%	2.5%
2.5+1.25	12	6	463	359	366	600	776	4.0%	2.6%
5.0+1.25	12	6	435	346	366	600	714	3.8%	2.8%
2.5+1.25	12	9	587	445	627	700	970	3.8%	2.6%
5.0+1.25	12	9	548	423	627	700	893	3.5%	2.8%
2.5+1.25	15	7.5	565	444	509	750	1034	3.6%	3.2%
5.0+1.25	15	7.5	520	423	509	750	963	3.3%	3.0%
2.5+1.25	15	9	660	520	673	800	1125	3.1%	3.6%
5.0+1.25	15	9	607	483	673	800	1048	2.8%	3.4%

Table 8.12 *Deflection of the floor and elongation of reinforcing steel for fire duration R90 (without mechanical link between slab and columns)*

Load [kN/m²]	Span1 L [m]	Span2 ℓ [m]	ANSYS [mm]		SDM [mm]	$\frac{L+\ell}{30}$ [mm]	$\frac{L^2}{400\,d}$ [mm]	Elongation Span1 [%]	Elongation Span2 [%]
			Total add.	Slab					
2.5+1.25	6	6	363	275	295	400	474	4.1%	3.0%
5.0+1.25	6	6	338	257	295	400	439	4.3%	3.1%
2.5+1.25	9	6	433	331	359	500	585	2.6%	2.3%
5.0+1.25	9	6	403	303	359	500	542	3.8%	3.0%
2.5+1.26	9	9	531	402	569	600	810	3.3%	2.0%
5.0+1.25	9	9	521	408	569	600	750	2.2%	2.2%
2.5+1.25	12	6	497	375	369	600	763	2.5%	2.4%
5.0+1.25	12	6	475	370	369	600	703	3.2%	2.2%
2.5+1.25	12	9	644	477	633	700	953	3.0%	2.4%
5.0+1.25	12	9	599	450	633	700	879	2.8%	2.2%
2.5+1.25	15	7.5	624	472	513	750	1019	2.2%	3.0%
5.0+1.25	15	7.5	582	457	513	750	950	1.9%	2.8%
2.5+1.25	15	9	726	548	679	800	1109	2.6%	2.8%
5.0+1.25	15	9	670	514	679	800	1034	2.3%	2.5%

Table 8.13 *Deflection of the floor and elongation of reinforcing steel for fire duration R120 (without mechanical link between slab and columns)*

Load [kN/m²]	Span1 L [m]	Span2 ℓ [m]	ANSYS [mm]		SDM [mm]	$\frac{L+\ell}{30}$ [mm]	$\frac{L^2}{400\,d}$ [mm]	Elongation Span1 [%]	Elongation Span2 [%]
			Total add.	Slab					
2.5+1.25	6	6	393	280	287	400	462	4.9%	3.8%
5.0+1.25	6	6	353	270	287	400	429	5.2%	3.7%
2.5+1.25	9	6	466	326	351	500	574	4.6%	4.1%
5.0+1.25	9	6	434	320	351	500	532	4.5%	3.9%
2.5+1.26	9	9	567	423	551	600	794	2.8%	2.9%
5.0+1.25	9	9	548	421	551	600	736	3.6%	4.5%
2.5+1.25	12	6	537	392	360	600	750	4.1%	2.6%
5.0+1.25	12	6	509	372	360	600	692	3.8%	2.6%
2.5+1.25	12	9	686	493	614	700	938	3.7%	2.8%
5.0+1.25	12	9	663	469	614	700	865	3.5%	2.7%
2.5+1.25	15	7.5	677	501	501	750	1004	3.2%	3.2%
5.0+1.25	15	7.5	625	485	501	750	938	2.8%	3.1%
2.5+1.25	15	9	767	560	661	800	1093	2.7%	3.5%
5.0+1.25	15	9	717	539	661	800	1020	2.8%	3.1%

8.4 Conclusion

The objective of the parametric study was to make a detailed investigation of the simple design method with the help of advanced calculation models validated against an ISO fire test. From the results, it can be concluded that:

- With respect to load bearing capacity, the simple design method gives conservative results compared to advanced calculation models;
- When using traditional deflection criteria based on the behaviour of single flexural structural members, the fire performance of composite flooring systems predicted with the simple design method are on the safe side;
- Concerning the elongation of reinforcing steel mesh, it remains generally below 5%, the minimum elongation requirement recommended by EN 1992-1-2 for all types of reinforcing steel;
- Mechanical links between slab and columns are not necessary. Nevertheless, this constructional detail could reduce the deflection of a composite flooring system under a fire situation.

The results derived from this parametric study show clearly that the simple design method is fully capable of predicting in a safe way the structural performance of composite steel and concrete floors subjected to an ISO fire condition, which may be taken as evidence that the design method can be used in structural fire engineering design.

9 REFERENCES

1. 'Fire Safe Design: A new approach to multi-storey steel framed buildings' P288, The Steel Construction Institute, 2006.
2. 'The behaviour of Multi-storey steel framed buildings in fire', A European joint research programme, British Steel Swinden Technology Centre, 1999
3. Lennon, T., 'Cardington fire tests: instrumentation locations for large compartment fire test.', Building Research Establishment Report N100/98, June 1996.
4. Lennon, T., 'Cardington fire tests: instrumentation locations for corner fire test.', Building Research Establishment Report N152/95, June 1996
5. Wainman, W. and Kirby, B., Compendium of UK standard fire test data, No.1 - Unprotected structural steel, British Steel, Swinden Technology Centre, 1987
6. Investigation of Broadgate Phase 8 Fire, SCI, Ascot, 1991.
7. Thomas, I. R., Bennetts, I. D., Dayawansa, P., Proe, D. J. and Lewins, R. R., 'Fire Tests of the 140 William Street Office Building.', BHPR/ENG/R/92/043/SG2C, BHP Research, Melbourne Australia, 1992
8. Proe, D. J. and Bennetts, I. D., 'Real Fire Tests in 380 Collins Street Office Enclosure.', BHPR/PPA/R/94/051/SG021A, BHP Research Melbourne Australia, 1994.
9. Brand Verhalten Von Stahl und Stahlverbund Konstructionen (Fire behaviour of steel and composite construction), Verlag TUV Rheinland, 1986.
10. Johansen, K.W., 'The Ultimate strength of Reinforced Concrete Slabs.', International Association for Bridge and Structural Engineering, Final Report, Third Confress, Liege, September 1948.
11. Ockleston AJ. Load tests on a 3-storey reinforced concrete building in Johannesburg. Struct Eng 1955;33(10):304-22
12. Bailey C.G. and Moore D.B., The structural behaviour of steel frames with composite floor slabs subjected to fire: Part 1: Theory
13. Bailey C.G. and Moore D.B., The structural behaviour of steel frames with composite floor slabs subjected to fire: Part 2: Design
14. Park, R, Ultimate strength of rectangular concrete slabs under short term uniform loading with edges restrained against lateral movement. Proceedings, Institution of Civil Engineers, 28, pp125-150.
15. Wood R. H. Plastic and elastic design of slabs and plates, with particular reference to reinforced concrete floor slabs Thames and Husdon, London. 1961.
16. Taylor R. A note on a possible basis for a new method of ultimate load design of reinforced concrete slabs. Magazine of concrete research VOL 17 NO. 53 Dec 1965 pp. 183-186
17. Kemp. K.O. Yield of a square reinforced concrete slab on simple supports allowing for membrane forces. The structural Engineer Vol 45, No.7 July 1967 pp. 235-240.
18. Sawczuk A. and Winniki L. Plastic behaviour of simply supported reinforced concrete plated are moderately large deflections. Int J. Solids Structures Vol 1 1965 pp. 97 to 111.

19. Hayes B. Allowing for membrane action in the plastic analysis of rectangular reinforced concrete slabs Magazine of concrete research Vol. 20 No. 81 Dec 1968. pp 205-212.
20. Bailey C. G., White D.S. and Moore D.B. The tensile membrane action of unrestrained composite slab under fire conditions, Engineering Structures, vol. 22, no12, pp. 1583-1595
21. Bailey C. G. & Toh, W.S. 'Behaviour of concrete floor slabs at ambient and elevated temperature', Fire Safety Journal, 42, oo425-436, 2007.
22. Hayes B. and Taylor R. Load-Testing RC slabs. The Consulting Engineer. Nov. 1969. pp 46-47
23. Taylor R., Maher D.R.H. and Hayes B. Effect of arrangement of reinforcement on the behaviour of the reinforce concrete slabs. Magazine of concrete research Vol 18 No. 55. June 1966. pp 85-94
24. Moy S.S.J. Load-deflection characteristics of rectangular reinforced concrete slabs. Magazine of concrete research Vol 24 No. 81 Dec. 1972. pp 209-218.
25. Bailey, C.G., Efficient arrangement of Reinforcement for membrane behaviour of composite slabs in fire conditions, Journal of Constructional Steel Research, 59, 2003, pp931-949.
26. Bailey C.G., Membrane action of lightly reinforced concrete slabs at large displacements, Engineering Structures, 23, 2001, pp470-483.
27. Bailey, Colin G. and Toh, Wee Siang. Experimental behaviour of concrete floor slabs at ambient and elevated temperatures. SIF06
28. O'Conner MA, Kirby BR, Martin DM. Behaviour of a multi-storey composite steel framed building in fire. Struct Eng 2003;81(2):27–36.
29. Bailey CG, Lennon T, Moore DB. The behaviour of full-scale steel framed buildings subjected to compartment fires. Struct Eng 1999; 77(8):15–21.
30. Bailey CG, Membrane action of slab/beam composite floor systems in fire. Engineering Structures 26 2004:1691-1703.
31. Wang YC. Tensile membrane action in slabs and its application to the Cardington fire tests. Fire, static and dynamic tests of building structures. Proceeding of the second Cardington conference, England, 12-14 March1996: 55–67
32. EN 1992-1-2, Eurocode 2, Design of concrete structures. Part 1.2: General rules. Structural fire design, CEN
33. EN 1994-1-2, Eurocode 2, Design of composite steel and concrete structures. Part 1.2: General rules. Structural fire design, CEN
34. EN 1994-1-1, Eurocode 4 Design of composite steel and concrete structures – Part 1-1: General rules and rules for buildings, CEN
35. EN 1993-1-8, Eurocode 3 Design of steel structures – Part 1-8: Design of joints, CEN
36. EN 1992-1-1, Eurocode 2 Design of Concrete Structures – Part 1-1: General rules and rules for buildings, CEN
37. EN 1991-1-2 - Eurocode 1 " Actions on structures. General actions. " – Part 1-2: Actions on structures exposed to fire, CEN.
38. ARRETE DU 21 AVRIL 1983, Ministère de l'Intérieur Français Détermination des degrés de résistance au feu des éléments de construction.

39. EN 1363-1 - Fire resistance tests – Part 1: General requirements, CEN.(35)